Sound absorption in porous materials

Jose María Cucharero Moya

School of Electrical Engineering

Thesis submitted for examination for the degree of Master of Science in Technology.

Espoo 5.12.2017

Thesis supervisors:

Prof. Tapio Lokki

Thesis advisor:

D.Sc. Tuomas Hänninen

Aalto University
School of Electrical
Engineering

AALTO UNIVERSITY
SCHOOL OF ELECTRICAL ENGINEERING

ABSTRACT OF THE
MASTER'S THESIS

Author: Jose María Cucharero Moya

Title: Sound absorption in porous materials

Date: 5.12.2017 Language: English Number of pages: 13+79

Department of Signal Processing and Acoustics

Professorship: Acoustics and Audio Signal Processing

Supervisor: Prof. Tapio Lokki

Advisor: D.Sc. Tuomas Hänninen

Porous materials have been the most commonly used materials to dissipate sound energy and reduce sound reflections. The popularity of these materials resides in their ability to efficiently absorb sound at mid and high frequencies using relatively thin layers. Dissipation of sound energy in porous materials occurs through the interconnected pores due to viscous, thermal and inertial effects caused by the interaction between the fluid and the solid phases.

Measurements of the sound absorption coefficients of sound absorbing materials are generally performed using the reverberation chamber or the impedance tube methods. The two of them are laboratory measurement techniques. The impedance tube methods compute the absorption coefficients only considering normal incident sound waves, whereas the reverberation chamber method assumes a diffuse field, where sound arrives the surface of the absorbing material from all directions.

The ability of porous materials to absorb sound strongly depends on their physical characteristics. These include porosity, tortuosity, shape of the pores, and flow resistivity. The physical properties of the total system determine the final sound absorption coefficients. The physical properties of the system include thickness and bulk density of the porous layer, and size of the particles forming the material.

Theoretical, semi-phenomenological, and empirical models have been developed to predict the sound absorption properties of porous materials. It has been demonstrated that the most popular models, which were developed to predict the sound absorption properties of mineral wool porous materials, do not accurately predict the sound absorption coefficient of porous materials made of natural cellulose fibres. New parameters have to be added to the models.

Keywords: Porous material, sound absorption, cellulose, modelling, impedance tube, reverberation chamber.

Preface

I would like to thank Professor Tapio Lokki for giving me the opportunity to develop my Master's thesis under his supervision and for his support and ideas. I am extremely thankful to him for giving me the opportunity to continue investigating on sound absorbing materials after the end of this thesis.

I would also like to express my gratitude to my advisor Tuomas Hänninen for his support and contagious enthusiasm for the subject. His help in the preparation of the cellulose fibres, the supply of many different porous materials, and all his ideas and comments which helped me to successfully complete this thesis work.

I am very thankful to Ritva Kivelä for all the time she spent helping me in making cellulose fibres. Also, my gratitude to Kristiina Lillqvist for the great scanning electron microscopy images of porous materials.

My most special thanks go to Mira Savolainen, for her love, patience and support throughout all these years. You always believed in me despite all the adversities.

Finally, but no less important, I would like to thank my parents and siblings for supporting me and encourage me to pursue my dreams.

Otaniemi, 5.12.2017

Jose María Cucharero Moya

Contents

Symbols and abbreviations

Symbols

a	Acceleration
A_{cr}	Cross-sectional area
A_0	Complex amplitude of the incident sound wave
A	Absorption area
$\hat{A}$	Empirical coefficient
A_T	Equivalent sound absorption area of a test sample
$\hat{B}$	Empirical coefficient
c	Speed of sound
c_0	Speed of sound in air
$c_1 - c_8$	Empirical coefficients
C	Compressibility factor
$\hat{C}$	Empirical coefficient
d_f	Diameter of a fibre
d_{tube}	Diameter of a tube
dx	Length of an elemental volume
dV	Volume of an elemental volume
D	Characteristic particle dimension
E	Dimensionless variable, empirical models
f	Frequency
f_{cr}	Transition frequency
f_u	Upper frequency limit
f_l	Low frequency limit
F	Force
H_i	Transfer Function of the incident sound wave
H_r	Transfer Function of the reflected sound wave
H_{12}	Transfer Function of the total sound field
H_c	Calibration factor
$H_{12,cal}$	Calibrated Transfer Function of the total sound field
$H_{12,A}$	Transfer Function of the total sound field with microphones in configuration A for the calculation of H_c
$H_{12,B}$	Transfer Function of the total sound field with microphones in configuration B for the calculation of H_c
I	Sound intensity
k	Wave number
k_s	Structure factor
k'	Real part of the wave number
k''	Imaginary part of the wave number
k_0	Wave number in air
J_0	Zeroth-order Bessel function
J_1	First-order Bessel function
l_f	Length of a fibre
L	Thickness
L_{air}	Thickness of air layer

l_{tube}	Length of the tube
m	Mass
m'	Power attenuation coefficient
M	Parameter that relates ρ_m to ρ_0
N_{pr}	Prandtl number
P	Pressure
P_0	Static pressure in air
p_{max}	Maximum pressure
p_{min}	Minimum pressure
$P_i(x, f)$	Fourier Transform of the incident wave at microphone position x
$P_r(x, f)$	Fourier Transform of the reflected wave at microphone position x
$P1(x_1, f)$	Fourier Transform of the pressure measured at microphone position x_1
$P1(x_1, f)*$	Conjugate of $P1(x_1, f)$
$P2(x_2, f)$	Fourier Transform of the pressure measured at microphone position x_2
$P2(x_2, f)*$	Conjugate of $P2(x_2, f)$
P_T	Total pressure
P_i	Incident sound wave
P_r	Reflected sound wave
P_t	Transmitted sound wave
Q	Structural characteristic
q_0	Parameter that accounts for the motion of fibres
r	Radius
$\hat{r}$	Hydraulic radius
R	Reflection factor
R_g	Constant of a gas
RT_{60}	Reverberation time
s	Tortuosity
$\hat{s}$	Share wave number (pore shape)
s_a	Acoustic condensation
s_{pore}	Parameter accounting for the shape of the pores
S_{spec}	Area covered by the test specimen
t	Time
T	Absolute temperature
U	Steady flow velocity
$v(r)$	Velocity of an inviscid fluid within a pore
$v(r_w)$	Velocity of an inviscid fluid at the surface of pore walls
V	Volume
V_a	Volume of air in a porous material
V_b	Volume of solid in a porous material
V_g	Equivalent volume of one grain
w	Angular frequency
W_i	Incident sound energy
W_r	Reflected sound energy

W_t	Transmitted sound energy
$\hat{X}$	Dimensionless variable, empirical models
x_0	Reference plane
x_1	Position of microphone 1 in the impedance tube
x_2	Position of microphone 2 in the impedance tube
Z_a	Characteristic impedance
Z_a'	Real part of the characteristic impedance
Z_a''	Imaginary part of the characteristic impedance
Z_{a0}	Characteristic impedance of air
Z_s	Surface impedance
α	Absorption coefficient
$\bar{\alpha}$	Average absorption
α_∞	Tortuosity, equivalent to s, and k_s
γ	Adiabatic index
Γ_a	Propagation constant
Γ_a'	Real part of the propagation constant, Attenuation constant
Γ_a''	Imaginary part of the propagation constant, Phase velocity
δ_v	Viscous boundary layer
$\triangle\rho$	Density fluctuations
$\triangle p$	Pressure fluctuations
$\triangle P$	Pressure difference across the sample
η	Dynamic viscosity
θ_i	Angle of incident sound wave
θ_r	Angle of reflected sound wave
θ_t	Angle of transmitted sound wave
κ	Bulk modulus
κ_d	Dynamic bulk modulus
μ	Particle velocity
ξ	Parameter accounting for viscous losses
σ	Flow resistivity
σ_s	Flow resistance
ρ	Density
ρ_d	Dynamic density
ρ_0	Static density in air
ρ_T	Total density
ρ_m	Specific density of a material
ρ_s	Bulk density of a specimen
ϕ	Porosity
$\wedge$	Viscous characteristic length
$\wedge'$	Thermal characteristic length

Abbreviations

AC	Activated Carbon
$A\&C$	Allard & Champoux
$B\&I$	Berardi & Iannace
$D\&B$	Delany & Bazley
FT	Fourier Transform
$G\&P$	Garai & Pompoli
ISO	International Organization of Standardization
MCC	Microcrystalline Cellulose
MPP	Microperforated Panels

List of Figures

List of Tables

1 Introduction

In a world where people are looking for more and more comfort, the control of sound levels enclosures is indispensable to achieve a high level of satisfaction among users. It is not only comfort but many other aspects that can be benefited by an appropriate acoustic design. The ability of employees to concentrate in an office, the performance of students in a classroom, or the experiences of users in entertainment halls, such as cinemas or theatres. These are some examples of situations where a good acoustic design would make a difference. Sound levels within enclosures are controlled by the use of diffusers and sound absorbing materials. Diffusive elements scatter sound reflections as to achieve a more homogeneous sound field within a room, whereas sound absorptive materials dissipate sound energy and reduce sound reflections.

The development of sound absorbing materials has undergone intense study for over the last century. The advent of acoustic meta-materials, together with the development of biodegradable and sustainable products has intensified the interest in the subject. The aim of the developers is the design of sound absorbers that are environmental-friendly, non-hazardous for human beings, resistant to hostile environments (high temperatures or hits, among others), economical, aesthetic, and of reduced size. There are mainly four types of absorber, porous materials, membranes or panel absorbents, Helmholtz resonators, and meta-materials.

Porous materials are the most commonly used absorbers due to their ability to efficiently absorb sound at mid and high frequencies with relatively thin layers. They are seen as a network of interconnected pores through which sound waves may propagate. When sound waves propagating in air impact the surface of a porous material, part of the sound energy is dissipated due to the interactions between the solid structure of the porous media and the molecules of air disturbed by the sound waves. The main mechanisms causing this dissipation of energy are viscous, thermal and inertial effects.

However, when low frequencies are needed to be absorbed, very thick porous layers are needed. In general, this is an undesirable solution because the available space, or maximum weight is limited. This is the case, for example, of the light-weighting of vehicles. Making lighter vehicles is seen as the best approach to reduce the consumption of fuel and CO_2 emissions, as well as to achieve higher acceleration. However, the use of lighter and stiffer elements in the body of the vehicle causes higher noise levels. Low frequency sound absorbers are needed to reduce the noise levels produced by the engines. A solution based on the use of thick layers of porous materials would be conflicting with the light-weighting design of the vehicle. Therefore, alternatives to porous materials need to be developed.

Membranes, perforated and micro-perforated panels are the most common alternatives used to absorb sound at low frequencies. The three of them are resonant absorbers, and therefore, they are limited to attenuate sound energy over a certain frequency band. Perforated panels and membranes require a cavity of air behind them in order to achieve effective sound absorption. For membranes, sound absorption is determined by the mass of the panel, the air cavity thickness between the panel and the rigid wall, and the method of attachment.

The perforations of perforated panels act as Helmholtz resonators. These type of resonator is a mass-spring system, where the mass is the air contained in the opening of the perforation and the spring is the air contained in the cavity behind the perforated panel. The resonator can be tuned by adjusting the following parameters related to the perforated board: size of the holes, the total open area, and the thickness of the perforated panel and the air space between the perforated panel and the rigid wall. The effective frequency range of both, membranes and perforated panels, can be broadened by placing porous materials in the air cavity.

Micro-perforated panels (MPPs) absorb sound due to the sub-millimetre size of the perforations, which causes viscous losses as sound waves propagate through the holes. MPPs also need an air cavity between themselves and a rigid back in order to efficiently absorb sound (porous material behind the panel is not needed). Sound waves reflected from the rigid back causes a destructive interference with the incident sound within the holes. The destructive interference together with the viscous effects provides MPPs with effective sound absorption. The characteristic of the destructive interference can be improved by modifying the shape of the rigid back.

Meta-materials aim the design of low frequency absorbers by using a number of periodically distributed sub-wavelength Helmholtz resonators. The presence of the Helmholtz resonators cause strong dispersion which results in slow-sound propagation. The slow-sound propagation shifts the resonance of the Helmholtz resonators towards low frequencies, thus allowing for the design of very thin absorbers able to achieve perfect absorption at very low frequencies. Meta-materials are narrow-band absorbers in nature. However, researchers are devoting much work to the design of broadband meta-materials absorbers.

The objective of this thesis is to investigate the sound absorption of porous materials and analyse the laboratory measurement methods used to obtain the sound absorption coefficients. The thesis has been structured as follows. Section 2 introduces all the necessary theory for this topic. Section 3 presents the laboratory methods used for measurements of sound absorption coefficients. The main methods are the reverberation chamber method, defined in the standard *ISO-354*, and the impedance tube methods, defined in the standards *ISO 10534-1* and *ISO 10534-2*. Section 4 focuses on the characterization of porous materials. The macroscopic parameters of porous materials, as well as the effects of varying the physical properties of a porous layer are explained. The three main types of porous materials, fibrous, foams, and granular materials are discussed in detail. Section 5 reviews models developed to predict sound absorption of porous materials. Section 6 presents measurements of sound absorption coefficients of materials made of natural cellulose fibres and micro-crystalline cellulose spheres. The transfer-function impedance tube method was used to perform the measurements. The results are compared with some of the models introduced in section 5.

2 Theory

2.1 Wave equation for sound waves propagating in air

In the absence of sound, air particles are constantly moving in all directions, colliding with surrounding particles. This continuous movement of particles results in a balanced state of the medium characterized by a static air pressure (P_0), static density (ρ_0) and a null apparent total velocity of particles.

When a sound wave is introduced in a medium it disturbs the balance state of the medium, producing fluctuations in pressure, density and particle velocity. The total pressure in the medium, P_T, becomes:

$$P_T = P_0 + \triangle p \tag{1}$$

Where P_T is the total pressure, P_0 is the static pressure, and $\triangle p$ is the acoustic wave, pressure fluctuations with respect to the static pressure.

The wave equation can be derived by establishing a relationship between pressure, density and particle velocity variations in the disturbed medium. This relationship lies on the following three principles: equation of state of an ideal gas; equation of conservation of mass (also known as the continuity equation); and Newton's laws of motion.

Let us first derive the wave equation for plane waves propagating in air. Plane waves are a mathematical representation of waves in which all the acoustic quantities vary with time and with one Cartesian coordinate, generally x. In order to derive the wave equation let us consider sound waves propagating in air as an adiabatic process for all the audible frequencies. This assumption implies that pressure fluctuations do not cause heat exchange of a gas with the surrounding. This can be true only when pressure fluctuations happen so fast that there is no sufficient time for the heat to flow. It is shown later in this work that this assumption is not totally true, and the adiabatic process in sound propagation can be considered only at high frequencies, but not at low frequencies. Nevertheless, at this stage of this work sound propagation in air is considered as an adiabatic process at all frequencies. Under adiabatic conditions the state equation of an ideal gas is:

$$P_T V^\gamma = constant \tag{2}$$

where V is volume and γ is the adiabatic index (1.4 for air). The adiabatic index is calculated as the ratio between the specific heat at constant pressure and the specific heat at constant volume. Eq (2) leads to the following expression:

$$\frac{P_T}{P_0} = \left(\frac{\rho_T}{\rho_0}\right)^\gamma \tag{3}$$

where again the indexes T and 0 refers to total and static values, respectively. Eq. (3) can be expressed using the concept of acoustic condensation, s_a. The acoustic condensation describes changes in density caused by fluctuations in pressure.

$$\frac{P_T}{P_0} = \left(\frac{\rho_T - \rho_0 + \rho_0}{\rho_0}\right)^{\gamma} = (1 + s_a)^{\gamma} \tag{4}$$

and s_a is defined as:

$$s_a = \frac{\rho_T - \rho_0}{\rho_0} = \frac{\triangle\rho}{\rho_0} \tag{5}$$

P_T can be written as:

$$P_T = P_0\,(1 + s_a)^{\gamma} \tag{6}$$

Using Taylor series Eq. (6) can be expanded:

$$P_T = P_0\left[1 + \gamma s_a + \gamma\,(\gamma - 1)\,\frac{s_a^2}{2!} + ...\right] \tag{7}$$

The higher order terms can be neglected because at normal sound pressure levels they are very small. Elimination of the high order terms is not valid for very high sound levels such as those coming from explosions or air plane engines. At such sound pressure levels, these high order terms become significant, thus having a relevant influence on the total pressure. From Eq. (7), P_T can be expressed as:

$$P_T = P_0\,(1 + \gamma s_a) \;\longrightarrow\; P_T - P_0 = \triangle p = P_0 \gamma s_a \tag{8}$$

where $P_T - P_0$ is the acoustical pressure $\triangle p$. By using the definition of acoustic condensation, Eq. (8) can be expressed as follows:

$$\triangle p = \gamma P_0 \frac{\triangle\rho}{\rho_0} \tag{9}$$

where $\triangle\rho$ represents fluctuations in density. The term γP_0 is known as bulk modulus, denoted as κ. It is a characteristic property of a gas that determines how stiff the gas is. The inverse of the bulk modulus is the compressibility factor C, which describes how compressible a gas is. The ratio between fluctuation in pressure and density results in the speed of sound:

$$c = \sqrt{\frac{\kappa}{\rho_0}} = \sqrt{\frac{\gamma P_0}{\rho_0}} \tag{10}$$

Using the state equation of an ideal gas, Eq. (11), where T is absolute temperature in Kelvin units, and R_g is a constant related to the gas, it can be shown that speed of sound, c, depends on temperature:

$$\frac{P}{\rho} = R_g * T \tag{11}$$

$$c = \sqrt{\frac{\kappa}{\rho_0}} = \sqrt{\frac{\gamma P_0}{\rho_0}} = \sqrt{\frac{\gamma R_g T_0 \rho_0}{\rho_0}} = \sqrt{\gamma R_g T_0} \tag{12}$$

So far, the speed of sound has been computed by finding the relationship between fluctuations in density and pressure using the state equation of an ideal gas under adiabatic conditions. Next, the equation of continuity will be used to derive a relationship between density and particle velocity. Let's begin by assuming that a medium consists of multitude particles that are grouped in elemental volumes. Fig. 1 shows one of these elemental volumes contained in a cylindrical tube.

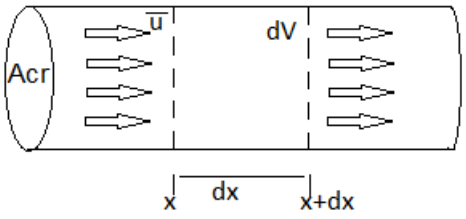

Figure 1: Sound waves propagating in a cylindrical tube.

The cross-sectional area of the tube is A_{cr}. The elemental volume has a length dx and a volume dV. When the medium is undisturbed, there is no sound, the volume of the elemental volume is:

$$dV = A_{cr}\ dx \tag{13}$$

Consider a flow μ entering the elemental volume at position x. The total mass entering the elemental volume during a time t is:

$$\rho(x)\mu(x)A_{cr}\ dt \tag{14}$$

Similarly, the total mass leaving the elemental volume at position $x + dx$ during a time t is:

$$\rho(x + dx)\mu(x + dx)A_{cr}\ dt \tag{15}$$

The net change in mass in the elemental volume within a distance dx and during a time t is then calculated by subtracting Eq. (15) from Eq. (14). This can be expressed in the form of Eq. (16):

$$-dx\ A_{cr}\frac{\partial(\rho\mu)}{\partial x}\ dt \tag{16}$$

By solving the partial derivative in Eq. (16) the following expression is obtained:

$$-\rho\ A_{cr}\frac{\partial(\mu)}{\partial x}\ dtdx + ...(Higher\ order\ terms) \tag{17}$$

Next, the net change in density in the elemental volume during a time t can be computed in a similar way:

$$dx\ A_{cr}\frac{\partial\rho}{\partial t}\ dt \tag{18}$$

By equating Eq. (17) and (18) and neglecting the high order terms from Eq. (17):

$$\frac{\partial \mu}{\partial x} = -\frac{1}{\rho_0}\frac{\partial \rho}{\partial t} \tag{19}$$

Eq. (19) can be expressed as a function of pressure and particle velocity by using Eq. (9):

$$\frac{\partial \mu}{\partial x} = -\frac{1}{\rho_0 c^2}\frac{\partial p}{\partial t} \tag{20}$$

Eq. (20) describes the relationship between spatial changes in particle velocity and temporal changes in pressure. The following step involves finding a relationship between temporal changes in particle velocity and spatial changes in pressure. This will be done based on Newton's laws of motion.

Going back to Fig. (1), when a sound wave penetrates the tube, the pressures at each side of the elemental volume become different. This pressure difference is a net pressure acting on the fluid. The net pressure multiplied by the area of the elemental volume becomes a net Force. By the second Newton's law, a net force applied on a mass causes an acceleration. Let's apply this reasoning to the elemental volume located inside the tube. The net force acting on the elemental volume is:

$$A_{cr}(p(x) - p(x + dx)) \tag{21}$$

Eq. (21) can be expressed as:

$$-A_{cr}\frac{\partial p}{\partial x}dx \tag{22}$$

The mass of the elemental volume and the acceleration are given by Eq. (23) and (24), respectively:

$$m = \rho_0 A_{cr} dx \tag{23}$$

$$a = \frac{\partial \mu}{\partial t} \tag{24}$$

Eq. (25) is then derived using the second law of Newton, $F = m\ a$:

$$-A\frac{\partial p}{\partial x}dx = \rho_0 A dx \frac{\partial \mu}{\partial t} \tag{25}$$

The last relationship is given by simplifying Eq. (25):

$$\frac{\partial p}{\partial x} = -\rho_0 \frac{\partial \mu}{\partial t} \tag{26}$$

The wave equation is calculated based on the three relationships given by Eq. (9), (20) and (26). It is obtained by equating the partial derivative of Eq. (20) with respect to t and the partial derivative of Eq. (26) with respect to x:

$$\frac{\partial^2 p}{\partial^2 t} = c^2 \frac{\partial^2 p}{\partial^2 x} \tag{27}$$

The solution for the wave equation can be expressed as two waves travelling in opposite directions:

$$p(x,t) = g_1(x - ct) + g_2(x + ct) \tag{28}$$

Where g_1 represents a wave travelling forward at a velocity c, and g_2 accounts for a wave travelling backwards at the same velocity c. Eq. (28) can be expressed in exponential form:

$$p(x,t) = \hat{p}e^{j(wt \mp k_0 x)} \tag{29}$$

where w is the angular frequency and k_0 is the wavenumber in air. They are defined in Eq. (30) and (31), respectively:

$$w = 2\pi f \tag{30}$$

$$k_0 = w\sqrt{\frac{\rho_0}{\kappa}} \tag{31}$$

Where ρ and κ are the density and bulk modulus of the fluid, in this case air.

For sound waves propagating in air, particle velocity μ is related to pressure through the characteristic impedance of air Z_{a0}. The characteristic impedance of air under standard conditions is approximately 400 MKS rayls.

$$\mu(x,t) = \frac{p(x,t)}{Z_{a0}} = \frac{p(x,t)}{\rho_0 c_0} \tag{32}$$

The concept of characteristic impedance is explained in more detail in section 2.5.

2.2 Sound propagation in porous materials

Sound waves penetrating a porous medium set air molecules within the pores to oscillate. The interaction between the gas and the frame causes sound energy losses by different mechanisms. The following lines describe the more general mechanisms of sound absorption within porous materials.

The first mechanism of sound energy dissipation due to the interaction between the gas and the frame is related to viscous losses. Viscous losses are caused by the generation of shear forces, also known as viscous stresses, that aim to equal the velocity of the two mediums by dissipating some of the fluid kinetic energy into heat. Viscous forces has the effect of increasing the effective density of the fluid travelling through the pores. Dissipation of sound energy due to viscous forces decreases with distance from the frame, and it is frequency dependent. Furthermore, viscous forces within the passages of porous materials depend on many other factors, including geometrical properties of the pores, dynamic viscosity of the gas, and the contact surface between the gas and the frame. The area within the path where viscous forces

efficiently dissipate sound energy is known as viscous boundary layer. The sound velocity within the viscous boundary layer is minimum at the surface of the rigid frame, where the effect of viscous forces is maximum. The speed of the fluid increases with distance from the surface and reaches its maximum outside the boundary layer. The dimensions of the viscous boundary layer relative to the pore size is greater at lower frequencies than at higher frequencies. Consequently, sound energy dissipation due to viscous stresses is more significant at lower frequencies [1].

A second mechanism for sound energy losses is explained by the energy exchange between molecules of the fluid and the frame to achieve thermal equilibrium between the two mediums [1]. Molecules from the fluid are temporally stuck in the solid surface. During this time there is an energy exchange that aims thermal equilibrium between the fluid and the solid. After the exchange of energy, molecules are released with a modification in the magnitude of their particle velocity.

Analogously to the viscous boundary layer, the area within the passages where molecules from the fluid and frame exchange thermal energy to achieve thermal equilibrium is known as thermal boundary layer. The thickness of the boundary layer depends on the thermal properties of the gas and material the frame is made of, as well as on frequency. At low frequencies the thermal boundary layer is of the same dimensions than the radius of the pores, whereas at high frequencies the boundary layer is very small, thus having insignificant effect on energy losses. The thermal boundary layer has an influence on the bulk modulus of the gas. At low frequencies κ approaches its isothermal value (P_0), whereas at high frequencies it goes to its adiabatic value (γP_0). At intermediate frequencies κ becomes complex.

Another mechanism for energy losses can be explained by the exchange of momentum between molecules of the fluid [1]. When fluid molecules impact the frame, a process of energy exchange between molecules of the frame and fluid is initiated. When this process is finished, the fluid molecules are released from the frame to the fluid in opposite direction, thus reducing the velocity of the fluid molecules that have not impacted the surface. In this case energy losses are mainly dependent on the geometry of the frame.

Energy losses can also be found in the skeleton of porous materials. However, these losses are believed to be of minor importance [2]. In most cases, porous materials are placed against rigid elements. Under these conditions the elastic properties of porous materials are constrained, and consequently the frame of the porous materials can be assumed to be rigid.

Slowing down the speed of sound is another approach that can be used to enhance sound absorption at lower frequencies. The speed of sound in typical porous materials has been reported to be of the same order than the speed of sound in the air [23]. Furthermore, at high frequencies, the speed of sound waves travelling within porous materials tend to equal the speed of air, where the effects of the viscous and thermal boundary layers can be neglected (see subsection 4.1.1). Reducing the speed of sound is of special interest because it results in a shifting of the first maximum absorption peak towards lower frequencies. As a result, thinner materials are needed to efficiently absorb sound energy at lower frequencies.

Summarizing, at low frequencies, viscous-thermal losses dominate. At high

frequencies, the inertial effects dominate and the viscous and thermal boundary layers are so small that their effect on sound absorption is insignificant. Viscous and inertial forces influence the dynamic density of the air within the porous material. While the presence of the thermal boundary layer affects the dynamic bulk modulus of the gas. Its value varies from the isothermal value at low frequencies to the adiabatic value at high frequencies. Additionally, slowing down the speed of sound results in more efficient sound absorption at low frequencies, which allows the use of thinner materials.

2.3 Modified wave equation for sound waves propagating in porous media

In this section the wave equation is derived for sound waves that travel in porous materials. This is accomplished by modifying the conservation equations used in the previous section to take into account the effects caused by porosity, flow resistivity and tortuosity [1]. These macroscopic physical characteristics of porous materials are described in section 4.1.1.

In first place the equation of conservation of mass calculated for sound propagation in air, Eq. (20), is modified to take into account the material porosity, ϕ, as to account for the volume occupied by the solid phase. Furthermore, the modified conservation of mass equation must consider the deviations of the bulk modulus, κ, going from its isothermal value at low frequencies, ($\kappa = P_0$), to the adiabatic value at high frequencies ($\kappa = \gamma P_0$).

$$\frac{\rho_0}{\kappa}\frac{\partial p}{\partial t} = -\frac{\rho_0}{\phi}\frac{\partial \mu}{\partial x} \tag{33}$$

Secondly, Eq. (26) is modified to account for the porosity, ϕ, flow resistivity, σ, and tortuosity, s, of the material. Changes are based on the second law of Newton, $F = m \cdot a$

$$\frac{\partial p}{\partial x} = -(\frac{s\rho_0}{\phi})\frac{\partial \mu}{\partial t} - \sigma\mu \tag{34}$$

Lastly, the modified wave equation can be derived by differentiating Eq. (33) and (34) with respect to time (t) and position (x) and equating the two equations:

$$\frac{\partial^2 p}{\partial^2 x} - \frac{s\rho_0}{\kappa}\frac{\partial^2 p}{\partial^2 t} - \frac{\sigma\phi}{\kappa}\frac{\partial p}{\partial t} = 0 \tag{35}$$

The effect of the three parameters porosity, flow resistivity and tortuosity in the modified wave equation is to attenuate sound waves and change the speed of sound as waves propagate within porous materials.

2.4 Attenuation

A plane wave propagating forward in the x axis can be defined as:

$$p(x,t) = \hat{p}e^{j(wt-kx)} \tag{36}$$

In a medium where attenuation effects are insignificant, the bulk modulus and density of the medium can be regarded as values only having real components. Real bulk modulus and density lead to real wave number and characteristic impedance (section 2.5 describes the concept of characteristic impedance). In air, for instance, where sound energy losses are generally neglected, the wave number and characteristic impedance have only real component.

In a medium where dissipation effects cannot be neglected, the density and bulk modulus of the medium become complex, and consequently the wave number and characteristic impedance of the medium are replaced by complex quantities as well, $k = k' + jk''$ and $Z_a = Z'_a + jZ''_a$ [3]. Where k'' is known as the attenuation constant and represents the energy losses within the medium, and k' is related to the speed of sound propagating through the media. A plane wave propagating in an attenuating medium is expressed as follows:

$$p(x,t) = \hat{p}e^{-jk''x}e^{j(k'x-wt)} \tag{37}$$

From Eq. (37) it can be seen that the amplitude of a sound wave propagating in a medium with $k'' \neq 0$ is driven to 0 when $x \longrightarrow \infty$.

2.5 Acoustic characteristics of porous materials

Acoustic characteristics of porous materials refer to characteristic impedance Z_a [Pa*s/m] and propagation constant Γ_a [1/m]. The latter is directly related to the complex wave number (see Eq. (38)). These two parameters are complex values of a medium where sound energy is dissipated as sound waves propagate. The acoustic characteristics together with the sound absorption coefficient completely characterize the sound absorption properties of porous materials [4]. The calculation of these parameters assumes that porous materials are of infinite thickness.

$$Z_a = jk = Z'_a + jZ''_a \tag{38}$$

$$\Gamma_a = \Gamma'_a + j\Gamma''_a \tag{39}$$

The propagation constant is given by the complex wave number as $\Gamma_a = jk$. The real part of the propagation constant Γ'_a represents the attenuation taking place within the porous material (it corresponds to the imaginary part of the complex wave number), while the imaginary part Γ''_a is related to the speed of sound propagating through the media (real part of the complex wave number). The characteristic impedance refers to the ratio between pressure and particle velocity at any point of the porous material.

Many models have been proposed to predict sound absorption propagation in porous media. These models use microscopic characteristics of the materials to calculate their propagation constant and acoustic characteristic. Some models, in particular semi-phenomenological models (see section 5.2.2), calculate Z_a and Γ_a by first calculating the dynamic bulk modulus and density of the gas interacting with the solid, and then computing Z_a and Γ_a as follows:

$$\Gamma_a = j2\pi f\sqrt{\frac{\rho_d}{\kappa_d}} = \Gamma'_a + j\Gamma''_a \tag{40}$$

$$Z_a(w) = \frac{p(x,t)}{\mu(x,t)} = \sqrt{\rho_d \kappa_d} = Z'_a + jZ''_a \tag{41}$$

On the other hand, empirical models provide expression for Z_a and Γ_a that are calculated directly by applying regression models to a large number of measurements taken on the materials. A more in-detail description of different models for sound propagation in porous materials can be found in chapter 5.

Acoustic characteristics can also be obtained via measurements based on the method introduced by Utsumo *et al.* in [5]. The method relies on the use of an impedance tube. The surface impedance (this concept is introduced in section 2.6) of a sample is computed having two different air layers behind the sample. Let us consider Z_{s1} to be the surface impedance of a sample of thickness L with an air gap of thickness L_{air1}, and $\hat{Z}_{s1}$ the surface impedance of the same sample with a second air gap of thickness L_{air2}. Z_{s2} and $\hat{Z}_{s2}$ are the surface impedances of the air layer 1 and 2, respectively. The characteristic impedance and propagation constant are then calculated using the following expressions:

$$Z_a = \pm\sqrt{\frac{Z_{s1}\hat{Z}_{s1}(Z_{s2}-\hat{Z}_{s2}) - Z_{s2}\hat{Z}_{s2}(Z_{s1}-\hat{Z}_{s1})}{(Z_{s2}-\hat{Z}_{s2}) - (Z_{s1}-\hat{Z}_{s1})}} \tag{42}$$

$$\Gamma_a = \frac{1}{2jL}\ln\left(\frac{Z_{s1}+Z_a}{Z_{s1}-Z_a}\frac{Z_{s2}+Z_a}{Z_{s2}-Z_a}\right) \tag{43}$$

where Z_{s2} and $\hat{Z}_{s2}$ are given by Eq. (44) and (45):

$$Z_{s2} = -jZ_{a0}cot(k_0 L_{air1}) \tag{44}$$

$$\hat{Z}_{s2} = -jZ_{a0}cot(k_0 L_{air2}) \tag{45}$$

Z_{a0} and k_0 are the characteristic impedance and wave number in air.

2.6 Surface impedance

Real sound absorbing materials have finite thickness. As mentioned above, the acoustic characteristics Z_a and Γ_a assume that materials are infinitely thick. Therefore, a new parameter must be added that takes into account the thickness of the material and the medium located behind the material. This parameter is called surface impedance, and in this work it is denoted by Z_s.

2.7 Sound absorption coefficient

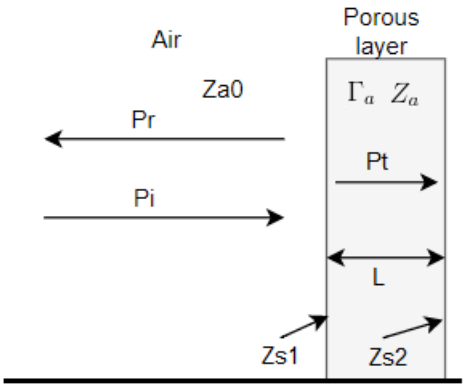

Figure 2: Plane waves propagating perpendicularly to a surface.

Generally, when a sound impacts a surface part of its energy is reflected, part is absorbed by the surface and converted into heat, and part is transmitted to the other side of the surface as shown in Fig.2. The sound absorption coefficient is defined as the ratio of absorbed to incident sound energy:

$$\alpha = \frac{W_i - W_r}{W_i} \tag{46}$$

The value of the sound absorption coefficient ranges within 0 and 1. Surfaces that poorly absorb sound have a α value close to 0, $W_r \leq W_i$, whereas efficiently absorbing porous materials have a α value close to 1, $W_r \ll W_i$. Absorption coefficient is frequency dependent, and in general, it increases at higher frequencies for porous materials.

2.7.1 Sound absorption for normal incident plane waves

Assuming plane waves propagating perpendicularly to a surface as shown in Fig. 2, the sound absorption coefficient values can be calculated as follows [6]. Incident sound pressure and particle velocity can be expressed as:

$$p_i(x,t) = \hat{p_i} e^{j(wt - k_0 x)} \tag{47}$$

$$\vec{\mu_i}(x,t) = \frac{\hat{p_i}}{Z_{a0}} e^{j(wt - k_0 x)} \tag{48}$$

The pressure and particle velocity of the reflective wave are:

$$p_r(x,t) = \hat{p_r} e^{j(wt + k_0 x)} \tag{49}$$

$$\vec{\mu_r}(x,t) = \frac{\hat{p_r}}{Z_{a0}} e^{j(wt + k_0 x)} \tag{50}$$

and the p and μ of the transmitted wave are

$$p_t(x,t) = \hat{p}_t e^{j(wt-k_1 x)} \tag{51}$$

$$\vec{\mu_t}(x,t) = \frac{\hat{p}_t}{Z_{a1}} e^{j(wt-k_1 x)} \tag{52}$$

where Z_{a0} and Z_{a1}, as well as k_0 and k_1 correspond to the characteristic impedance and complex wave number of air and the absorbing material, respectively. In the boundary between medium 1 and 2 the following boundary conditions must be met:

$$p_i(x=0,t) - p_r(x=0,t) = p_t(x=0,t) \tag{53}$$

$$\vec{\mu_i}(x=0,t) - \vec{\mu_r}(x=0,t) = \vec{\mu_t}(x=0,t) \tag{54}$$

By substituting Eq. (47), (49), and (51) in Eq. (53)

$$\hat{p}_i - \hat{p}_r = \hat{p}_t \tag{55}$$

and similarly, by substituting Eq. (48), (50), and (52) in Eq. (54)

$$\frac{\hat{p}_i}{Z_{a0}} - \frac{\hat{p}_r}{Z_{a0}} = \frac{\hat{p}_t}{Z_{a1}} \tag{56}$$

Now, the reflection coefficient R, defined as the ratio of reflected and incident pressures at the surface of the porous layer, can be obtained by using Eq. (55) to eliminate $\hat{p}_t$ in Eq. (56)

$$\frac{\hat{p}_r}{\hat{p}_i} = \frac{Z_{a1} - Z_{a0}}{Z_{a1} + Z_{a0}} = R \tag{57}$$

From the definition of absorption coefficient given in Eq. (46), and considering that sound energy is directly related to sound intensity, I, which in turn depends on pressure and particle velocity $I = p\vec{\mu} = p^2/Z_a$, the following expression can be derived

$$\alpha = 1 - \frac{W_r}{W_i} = 1 - \frac{I_{x,r}}{I_{x,i}} = 1 - \left(\frac{\hat{p}_r}{\hat{p}_i}\right)^2 = 1 - \mid R \mid^2 = 1 - \left|\frac{Z_{a1} - Z_{a0}}{Z_{a1} + Z_{a0}}\right|^2 \tag{58}$$

Eq. (58) has been obtained by assuming that the material has infinite thickness. In such case there are no reflections coming from the back surface of the material. This situation, however, is not real. Sound absorbing materials are of finite length and in most cases they are placed in front of other surfaces, which would cause reflections or sound energy going from the back surface to the front surface of the absorbing material. In these situations the concept of surface impedance is used (see section 2.6). Eq. (58) can be modified to take into account the thickness of the material by substituting the characteristic impedance term, Z_{a1}, by its corresponding surface impedance Z_{s1}:

$$\alpha = 1 - \left|\frac{Z_{s1} - Z_{a0}}{Z_{s1} + Z_{a0}}\right|^2 \tag{59}$$

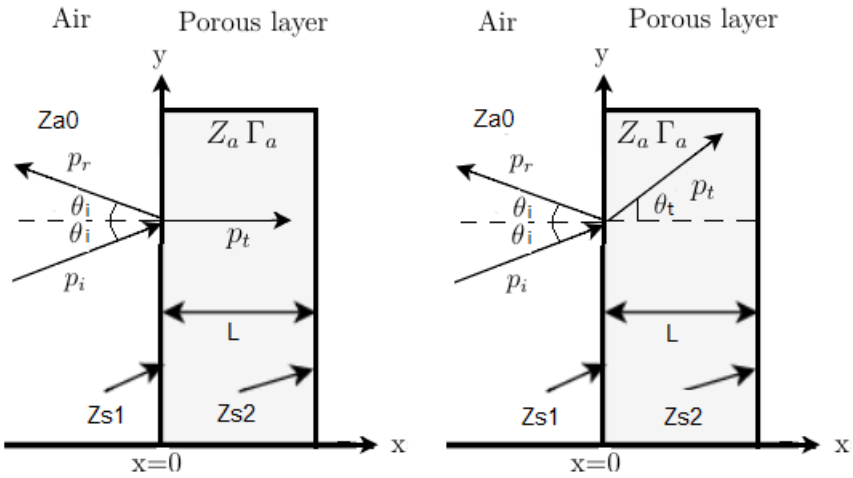

Figure 3: Transmission of sound into local and bulk reacting materials, on the left and right, respectively.

2.7.2 Sound absorption for oblique incident plane waves

For plane sound waves arriving a surface at oblique angle, sound absorption depends on the angle of incidence and transmission. Two cases may be distinguished in the analysis of sound absorption for oblique incident plane waves [6]. The first case involves *locally reacting materials*, which are defined as materials in which sound waves propagate only perpendicularly to the boundary (this is the general case considered for porous materials). The second case involves *bulk reacting materials*. In these materials, sound waves propagate perpendicularly and in parallel to the boundary. As a consequence, sound energy at any point within the material depends on the sound wave impacting that point and other sound waves propagating within the material. In bulk reacting materials, the angle of the transmitted wave is determined by the Snell's law (shown in Eq. (60)). The concepts of local and bulk reacting materials are depicted in Fig. 3.

$$\frac{c_1}{sin\theta_i} = \frac{c_2}{cos\theta_t} \tag{60}$$

The reflection factor for oblique incident plane waves is calculated as follows [1]. Let's assume p_1 be the total pressure at the boundary between the mediums 1 and 2:

$$p_1(x,y,t) = p_i(x,y,t) + p_r(x,y,t) = e^{-j(wt+k_{0,y}y)}(\hat{p_i}e^{-jk_{0,x}x} + \hat{p_r}e^{jk_{0,x}x}) \tag{61}$$

where $k_{0,x}x$ and $k_{0,y}y$ are the components x and y of the wave number (see Fig. 4).

$$k_{0,x}x = k_0 cos\theta, \qquad k_{0,y}y = k_0 sin\theta \tag{62}$$

The particle velocity at the boundary is then given by Eq. (63):

$$\vec{\mu_1}(x,y,t) = cos\theta_i \frac{1}{Z_{a0}} e^{-j(wt-k_{0,y}y)}(\hat{p_i}e^{-jk_{0,x}x} + \hat{p_r}e^{jk_{0,x}x}) \tag{63}$$

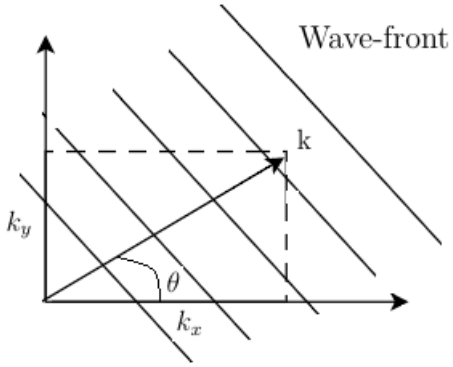

Figure 4: Plane wave front in two dimensions, adapted from [1].

The boundary conditions given in Eq. (53) and (54) are fulfilled if:

$$\frac{cos\theta_i}{Z_{a0}} e^{-j(wt-k_{0,y}y)}(\hat{p_i}e^{-jk_{0,x}x} + \hat{p_r}e^{jk_{0,x}x}) = \frac{cos\theta_t}{Z_{a1}} e^{-j(wt-k_{0,y}y)}(\hat{p_i}e^{-jk_{0,x}x} + \hat{p_r}e^{jk_{0,x}x}) \tag{64}$$

An expression for the reflection factor can be derived from Eq. (64):

$$R = \frac{Z_{a1}cos\theta_i - Z_{a0}cos\theta_t}{Z_{a1}cos\theta_i + Z_{a0}cos\theta_t} \tag{65}$$

Finally, the absorption coefficient is calculated by Eq. (66). This equation is valid for both, local and bulk reacting materials.

$$\alpha_{oblique} = 1 - \mid R \mid^2 = 1 - \left| \frac{Z_{a1}cos\theta_i - Z_{a0}}{Z_{a1}cos\theta_i + Z_{a0}} \right| \tag{66}$$

Before going forward, let us introduce the concept of sound absorption modelling of multilayer structures.

2.7.3 Sound absorption modelling of multilayer structures

A generalized expression for modelling sound absorption of multilayer structures is given in [6]. This expression is based on the transfer matrix method. It aims to calculate the surface impedance of the whole structure ($Z_{s,1}$) by recursively calculating the surface impedance of each layer ($Z_{s,i}$, $Z_{s,i+1}$,...,$Z_{s,N}$, where N corresponds to the sub-index of the farthest layer from the sound source). Fig. 5 is an instructive image of a multilayer structure comprised of air, porous layers, and a rigid surface or layer of air at the back.

The expression used to calculate the surface impedance of each layer is given in Eq. (67), where $Z_{s,i}$ refers to the surface impedance to be calculated, and $Z_{s,i+1}$ corresponds to the surface impedance of the layer behind. The parameters Z_{ai}, Γ_{ai}, and L_i are the acoustic characteristics and thickness of the layer i:

$$Z_{s,i} = Z_{a,i} \frac{Z_{s,i+1}coth(\Gamma_{a,i}L_i) + Z_{a,i}}{Z_{s,i+1} + Z_{a,i}coth(\Gamma_{a,i}L_i)} \tag{67}$$

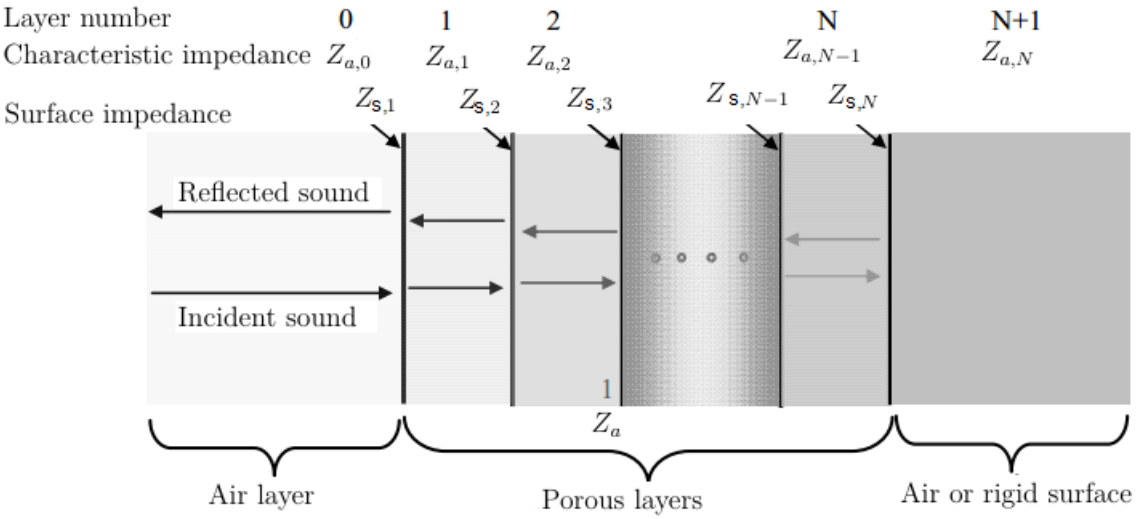

Figure 5: Multilayer structure. Adapted from [6].

In general, the last layer (denoted by N), the farthest away from the sound source, is air or a rigid surface. Their surface impedance are considered to be known. For a rigid wall, the real and imaginary parts of the surface impedance are infinite. For a layer of air, the surface impedance is equal to the characteristic impedance of air. That is, imaginary part equal to zero, and real part equal to 443 kg/m^2s.

Let us consider the layer of porous material of thickness L shown in Fig. 2. Assuming that the impedance Z_{s2} as well as the characteristic impedance (Z_a) and propagation constant (Γ_a) of the porous layer are known, the surface impedance Z_{s1} can be calculated by using the expression given in Eq. (67):

$$Z_{s1} = Z_a \frac{Z_{s2} coth(\Gamma_a L) + Z_a}{Z_{s2} + Z_a coth(\Gamma_a L)} \tag{68}$$

Assuming that the last layer is air, Eq. (68) becomes:

$$Z_{s1} = Z_a \frac{Z_{a0} coth(\Gamma_a L) + Z_a}{Z_{a0} + Z_a coth(\Gamma_a L)} \tag{69}$$

Once the surface impedance Z_{s1} has been calculated, the absorption coefficient can be computed using Eq. (59) or (66), for normal or oblique incident sound.

Let us now consider the case where instead of a layer of air, a rigid wall is located behind the porous layer shown in Fig. 2. A rigid wall can be assumed to reflect all the incident sound, and therefore its surface impedance Z_s tends to ∞. Under these conditions Eq. (67) becomes:

$$Z_{s1} = Z_a coth(\Gamma_a L) \tag{70}$$

Now, let us assume a more complex case where a layer of air is located between a porous layer and a rigid wall, this is shown in Fig. 6. Again, the impedance of the rigid wall is ∞. By using Eq. (67) the surface impedance Z_{s2} becomes:

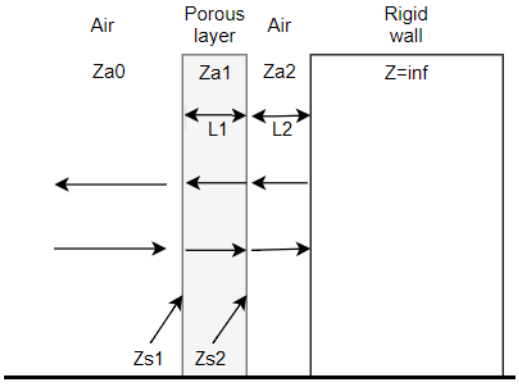

Figure 6: Sound absorption of a porous layer of thickness L with an air layer between the porous layer and a rigid wall.

$$Z_{s2} = Z_{a0} coth(\Gamma_0 L_2) \tag{71}$$

Where Γ_0 is the propagation constant of air ($\Gamma_0 = jk_0$). The surface impedance Z_{s1} is also calculated using Eq. (67), and the sound absorption coefficient is then given by Eq. (59).

$$Z_{s1} = Z_{a,1} \frac{Z_{s2} coth(\Gamma_{a,1} L_1) + Z_{a,1}}{Z_{s2} + Z_{a,1} coth(\Gamma_{a,1} L1)} \tag{72}$$

So far, theoretical expressions needed to calculate the sound absorption coefficient of materials have been presented. These expressions require the characteristic impedance and propagation constant of the material under study. These parameters can be calculated using models devised for sound propagation in porous materials. Some of these models are presented in chapter 5.

3 Methods for measuring sound absorption

Various methods have been devised to compute the absorption coefficient of sound absorbing materials. Among these methods, the two most used are *Measurements of sound absorption in a reverberation room* [7], defined in *ISO 354:2003*, and *Determination of sound absorption coefficients and impedance in impedance tubes - Part 2: Transfer-function method* [9], defined in *ISO 10534-2:1998*. There is one more impedance tube method that is defined in *ISO 10534-1:1996* and it is known as *Determination of sound absorption coefficients and impedance in impedance tubes - Part 1: Standing wave ratio method* [8]. None of them is an in-situ measurement technique.

The main difference between the impedance tube and the reverberation chamber method is that the reverberation chamber technique determines absorption coefficient values for diffuse field (sound coming from all directions), whereas the impedance tube techniques are limited to the calculation of the coefficient values for normal sound incidence. The impedance tube methods are generally used for the development and research of sound absorbing materials. These methods require much smaller samples than the reverberation chamber method, thus allowing for much faster preparation of samples, measuring and optimization of materials. Furthermore, among the impedance tube techniques, the transfer-function method is generally used because it is much faster than the standing wave ratio method. On the other hand, more realistic results are obtained by the reverberation chamber technique, as it considers sound arriving from all directions.

In the following sections the impedance tube and the reverberation chamber methods are described and analysed.

3.1 Impedance tube methods

The impedance tube methods require the use of an impedance tube with a loudspeaker at one end and a sample holder at the other end. The sample under study is placed in the sample holder. The sample must tightly fit the tube. However, too much tightness may be problematic and causes errors in the measurement. The methods rely on the fact that only normal incident and reflected plane waves propagate along the tube. Sound pressure is measured at two positions within the tube. The measurement technique aims to derive the absorption coefficient by finding a relation between the incident plane wave and the plane wave reflected from the sample. The following subsections describe in detail the standing wave and the transfer function methods.

3.1.1 Impedance tube standing wave ratio method

The loudspeaker located at one end of the tube generates a tone that propagates as a plane wave towards the specimen located at the other end of the tube. The superposition between the incident plane wave and the plane wave reflected from the specimen produces a standing wave in the tube. The absorption coefficient is determined by measuring sound pressure at points of maximum and minimum

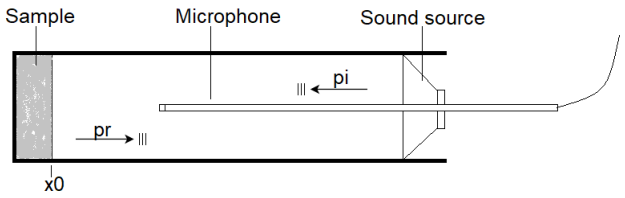

Figure 7: Set-up for the impedance tube standing wave ratio method.

pressure in the standing wave, p_{max} and p_{min}, respectively [8]. These pressures are measured using a moveable microphone. The set-up for this method is shown in Fig. 7. In order to avoid sound energy losses due to absorption caused by the walls of the tube, it is recommended to measure the first minimum pressure and the next maximum found when the microphone probe is moved from the surface of the sample to the sound source. The mathematics involved in this procedure are explained in the following equations.

The incident and reflected sound plane waves, p_i and p_r, are defined as:

$$p_i = A_0 e^{jk_0 x} \qquad p_r = R \cdot A_0 e^{-jk_0 x} \tag{73}$$

where k_0 is the wave number in air, A_0 is the complex amplitude, and R is the reflection factor. The reference position $x_0 = 0$ is assumed at the front surface of the specimen (in case the surface of the sample was not smooth, the reference position is place at some distance from the surface of the specimen). At a point of maximum pressure p_i and p_r are in phase, and $\mid p_{max} \mid$ is given by:

$$\mid p_{max} \mid = \mid A_0 e^{jk_0 x} \mid + \mid R \cdot A_0 e^{-jk_0 x} \mid = \mid A_0 \mid \cdot (1 + \mid R \mid) \tag{74}$$

$\mid p_{min} \mid$ occurs when p_i and p_r are in opposite phase:

$$\mid p_{min} \mid = \mid A_0 e^{jk_0 x} \mid - \mid R \cdot A_0 e^{-jk_0 x} \mid = \mid A_0 \mid \cdot (1 - \mid R \mid) \tag{75}$$

The ratio between pressure maxima and minima is then given by Eq. (76):

$$\frac{p_{max}}{p_{min}} = \frac{1 + \mid R \mid}{1 - \mid R \mid} \tag{76}$$

And the reflection factor can be solved from Eq. (76):

$$\mid R \mid = \frac{\frac{p_{max}}{p_{min}} - 1}{\frac{p_{max}}{p_{min}} + 1} \tag{77}$$

Once the reflection factor has been obtained, the absorption coefficient value at the frequency of the tone emitted by the loudspeaker can be calculated using Eq. (58), $\alpha = 1 - \mid R \mid^2$.

The fact that this method computes sound absorption for one frequency at a time makes it very slow. Nevertheless, this method does not require calibration since a single moveable microphone is used to measured maximum and minimum pressures in the standing wave.

The valid frequency range is defined by the tube diameter, d_{tube}, and the length of the tube, l_{tube} [8]. The tube diameter is the lowest dimension of the tube, and therefore it causes the first mode to interfere with the sound field of plane waves, thus determining the upper frequency limit, f_u. On the other hand, the frequency limit at low frequencies, f_l, is determined by the length of the tube. In order for the sound field of plane waves to become stable the length of the tube must be at least three tube diameters long:

$$f_u = 0.58\frac{c_0}{d_{tube}} \tag{78}$$

$$l_{tube} = \frac{250}{f_l} + 3d_{tube} \tag{79}$$

The working frequency range defined in Eqs. (78) and (79) corresponds to circular impedance tubes. For rectangular impedance tubes the reader is directed to [8].

3.1.2 Impedance tube transfer function method

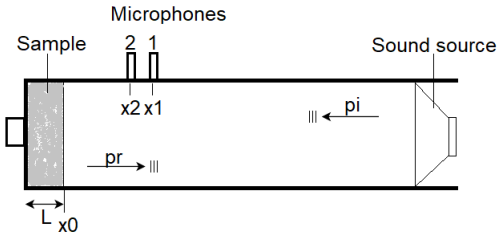

Figure 8: Set-up for the impedance tube transfer-function method.

The transfer function technique is considerably more efficient than the standing wave ratio method. It computes the absorption coefficient of a broad frequency range by doing one single measurement. The spectrum of the input signal should cover the frequency range of interest. It has been shown by Farina [10] that using deterministic signals, such as a sweep, provides better results due to an increase in the signal to noise ratio. However, this involves the computation of the impulse responses of the measured pressures. It is noted here that according to the standard, the measured pressures has to be at least 10 dB higher than the background noise at all frequencies of interest.

This method is based on the measurement of sound pressure at two locations in the tube. The complex transfer function between the two measured pressures is computed using a multi-channel spectrum analyser. The computed transfer function is used to calculate the reflection factor. Once the reflection factor has been obtained the absorption coefficient and surface impedance can be calculated. The mathematics involved in this procedure are explained in the following lines.

The Fourier Transform (FT) of the sound pressure measured at the two points x_1 and x_2 in the impedance tube are:

$$P_1(x_1, f) = P_i(x_1, f) + P_r(x_1, f) = A_0(f)e^{jk_0x_1} + R(f) \cdot A_0(f)e^{-jk_0x_1} \tag{80}$$

$$P_2(x_2, f) = P_i(x_2, f) + P_r(x_2, f) = A_0(f)e^{jk_0x_2} + R(f) \cdot A_0(f)e^{-jk_0x_2} \tag{81}$$

where $P_i(x_1, f)$ and $P_i(x_2, f)$, and $P_r(x_1, f)$ and $P_r(x_2, f)$ are the Fourier Transforms of the incident and reflective pressures at microphone positions $x1$ and $x2$. A_0 and R are the complex amplitude and reflection factor. The transfer functions for the incident and reflected waves are given by $H_i(f)$ and $H_r(f)$:

$$H_i(f) = \frac{P_i(x_2, f)}{P_i(x_1, f)} = \frac{A_0(f)e^{jk_0x_2}}{A_0(f)e^{jk_0x_1}} = e^{-jk_0(x_1-x_2)} \tag{82}$$

$$H_r(f) = \frac{P_r(x_2, f)}{P_r(x_1, f)} = \frac{A_0(f)e^{-jk_0x_2}}{A_0(f)e^{-jk_0x_1}} = e^{jk_0(x_1-x_2)} \tag{83}$$

The transfer function for the total sound field, $H_{12}(f)$, is given by the ratio between $P_2(x_2, f)$ and $P_1(x_1, f)$ defined in Eq. (81) and (80), respectively:

$$H_{12}(f) = \frac{P_2(x_2, f)}{P_1(x_1, f)} = \frac{e^{jk_0x_2} + R(f) \cdot e^{-jk_0x_2}}{e^{jk_0x_1} + R(f) \cdot e^{-jk_0x_1}} \tag{84}$$

The reflection factor can be solved from Eq. (84). The absorption coefficient is then calculated as $\alpha = 1 - \mid R \mid^2$.

$$R(f) = \frac{H_{12}(f) - H_i(f)}{H_r(f) - H_{12}(f)} e^{2jk_0x_1} \tag{85}$$

The surface impedance of the material is then calculated as:

$$Z_s = Z_{a0}\frac{1 + R(f)}{1 - R(f)} \tag{86}$$

Measurements of the pressures p_1 and p_2 may be performed by employing two microphones, one for each measurement location, or by using only one microphone that measures the pressure at the two locations. The former is more appropriate when faster measurements are desired. However, since two different microphones are used, a calibration factor must be calculated to eliminate the phase mismatch between the microphones. The standard provides two methods to eliminate the phase mismatch of the microphones. The first method is based on the repetition of measurements with the microphones interchanged. This method requires more time for each measurement, which is not convenient when many samples are to be measured. The second method calculates a predetermined calibration factor (H_c) that is directly applied to the transfer functions calculated for each measurement:

$$H_{12,cal} = \frac{H_{12}}{H_c} \tag{87}$$

The calibration factor H_c is calculated as follows:

$$H_c = \sqrt{\frac{H_{12,A}}{H_{12,B}}} \tag{88}$$

where $H_{12,A}$ is the transfer function H_{12} obtained with the microphones located in the standard configuration (configuration used in measurements), and $H_{12,B}$ is the transfer function obtained with the microphones placed in interchanged positions. The calculation of the calibration transfer functions requires the use of a test sample that is able to considerably reduce reflections in the tube. However, the calibration process is specially important when measuring very reflective specimens.

The standard defines three methods for the calculation of the complex transfer function $H_{12}(f)$. Expression for the three methods are shown below. These three methods can be also used for the calculation of the calibration factor H_c.

The first method is used under normal conditions. It uses the ratio of the cross-spectrum between the FT of the pressures measured at each location to the auto-spectrum of the FT of the sound pressure measured at location 1:

$$H_{12}(f) = \frac{P_2(x_2, f) \cdot P_1(x_1, f)^\star}{P_1(x_1, f) \cdot P_1(x_1, f)^\star} \tag{89}$$

The second method can be used to reduce the influence of input noise on the measurement. It computes H_{12} as the ratio of the auto-spectrum between the FT of the sound pressure measured at location 2 to the cross-spectrum between the FT of the pressures measured at each location:

$$H_{12}(f) = \frac{P_2(x_2, f) \cdot P_2(x_2, f)^\star}{P_1(x_1, f) \cdot P_2(x_2, f)^\star} \tag{90}$$

The last method calculates H_{12} using the expression given in Eq. (91). This method is recommended when noise at input and output are of concern.

$$H_{12}(f) = \sqrt{\frac{P_2(x_2, f) \cdot P_1(x_1, f)^\star}{P_1(x_1, f) \cdot P_1(x_1, f)^\star} \frac{P_2(x_2, f) \cdot P_2(x_2, f)^\star}{P_1(x_1, f) \cdot P_2(x_2, f)^\star}} \tag{91}$$

It is noted here that the use of expression (91) given in the standard *ISO 10534-2* to calculate H_{12} caused errors in the measurements. The problem was solved by using a modified expression that was mathematically equivalent. The modified expression is given in Eq. (92). Fig. 9 shows the results obtained using the two expressions.

$$H_{12}(f) = \sqrt{\frac{P_2(x_2, f) \cdot P_1(x_1, f)^\star}{P_1(x_1, f) \cdot P_1(x_1, f)^\star}} \sqrt{\frac{P_2(x_2, f) \cdot P_2(x_2, f)^\star}{P_1(x_1, f) \cdot P_2(x_2, f)^\star}} \tag{92}$$

The three methods are compared in Fig 10. There is not appreciable difference in the results, which indicates that there was not significant input or output noise in the measurements. It is noted here that the use of auto- and cross-spectrum functions for the calculation of the transfer function H_{12} is convenient because it increases the signal to noise ratio.

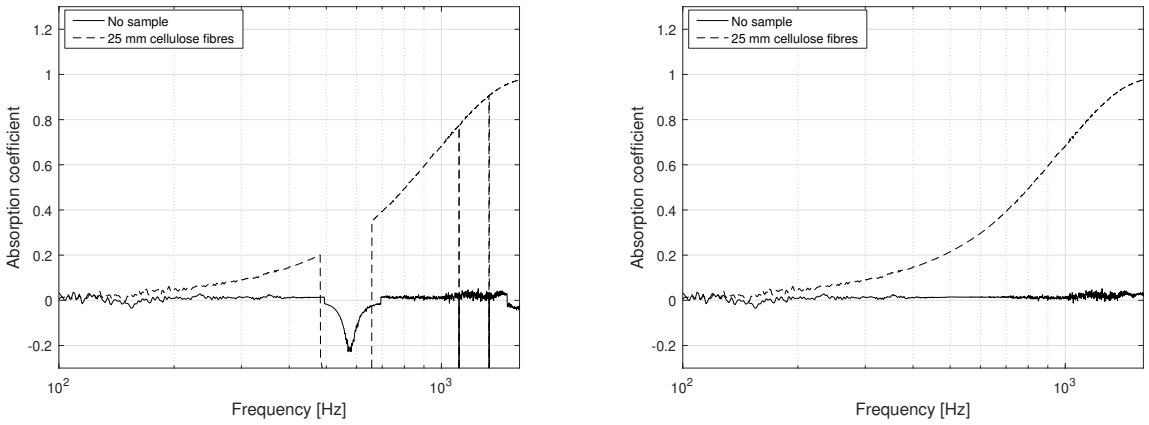

(a) (b)

Figure 9: Comparison between the measured results obtained by using Eqs. (91) and (92), on the left and right, respectively. _____ is the absorption curve for an empty impedance tube; − − − is the absorption curve for a sample of cellulose fibres of thickness 25 mm.

The usable frequency range for the transfer function method is determined by the diameter and length of the tube, the distance between microphone positions, and the distance between the loudspeaker and sample holder to the nearest microphone [9]. The upper frequency, f_u is constricted by the spacing between microphone positions, as well as the diameter of the tube:

$$f_u < 0.45 \frac{c_0}{\mid x_1 - x_2 \mid} \tag{93}$$

$$f_u < 0.58 \frac{c0}{d_{tube}} \tag{94}$$

According to Eq. (93), the smaller the distance between microphone positions, the higher the upper frequency limit. However, larger distances between the microphones provide more accurate measurements at lower frequencies, as larger differences in pressure are measured. Therefore, there must be a compromise between measurement accuracy and upper frequency limit [2]. This issue leads to the low frequency limit condition given in Eq. (95), which indicates that the spacing between microphones, x_1 - x_2, must exceed 5 % the wavelength of the lowest frequency of interest:

$$f_l = \frac{c_0}{20 \mid x_1 - x_2 \mid} \tag{95}$$

The distance between the loudspeaker and the closest microphone, as well as the distance between the front surface of the sample and its closest microphone must be considered. Near the sound source, the sound field is composed of plane waves and modes. No microphone should be located within a distance of 3 tube diameters to the loudspeaker in order to be able to have measurements taken in a stable sound field of plane waves. Similarly, the presence of the specimen may cause some distortion for

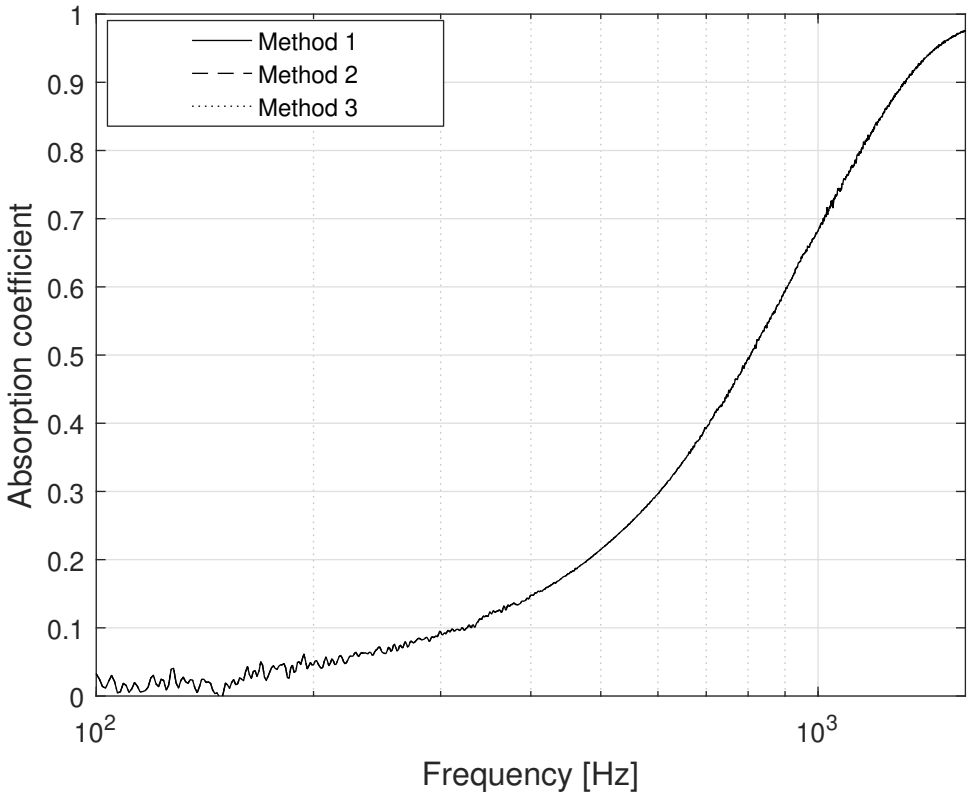

Figure 10: Comparison of the three methods available in the standard $ISO\,10534-2$ for the calculation of the transfer function H_{12}.

the acoustic field of plane waves. For this reason, for a homogeneous and isotropic sample the first microphone should be located at a distance of at least half tube diameter. For structured and anisotropic samples, the closest microphone to the specimen should be located at least two tube diameters away [9].

3.1.3 Drawbacks of the impedance tube method

The method is not an in-situ measurement technique and it only determines the normal incident sound absorption coefficient. The latter fact implies that only locally reacting materials can be measured successfully. This means that materials whose sound absorption properties change with the angle of incident cannot be measured accurately. Furthermore, the method requires small samples that in some cases may not correspond with their larger versions. This may be specially problematic when the samples are not completely homogeneous over the whole surface.

The effects of deviation in the sample size may have significant influence on the measurements. Naoki et al. [11] studied the effects of sample diameter deviation with respect to the impedance tube diameter. He showed that samples with diameter greater than the inner impedance tube diameter cause a resonance that can be clearly seen when examining the acoustic characteristics of the material. The resonance appears as a dip in the attenuation constant and a peak in the speed of sound within the

material. The absorption coefficient would show a reduction in sound absorption at the resonance frequency. On the other hand, samples with diameter smaller than the inner diameter of the impedance tube cause sound leakages on the sides of the samples. This leakages produce results characterized by a reduced attenuation constant. This effect is emphasized with smaller diameter of samples. Their work concluded that samples with diameter between 0.5 and 1 mm smaller than the impedance tube diameter are the best option to reduce possible resonances effect and diminish side leakages.

3.2 Reverberation room method

The reverberation room method is used to measure the absorption coefficient values of random incident sound. The method cannot be used to obtain the surface impedance. This is the reason why generally developers of sound absorbing materials use impedance tubes to develop their products as they can understand better the properties of the materials. Another reason is that the reverberation chamber method requires much larger test samples, 10-12 m^2, and still larger samples for reverberation rooms of volume larger than 200 m^3. The preparation of such samples may slow down the development process.

The method relies on the determination of the absorption coefficient values by computing the reverberation time (RT_{60}) of the reverberation room with and without the test sample. According to the standard, the RT_{60} is calculated using Sabine's formula (Eq. (96)). However, in [2] it is stated that Sabine's formula may not give accurate results for very absorptive materials. In such cases, the use of Eyring formula is suggested (Eq. (97)).

$$RT_{60} = \frac{0.161V}{A} \tag{96}$$

$$RT_{60} = \frac{55.3V}{-c_0\, S\ \ ln(1-\bar{\alpha})} \tag{97}$$

where $\bar{\alpha}$ is the average absorption in the room, c_0 is the speed of sound in air, V the volume of the room, and A is the absorption area.

The method begins with the measurement of the RT_{60} of the reverberation chamber with and without the test sample. The measured reverberation times are used then in Eq. (98) to calculate the equivalent sound absorption area of the test sample in m^2.

$$A_T = 55.3V\left(\frac{1}{c_2 RT_{60,2}} - \frac{1}{c_1 RT_{60,1}}\right) - 4V(m_2' - m_1') \tag{98}$$

where c_1 and c_2 are the sound speed in air with and without the test sample inside, $RT_{60,1}$ and $RT_{60,2}$ are the reverberation times with and without the test sample, and m_1' and m_2' are the power attenuation coefficients defined in the standard. These coefficients account for the atmospheric conditions in the chamber with and without

the sample. The diffuse sound absorption coefficient values of the absorber are then given by Eq. (99)

$$\alpha = \frac{A_T}{S_{spec}} \tag{99}$$

where S_{spec} is the area covered by the test specimen.

It should be noted here that the sound absorption coefficient values measured in a reverberation room may exceed unity. In theory, this should be incorrect, since the maximum absorption value by definition is one. There are two main factors that cause the exceeded value [12]. The first accounts for the sound absorption caused by the edges of the test sample, whose surface area is not considered in the calculations. The second reason is the use of Sabine's formula which may overestimate the results.

Despite of the many details of the measurement method prescribed in the standard ISO-354, many authors have reported the complexity to obtain hight rate of repeatability and reproducibility of measurements. The main factor causing the non-repeatability of measurements is the diffuseness of the sound field to which the test sample is exposed. The diffuseness of the sound field in a reverberation room is mainly determined by the shape of the reverberation room; the location of the microphones, loudspeaker, and test sample; as well as the changes in temperature and relative humidity between measurements [12].

Many authors have investaged the factors influencing the diffuseness of a reverberation room. D'Alessandro and Pispola [14] studied the performance of a rectangular reverberation chamber under different configurations. In their results, they explained that rectangular reverberation rooms are specially problematic due to their symmetrical shape which is inconvenient for the generation of a diffuse sound field. Furthermore, they stated that by placing test samples in such a way that no edge is parallel to the room walls the effects caused by horizontal axial modes are reduced.

The use of diffusers in reverberation rooms is a good practice to improve the properties of the sound field as well as to make the sound field more independent of the room shape. The standard recommends the area of the diffusers inside the room to be within the range 15 - 25 % of the total surface area of the room. D'Alessandro et al. also reported that diffusers placed on the lower corners of the chamber diminish the influence of tangential modes. In general, the use of hanging diffusers and diffusers located on the corners enhance the diffuse field on the entire frequency range. At mid-high frequencies the effect is more notorious. However, in the same paper the authors demonstrated that introducing diffusers in the reverberation chamber has also the negative effect of increasing the absorption area, thus decreasing the reverberation time. This results in a reduction in the accuracy of the measurements.

The effect of changes in temperature and relative humidity between measurements has been also investigated [14]. The authors reported that the correction for air absorption is more significant when temperature and relative humidity approach the limits given in the standard ($15°C$ 30 %). This influence is more noticeable at high frequencies.

4 Characterization of porous materials

Porous sound absorbing materials are solid media that contain multiple interconnected and isolated cavities through which a fluid may flow. These cavities, more known as pores, can be open or closed. Open pores are much more efficient at absorbing sound. They are communicated to the external surface of the body, thus allowing air to penetrate and consequently, causing energy dissipation due to the interaction between the solid and fluid as explained in section 2.2. Fig. 11 depicts a cross-section of a porous material illustrating the concepts of open and closed pores. The pores labelled as *b, c, d, e* and *f* are open pores.

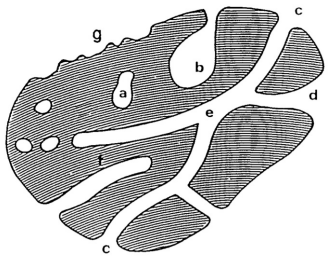

Figure 11: Cross-section of a porous solid material (adopted from [13]).

According to the microscopic configuration and physical characteristics of the elements forming the medium, three categories of porous materials can be distinguished, known as *cellular*, *fibrous* and *granular materials*. Fibrous materials are composed of a combination of several fibres that form a network containing irregular cavities through which air may flow. Fibrous materials can be made of natural and synthetic fibres. Cellulosic fibres and mineral wools are examples of natural and synthetic fibrous materials. Cellular porous materials contain a reticulated (net-like) skeleton that form the edges and faces of cells. If the solid is only contained in the edges of the cells, the material is said to be open-celled or fully reticulated. If the solid is contained in the edges and faces of the cells, it is said to be closed-celled or partially reticulated. Melamine and polyurethane foams are examples of cellular porous materials. Granular materials are made of grains gathered together forming a continuous medium that is surrounded by multitude of pores. Two main categories can be differentiated among granular materials, consolidated and unconsolidated granular media. Consolidated materials, also known as agglomerates, use binders to glue particles. These materials involve a relatively rigid and continuous media in which particles size notably exceeds the size of the pores. On the other hand, unconsolidated materials, also known as aggregate, are composed of discrete particles put together making loosely packed assemblages. Fig. 12 shows scanning electro micrograph (SEM) pictures of different types of porous materials.

Despite the differences in the basic elements forming the porous structure of these three types of porous materials, their sound absorption properties can be described in a similar way in all of them based on common macroscopic characteristics. These characteristics are known as porosity, flow resistivity, tortuosity and characteristic

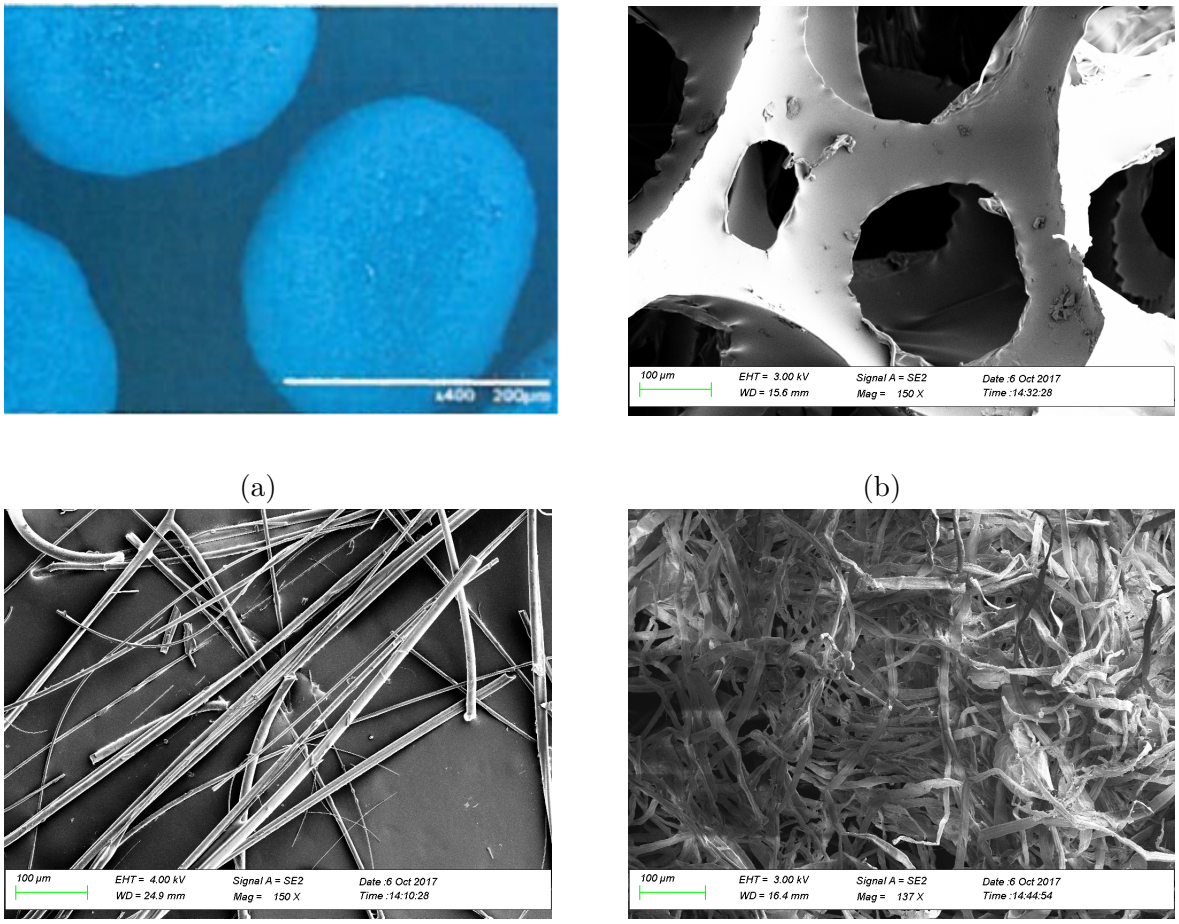

(a) (b)

(c) (d)

Figure 12: Scanning electro micrograph (SEM) pictures. (a) Granular particles (microcrystalline cellulose spheres of diameter 200 μm), adapted from [16]; (b) Cellular material (melamine foam); (c) Synthetic fibres (glass wool); (d) Natural fibres (cellulose).

lengths. They are described more in detail in the following section. Most of the models developed to model sound propagation within porous materials are based on these characteristics. Some of these models are presented in chapter 2.2.

This chapter continues with a description of the main physical characteristics that influence the sound absorption properties of porous materials. Then, different types of fibrous, cellular and granular materials used for acoustic purposes are presented. Data of sound absorption measurements of different materials collected from previous researches as well as measured for this work has been provided to the reader.

4.1 Parameters that influence sound absorption

The parameters that influence the sound absorption properties of porous materials can be classified in two categories. The first category accounts for the macroscopic

parameters of the materials, including flow resistivity, porosity, tortuosity, and characteristic lengths. These parameters are generally used in theoretical and empirical models to predict sound propagation within porous materials. The second category comprises parameters that describe the characteristic of the system, such as thickness, bulk density, fibre physical properties, and multilayers. These parameters are more associated to empirical models [17].

4.1.1 Macroscopic parameters

Flow resistivity and ***Flow resistance*** are the parameters that differ the most between different porous materials, and therefore, the parameters that best describe their sound absorption properties. Flow resistance is defined as the resistance of a material of thickness L to a steady flow of air moving through it [18]. Flow resistivity refers to a material flow resistance per unit thickness. The higher the flow resistance, the more complicated for the flow to move through the material. Expressions for flow resistance and resistivity are given in Eq. (100)

$$\sigma_s = \Delta P/U = \sigma L \tag{100}$$

Where σ_s is the flow resistance, ΔP is the pressure difference at the two sides of a sample of thickness L, U is the steady flow velocity, and σ is the flow resistivity. The unit of flow resistance is mks rayls ($N \cdot s \cdot m^{-3}$ or $Pa \cdot s \cdot m^{-1}$).

Porosity, denoted as ϕ, is defined as the ratio between the volume of air in the voids and the total volume of a material.

$$\phi = \frac{V_a}{V_a + V_b} \tag{101}$$

Where V_a and V_b are the volume of air and solid, respectively, and hence, the total volume is $V_a + V_b$. Porosity can also be computed based on the relation between the specific density and the bulk density of the material [18].

$$\phi = 1 - \frac{\rho_s}{\rho_m} \tag{102}$$

Where ρ_m is the specific density of the material and ρ_s is the bulk density of the sample [18]. The latter can be computed easily by the ratio between the dry weight of the sample and its total volume.

It is noted here that only open pores within the porous media contribute to sound absorption. Air penetrating porous media only has access to open pores, and therefore there is no much energy losses in close cavities. The higher the porosity, the more interaction between the frame and the sound waves propagating through the passages within the porous material, thus resulting in higher dissipation of sound energy.

Fibrous and cellular porous materials used for acoustic purposes generally have a porosity greater than 0.9, whereas granular materials commonly have an average

porosity of approximately 0.4 [18].

Tortuosity, denoted as s, can be defined as the ability of porous materials to prevent direct flow. Its value increases with the complexity of the passages interconnecting the pores. The longer the passages compared to the thickness of the material, the larger the tortuosity.

Many theoretical expressions have been developed to calculate the tortuosity of granular and fibrous porous materials. Attenborough and Umnova [19] suggested that the tortuosity of granular materials composed of identical spheres can be calculated by the following expression

$$s = 1 + \frac{1-\phi}{2\phi} \tag{103}$$

The tortuosity of materials composed of identical parallel fibres is calculated as [18]:

$$s = \frac{1}{\phi} \tag{104}$$

However, these formulas are idealized and they do not correspond with granular or fibre structures that can be found in real porous media. In practice, tortuosity is generally obtained by experimental techniques.

Allard et al. [20] showed that when a porous material is saturated by a nonviscous fluid, the dynamic density of the fluid is given by:

$$\rho_d = s\rho_0 \tag{105}$$

This implies, that at enough high frequencies, where the thickness of the viscous layer is so small that viscous losses can be neglected, the dynamic density of a viscous fluid must tend to $s\rho_0$. Therefore, at high audible and ultrasonic frequencies, tortuosity is the main factor defining the sound absorbing properties of porous materials. At these frequencies, the speed of sound within the material is approximately [18]:

$$c = \frac{c_0}{\sqrt{s}} \tag{106}$$

According to Eq. (106), the speed of sound waves travelling within typical porous materials, whose tortuosity is approximately one, at high frequencies tends to equal the speed of sound waves propagating in air.

Characteristic length is a microscopic parameter that is determined by the geometry of the pores. The concept was first introduced by Johnson [21]. In his work, he defined the viscous characteristic length, denoted as $\wedge$, that was used to calculate the high-frequency behaviour of the dynamic density of the fluid. Later, Champoux and Allard [20], introduced a second characteristic length, $\wedge$', that could be used to describe the high-frequency behaviour of the dynamic bulk modulus. Expressions for the two characteristic lengths developed by Johnson, and Champoux-Allard are given in Eq. (107) and (108)

$$\wedge = \frac{2\int_V \mid v(r)^2 \mid dV}{\int_A \mid v(r_w)^2 \mid dA} \tag{107}$$

$$\wedge' = \frac{2\int_V dV}{\int_A dA} \tag{108}$$

where $v(r)$ is the inviscid fluid velocity within the pore, and $v(r_w)$ is the velocity of the inviscid fluid at the surface of the pore walls. It can be seen that both expressions relate the volume to the area of the pores. The only difference between the two expressions is that $\wedge$ uses the squared flow velocity within the pores as weighting, whereas $\wedge$' does not. This weighting function implies that at narrower pores, $\wedge$ will be greater, since flow velocity increases with smaller constrictions. Consequently, narrower pores have greater influence on the effective density. On the other hand, $\wedge$' is not weighted, and according to Eq. (108) it increases for larger volumes of pore. This involves that larger pores have greater impact on the effective bulk modulus [20].

Therefore, as stated by Zwicker and Kosten [22], viscous forces that determine the effective density are due to the narrow parts of the pores, whereas the effective bulk modulus is governed by heat exchange taking place in larger pores.

In practice, calculations of $\wedge$ and $\wedge$' are unworkable due to the extremely complex geometry of pores in real porous materials. For this reason, characteristic lengths are generally computed from measurements of effective density and bulk modulus. Johnson [21] provided an expression that can be utilized to calculate the characteristic lengths of simple pore geometries. This expression relates $\wedge$ to flow resistivity

$$\wedge = s_{pore}\sqrt{\frac{8\eta s}{\sigma\phi}} \tag{109}$$

where η is the viscosity of air, s is tortuosity, σ is flow resistivity, ϕ is porosity and s_{pore} is a parameter that depends on the pore shape. It lies between 0.1 and 10 for most porous materials. For circular-cylindrical pores s_{pore}=1.

In general, $\wedge$' is larger than $\wedge$ [20]. However, in the case of cylindrical pores $\wedge$'=$\wedge$, as the flow velocity has no effect on Eq. (107). Additionally, it has been shown [20] that for fibrous materials, assuming the fibres to be of circular-cylindrical shape lying in layers perpendicular to the direction of the sound, $\wedge$'=2$\wedge$.

4.1.2 System properties

Thickness Thickness of a porous layer has an important impact on the absorption properties of the material. A useful rule of thumb is that doubling the thickness of the sample results in the sound absorption curve moved one octave towards low frequencies. Fig. 13 shows the behaviour of sound waves travelling perpendicularly to a sound absorbing surface. When a sound wave impacts a surface a standing wave is formed. At the surface, pressure and particle velocity are maximum and null, respectively. It is well known that porous materials are more efficient when they are placed at the location where incident particle velocity is maximum. This occurs at a

distance of $\lambda/4$ from the rigid wall. At such distance, maximum absorption can be achieved.

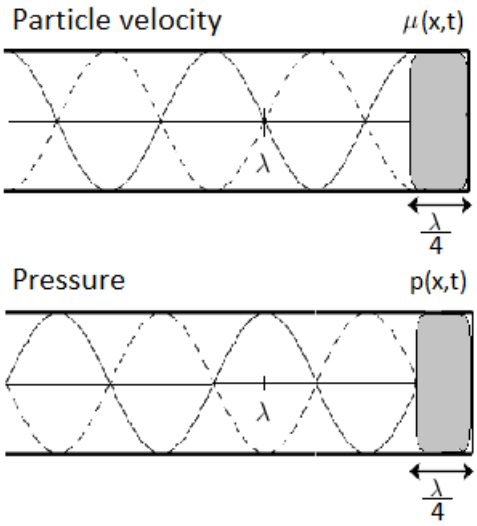

Figure 13: Points of maximum and minimum pressure and particle velocity for normal incidence sound waves [6].

.

In diffuse field, thinner layers of porous materials are required to achieve maximum absorption [6]. This can be explained by the fact that sound waves impact the surface arriving from all directions. As a result, oblique incident sound waves will see thicker porous layers compared to normal incident sound waves (see Fig. 14). Based on this explanation, a thickness of around $\lambda/10$ would be sufficient to achieve maximum absorption in diffuse field [6].

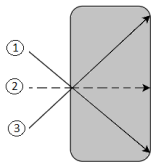

Figure 14: Oblique waves find thicker layers than normal incident sound waves.

While all the theory explained above in this subsection is completely true for the most typical sound absorbing materials used for acoustic purposes (mineral wools and foams), it is not generally valid for natural fibre-based materials, such as cellulose. It is shown in chapter 6 that materials made of natural cellulose fibres require lower thickness to achieve good sound absorption at lower frequencies. This phenomenon is believed to be caused by a reduction in the speed of sound waves propagating within cellulose fibrous materials. Decreasing the speed of sound while keeping the thickness of the material constant results in the first peak of the sound absorption curve moved towards lower frequencies [23].

The sound speed of the wave travelling within porous materials is given by:

$$c = \frac{w}{\Gamma_a''} = \frac{w}{Im\{j2\pi f\sqrt{\frac{\rho_d}{\kappa_d}}\}} = Re\{\sqrt{\frac{\kappa_d}{\rho_d}}\} \tag{110}$$

where Γ_a'' is the imaginary component of the propagation constant (see section 2.5), and ρ_d and κ_d are the dynamic density and bulk modulus, respectively. According to expression (110), the slowing-down of the speed of sound wave is caused by a reduction in the bulk modulus and/or an increase in the dynamic density of the fluid. The former implies an increase in the fluid compressibility which might be caused by the larger surface area with which the fluid may exchange thermal energy. This larger area is the result of the cellulose fibres being hollow. Thermal exchange may occur between the fluid and the interior and exterior surfaces of the fibres. Furthermore, the fact that cellulose fibres have micro-pores in their structure may increase the dynamic density of the fluid.

Air gap Adding an air gap between the back side of the porous layer and the rigid wall results in moving the maximum sound absorption peak towards low frequencies. However, sound absorption may be slightly deteriorated at some frequencies above the first peak if the porous layer is not thick or dense enough. The shape of the absorption curve is determined by the thickness of the porous layer, thickness of the air layer, and total thickness, as well as by the density [24]. Variations in the sound absorption curve can be diminished by increasing the density and thickness of the porous layer.

Maximum absorption is achieved by placing the material where particle velocity is maximum, $\lambda/4$. The present of an air layer behind the porous material generates points of minimum absorption. These points are identified as the locations where particle velocity is minimum. Fig. 15 depicts locations of maximum and minimum sound absorption. The frequencies of maximum and minimum sound absorption can be calculated using Eqs. (111) and (112), being L the total thickness of the samples (porous layer + air layer).

$$f_{max} = n\frac{c}{4L} \qquad n = 1, 3, 5, ... \tag{111}$$

$$f_{min} = n\frac{c}{2L} \qquad n = 1, 2, 3, ... \tag{112}$$

Once again, this theory is not valid for porous materials made of natural cellulose fibres. It is shown in Chapter 6 that a similar phenomenon happens for porous materials made of natural cellulose fibres but Eq. (111) and (112) are not valid for them.

Bulk density Hongisto et al. [24] studied the sound absorption properties of mineral wools with varying bulk density. Their results showed that the peak of maximum absorption is moved towards higher frequencies for denser materials. These outcomes are in agreement with many other studies on natural fibre-based porous

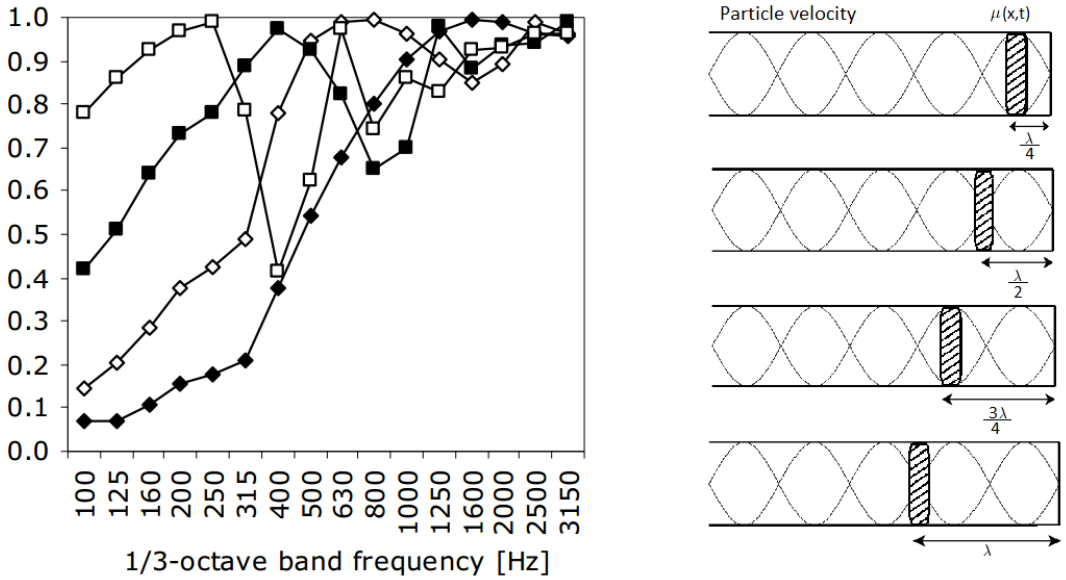

Figure 15: On the left, sound absorption coefficients measured in an impedance tube for a sample of glass wool of density 18 kg/m^3 with varying thickness of air layer behind: ♦ 50 mm glass wool, ◊ 50 mm glass wool + 50 mm air, ■ 50 mm glass wool + 150 mm air, □ 50 mm glass wool + 350 mm air. On the right, frequencies of maximum and minimum absorption of a multilayer (Eq. (111) and Eq. (112)) consisting of a porous layer, an air gap, and a rigid wall (adapted from [24]).

materials [17]. However, there are other studies in the literature that oppose these findings. In [25], Koizumi reported that the maximum peak of absorption is moved towards lower frequencies as density increases. This controversy is one more clue to the believe that porous materials may behave in different ways depending on the particle/elements they are made of. However, the author of this work believes that if Koizumi had used greater valuer of bulk density in his samples, his measurements would have probably agree with the results obtained in other works. It is shown in chapter 6 that cellulosic fibres harmonizes with the results reported by Hongisto et al.. At this point, it should be noted that high-density porous materials increase their ability to reflect sound at their surface. This explains the shift of the maximum absorption peak towards higher frequencies. On the other hand, very low-density materials may dissipate less sound energy because the particles are too separated from each other.

Fibre length, shape and diameter The interconnection of fibres differing in length, diameter, shape and any other physical characteristic may result in different pore geometries and structures within porous materials. This is the reason why most of the empirical models developed to predict sound absorption (e.g. Delany & Bazley) of porous materials do not give accurate results for materials made of natural fibres. These models have been developed to provide expressions to calculate sound absorption by applying regression models to several acoustical measurements

performed on materials made of mineral wool. The huge difference in the physical characteristics of mineral wool and natural fibres make these empirical models not suitable for predicting sound absorption properties of natural fibre-based materials. In [25], Koizumi used an impedance tube to measure the sound absorption coefficient of bamboo fibres of different diameters. He tested fibres of diameter 90-125 μm, 125-210 μm, and 210-245 μm. His results showed that sound absorption increases as the fibre diameter decreases. Koizumi reported that the more efficient sound absorption of lower diameter fibres is due to the fact that the number of fibres per unit area increases as the fibre diameter decreases. This results in more paths and surfaces for the sound to be dissipated. The influence of the fibre length might be analogous to that of the fibre diameter. More shorter fibres are required per unit area which results in more paths for the sound to flow.

4.2 Fibrous materials

In general, fibrous materials are assumed to be isotropic, meaning that the acoustic properties of the material are the same for all the possible directions of incident sound. However, this assumption is not completely correct because, generally, fibres are layered in the materials, which causes the medium to be anisotropic. Nevertheless, for the sake of simplicity most of the sources assume fibrous porous materials to be isotropic. This assumption is valid for most of the applications.

Synthetic fibrous materials made of mineral wools together with polyurethane or polyester materials dominate the market of products used for acoustic purposes [26]. Glass and mineral wool fibres have been found to be harmful. Handling these materials may cause skin irritation and harm due to the accumulation of fibres in the eyes. Furthermore, inhaling these fibres may cause problems in the respiratory system as some fibres may lay down on the lung alveoli. Especially hazard are respirable fibres, those with diameter less than 3 μm. In order to reduce these effects, glass/mineral wool fibrous materials must be properly overlaid when exposed to air. On the other hand, since 2001, glass and mineral wools are classified as materials *probably not carcinogenic to humans* by the International Agency for Research on Cancer [27].

The production of plastic fibrous materials, commonly involving petrochemical sources, requires considerably more energy than other sound insulating materials, thus implying much greater environmental impact [26]. The numerous disadvantages of synthetic fibres has given rise to develop natural and sustainable alternatives. Natural fibrous materials are already seen as sound absorbing alternatives to mineral wools. Natural fibres are characterized by having low toxicity, being completely biodegradable, and being lightweight. Furthermore, their production processes require less or similar magnitude of energy than the energy required by the production of mineral wools, and much less energy than the energy consumed in the manufacture of plastic fibres [26]. In addition, natural fibres are available as a waste product of the manufacture of other products, which makes them very attractive in term of cost. Moreover, the reuse of these wastes avoids their incineration, which reduces environmental impact. These facts together with the high acoustic performance that

they can provide make them excellent materials for sound absorption purposes.

Sources of natural fibres are plants, animals and minerals. A description of plant fibres is given in chapter 6. The same chapter presents measurements and analysis of the sound absorption properties of cellulose fibres. Examples of sources of plant fibres are cotton, kenaf, ramie, sisal, bamboo, hemp, coco fibre and flax. Sources of animal fibres are sheep, goat, and camel, among others. In the group of sources of mineral fibres asbestos is the most popular. However, the use of asbestos fibres in the building industry has considerably been reduced since it was detected that asbestos fibres may cause serious health hazards in building occupants. Table 1 shows the acoustic properties of natural fibre-based sound absorbing materials reported in the literature. Data of glass, rock wool and polyester fibres is also provided for comparisons.

	Density kg/m^3	Thickness cm	Absorption α coef. at 500 Hz	Absorption α coef. at 1 kHz
Kenaf [32]	50	6	0.33	0.68
Kenaf [32]	100	4	0.32	0.70
Kenaf [32]	100	6	0.61	0.99
Wood (Fibres) [32]	100	6	0.50	0.65
Wood (mineralized) [32]	260	3	0.10	0.20
Hemp [32]	50	3	0.25	0.51
Coconut [32]	60	5	0.34	0.67
Coconut [32]	60	10	0.83	0.81
Cane [32]	400	4	0.35	0.54
Cane [32]	470	8	0.56	0.52
Sheep wool [32]	40	4	0.36	0.73
Sheep wool [32]	40	6	0.66	0.95
Bamboo [25]	-	5	0.5	0.8
Cellulose	70	5	0.8	0.77
Cellulose	55	5	0.69	0.95
Glass wool	-	5	0.71	0.88
Rock wool	-	4	0.5	0.9
Polyester fibres [33]	40	4	0.28	0.54

Table 1: Sound absorption properties of some synthetic and natural fibrous materials (Impedance tube measurements). References to the papers are found in the table. The samples of cellulose, glass and rock wool were measured for this work.

4.3 Granular materials

Granular porous materials can provide high sound absorbing surfaces that are more durable and strong than fibrous and cellular materials. These surfaces are suitable for many industrial and outdoor applications, such as road pavements and noise barriers.

In granular media, the solid phase formed by the particles can be regarded as ideally rigid, and hence sound absorption due to vibration of the particles as sound waves propagate within the media can be neglected. Consequently, it can be considered that sound absorption in granular media is mainly caused by viscousthermal losses [28].

In general, porous granular materials have a rigid surface at their back. Under this condition, granular materials absorb sound due to the combination of two mechanisms. The first one is related to visco-thermal losses taking place within the material as sound waves propagate. The second mechanism is related to the destructive interference occurring at the surface of the sample between the direct and the reflected sound waves coming from the rigid backing behind the sample. The former provides absorption at higher frequencies while the latter increases attenuation of the lower frequencies [4]. Obviously, if there is no rigid surface behind the granular material, sound absorption will only happen due to visco-thermal losses.

Sound absorption properties of granular materials are more related to the average size of the particles and the geometries they formed rather than to the material properties. In [29], the authors reported that consolidated granular media made of particles of size smaller than 0.7 mm cannot be considered as acoustical materials due to their inefficient performance at absorbing sound. When such small particles gather together, very small pores are created and many of them will be closed after adding the binder to the material.

In the same work, it is shown that for consolidated materials, particle sizes greater than 2 mm of recycle rubber provide better sound absorption than smaller particle sizes. On the other hand, for unconsolidated materials, such large grain sizes absorb sound poorly and smaller diameter grains absorb more efficiently. Smaller grains form pores of smaller dimensions and therefore increase tortuosity and flow resistivity, thus causing an increase in viscous-thermal losses. Chapter 6 presents and analyses some sound absorption measurements performed on unconsolidated granular media. The acoustic properties of double porosity granular materials has been studied by many researchers [30]. These studies have revealed that media containing macro-pores (pores formed by interaction between particles) and micro-pores (pores within single particles) absorb more efficiently sound at low frequencies than granular media composed of non-porous grains (single porosity granular media). Moreover, among the different double porosity granular media there is a material that outperforms the others, this material is activated carbon. The material posses additional mechanisms for sound energy dissipation that makes it very attractive for acoustical purposes. Activated carbon is discussed in the following section.

4.3.1 Activated carbon

Activated carbon is a material that has been reported to have high sound absorption properties specially at low frequencies [31] (compared to typical sound absorbing materials). This material is carbonaceous and can be supplied in the form of grains or fibres. Its high absorption properties at low frequencies involves an absorption mechanism based on adsorption and desorption processes, in addition to the usual

viscous-thermal-inertial interactions between the fluid and solid phase.

This material is characterized by its complex porous structure and high adsorption capacity caused by free electrons in the deformed graphene layers. A single grain of activated carbon contains multitude of micro-pores, which results in very large internal surface areas. During the adsorption process, molecules of the fluid are attracted to the material and held on the surface by Van der Waals forces. In the desorption process the attracted molecules are realised to the fluid.

The sorption process (sorption refers to adsorption, desorption and absorption, as the penetration of the molecules of the fluid into the solid phase) is responsible of two phenomena that occur when sound waves propagate through activated carbon [31]. The first phenomenon consists in an increase of the volume compliance of an enclosure containing activated carbon. This is believed to be the result of an increase in the effective density of the gas caused by the sorption process. The second phenomenon is related to energy losses, such as heat transfer between the adsorbate molecules of the gas and the solid phase.

Increasing the volume compliance of enclosures is a desired phenomenon in many applications, such as in the design of loudspeakers boxes. For instance, an increase in the volume compliance of a loudspeaker cabinet enables the use of smaller cabinets while preserving reproduction bandwidth.

Bechwati et al. [31] showed that a Helmholtz resonator containing activated carbon in its backing cavity increases the volume compliance of the cavity, thus moving towards lower frequencies the resonance of the system. In this work, similar measurements has been performed. Different materials have been placed in the backing space of the Helmholtz resonator. The three different configurations of Helmholtz resonator are described below. In addition, different thickness for the backing layers were tested in order to explore the effects of having a thicker/thinner layer of air compared to the thickness of the layers of activated carbon and mycrocrystalline cellulose spheres (MCC). The results are shown in Fig. 17:

- A perforated board, and a second layer of air between the perforated layer and the rigid wall.
- A perforated board. A second layer of air behind the perforated layer, and a third layer of activated carbon between the rigid wall and the air layer.
- A perforated board. A second layer of air behind the perforated layer, and a third layer of microcrystalline cellulose spheres (MCC) between the rigid wall and the air layer.

The perforated board was made of natural cellulose fibres. The thickness of the board is 20 mm, the hole radius is 2.5 mm, and the total aperture is 8 %. The diameter of the activated carbon particles is within the range 0.4-1.4 mm. Diameter of the MCC is 0.7 mm. The three layers are shown in Fig. 16.

Table 2 shows the resonance frequencies measured for the three configurations of each resonator. It can be seen that the resonances for the resonators with backing spaces filled with activated carbon are located at lower frequencies. This happens

Figure 16: On the left, the perforated board made of cellulose fibres; in the middle, MCC particles of diameter 0.7 mm; and on the right, activated carbon particles of diameter 0.4-1.4 mm.

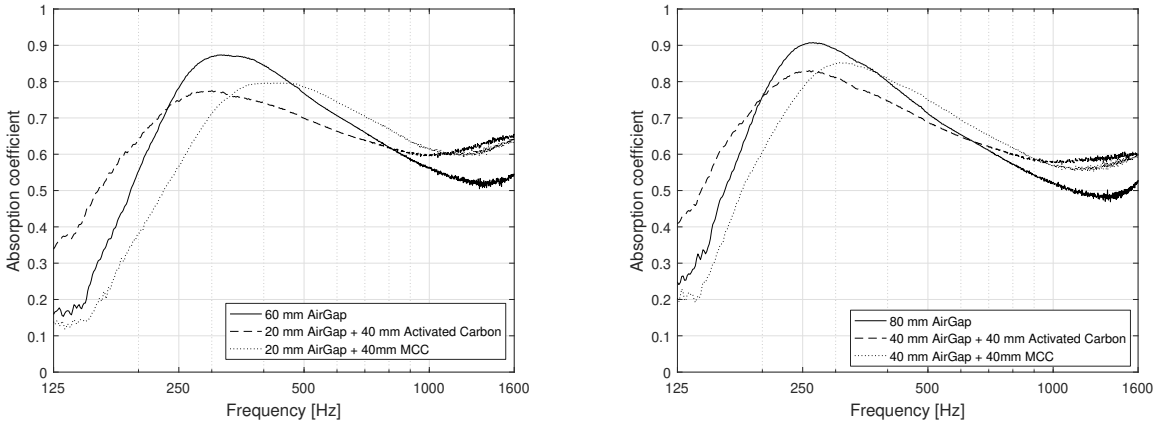

(a) (b)

Figure 17: Measured sound absorption for the two resonators and the three different backing configurations: _____ empty backing; − − − air layer + activated carbon; ... air layer + microcrystalline cellulose spheres (MCC). (a) resonator I, composed of a perforated board with 60 mm backing space. (b) Resonator II, composed of the perforated board with 80 mm backing space.

due to the increase in volume compliance caused by the sorption process that has its origin in the changes in pressure in the fluid caused by sound waves approaching the layer of activated carbon. [31]. When the backing space if partially filled with MCC, the resonance peak is shifted towards higher frequencies, which is the expected result for a reduction in the volume of air in the cavity of a Helmholtz resonator.

Differences in the measurements obtained for the two resonators reveal that the shifting of the resonance frequency towards lower frequencies is more effective when activated carbon is the dominant medium in the backing layer. If activated carbon is not the thicker layer in the backing space, the resonance peak of the system is approximately located at the same frequency than in the configuration where the backing space is only filled with air.

It is noted here that the sorption phenomenon is a process that needs some time

	Resonator I
Air (60 mm)	314 Hz
Air (20 mm) AC (40 mm)	301 Hz
Air (20 mm) MCC (40 mm)	426 Hz

	Resonator II
Air (80 mm)	263 Hz
Air (40 mm) AC (40 mm)	262 Hz
Air (40 mm) MCC (40 mm)	313 Hz

Table 2: Measured resonance frequencies for the two resonators.

to happen. This is the reason why sorption can only cause sound absorption at lower frequencies. At higher frequencies compression and rarefaction of sound waves happens so fast that there is no time for the sorption process to occur. Furthermore, the increase in sound absorption is related to the reduction in surface reactance rather than changes in surface resistance.

5 Models of sound propagation in porous media

Numerous models have been developed to predict sound propagation in porous media. These models can be divided in three groups, empirical, theoretical or phenomenological, and semi-phenomenological models. Empirical models are based on empirical formulas that are obtained by applying regression models to a large amount of acoustical measurements. Theoretical models predict sound propagation in porous materials characterized by simple pore geometries, such as slits or cylindrical pores with circular, triangular or square cross-section. Semi-phenomenological models consider more complex pore shapes but they require measurements of some properties of the materials.

5.1 Rigid vs elastic frame

The most accurate semi-phenomenological models assume the frame of the porous material to be elastic. This assumption implies sound waves propagating through the pores and the skeleton. Some waves propagate only through the frame or the pores, but others propagate through both the frame and the pores [2]. As a result, three different types of waves may propagate through the material. This leads to very complex theoretical models that require additional data of mechanical properties of the materials, such us the Young's modulus and Poisson's ratio. The most valuable advantage of elastic frame models is that they are able to predict the resonances of the frame, which can be measured when the motion of the material is not constrained by a rigid surface. The most popular elastic frame model was proposed by Biot [34, 35].

In general, most of the models assume the frame of the porous material to be rigid, motionless. This assumption involves that sound waves only propagate through the pores, thus providing the development of simplified models that give sufficient accuracy in most cases. For example, in many practical cases porous materials may be backed by a rigid wall, or they may be resting on the floor. In this cases, the rigid surface constrains the motion of the solid skeleton. Furthermore, some rigid-frame semi-phenomenological and empirical models are able to detect the resonances caused by the motion of the frame when the porous layer is placed free in air (no rigid surface constraining the motion of the material). This is due to those models using empirical fittings that may provide information related to the motion of the frame [2]. However, most of the semi-phenomenological models do not detect these resonances.

The assumption of rigid frame implies that the porous medium can be seen as a modified fluid characterized by a dynamic density, also known as complex or effective density, and a dynamic bulk modulus, also known as complex or effective bulk modulus. This assumption is true for all the absorbents with density and stiffness of the solid skeleton much greater than those of air [22]. The dynamic density accounts for viscous and inertial dissipation of the fluid propagating through the pores, whereas the dynamic bulk modulus takes into account losses due to thermal exchanges between the fluid and the solid frame.

In the following sections some semi-phenomenological and empirical models are reviewed. Only theoretical models based on the assumption of porous materials of rigid and motionless frame have been studied because they provide accurate predictions and are simpler compared to elastic-frame models.

5.2 Fully theoretical and semi-phenomenological models

In general, theoretical and semi-phenomenological models develop expression for the effective density (ρ_d) and bulk modulus (κ_d) of the fluid within porous materials. These expression are then used to calculate the acoustic characteristics Z_a and Γ_a:

$$Z_a(w) = \sqrt{\rho_d \kappa_d} \tag{113}$$

$$\Gamma_a(w) = jw\sqrt{\frac{\rho_d}{\kappa_d}} \tag{114}$$

5.2.1 Theoretical models

Kirchhoff was the first author to contribute to solving the problem of sound propagation in porous materials [36]. He developed an expression for sound propagation in cylindrical tubes that taked into account the effects caused by viscous and thermal losses. Later, Zwikker and Kosten [22] simplified the model of Kirchhoff and proposed expressions for dynamic density and bulk modulus for one single cylindrical tube by treating viscous and thermal effects separately:

$$\rho_d(w) = \frac{\rho_0}{1 - \frac{2J_1(\hat{s}\sqrt{-j})}{\hat{s}\sqrt{-j}J_0(\hat{s}\sqrt{-j})}} \tag{115}$$

$$\kappa_d(w) = \frac{\gamma P_0}{1 + (\gamma - 1)\frac{2J_1(\sqrt{N_{pr}}\hat{s}\sqrt{-j})}{\sqrt{N_{pr}}\hat{s}\sqrt{-j}J_0(\sqrt{N_{pr}}\hat{s}\sqrt{-j})}} \tag{116}$$

where ρ_0 and P_0 are the static density and pressure, N_{pr} is the Prandtl number, γ is the adiabatic index, and J_0 and J_1 are the zeroth- and first-order Bessel functions of first kind. The parameter $\hat{s}$ is the share wave number and it is related to the shape of the pore (s_{pore} specified for cylindrical pores of circular cross-sectional area):

$$\hat{s} = \sqrt{\frac{w\rho_0 r^2}{\eta}} \tag{117}$$

where r is the radius of the tube and η is the dynamic viscosity of the fluid. The expressions given by Zwikker and Kosten were justified at low and high frequencies. The real component of the dynamic density increases around 33% at low frequencies with respect to ρ_0. At high frequencies the real component of ρ_d tends to ρ_0 as the viscous boundary layer is so thin that it has no effect on the fluid. The real part of the dynamic bulk modulus given by Eq. (116) becomes P_0 at low frequencies

(isothermal limit) and γP_0 at high frequencies (adiabatic limit). At mid frequencies the two quantities become complex values.

The model of Zwicker and Kosten was also developed to compute the dynamic density and bulk modulus of cylindrical tubes with different geometrical cross-section, such as triangular, rectangular and hexagonal geometries [36]. Zwicker and Kosten extended their model for porous materials composed of multiple parallel cylindrical tubes perpendicular to the surface, see Fig. 18. They defined the porosity of such materials as $\phi = n\pi r^2$, where n is the number of pores (cylindrical tubes). Flow resistivity was determined as $\sigma = \frac{8\eta}{r^2\phi}$. And the share wave number became $\hat{s} = (\frac{8w\rho_0}{\sigma\phi})^{-1/2}$ [36].

Figure 18: A sample of porous material having perpendicular pores.

Expressions (118) and (119) can be used to compute the dynamic bulk modulus and density of porous materials with identical pores perpendicular to the surface and having simple cross-sectional geometry. At low frequencies porosity and flow resistivity are the main parameters defining ρ_d and κ_d:

$$\rho_d = \frac{\phi\sigma}{jw} + cte \tag{118}$$

$$\kappa_d = \frac{\gamma P_0}{\gamma - j(\gamma-1)\frac{wN_{pr}\rho_0}{\phi\sigma}} \tag{119}$$

where cte depends on the cross-sectional shape of the pore. At high frequencies, the main parameter determining ρ_d and κ_d is the hydraulic radius $\bar{r}$:

$$\rho_d = \rho_0\left(1 + \sqrt{\frac{2}{j}}\frac{\delta}{\bar{r}}\right) \tag{120}$$

$$\kappa_d = \gamma P_0\left[1 + (\gamma-1)\sqrt{\frac{2}{j}}\frac{\delta_v}{\bar{r}\sqrt{N_{pr}}}\right] \tag{121}$$

Expressions for the viscous boundary layer, δ_v, and the hydraulic radius, $\bar{r}$, can be found below:

$$\delta_v = \sqrt{\frac{2\eta}{w\rho_0}} \tag{122}$$

$$\bar{r} = \frac{2 \cdot cros - sectional\, area\, of\, a\, pore}{cross - sectional\, perimeter\, of\, a\, pore} \tag{123}$$

Figure 19: A sample of porous material having oblique pores.

Later, the model of Zwicker and Kosten was developed to account for porous materials composed of crosswise tubes. The inclination angle of the tubes, Θ, with respect to the normal of the surface affects the porosity and flow resistivity of the porous material as $\phi = n\pi r^2/cos\Theta$ and $\sigma = 8\eta/\phi r^2 cos\Theta^2$, respectively. Furthermore, a new parameter was needed that considered the longer paths for the sound waves to travel. The new parameter was called structure factor, k_s, and it was defined as $k_s = 1/cos^2\Theta$ (k_s is equivalent to tortuosity defined in section 4.1.1). The share wave number became $\hat{s} = \sqrt{8\rho_0 w/\phi\sigma cos\Theta^2}$ [36]. The obliqueness of the pores only influences the dynamic density at high frequencies:

$$\rho_d = k_s\rho_0\left(1 + \sqrt{\frac{2}{j}}\frac{\delta}{\bar{r}}\right) \tag{124}$$

5.2.2 Semi-phenomenological models

Porous materials having identical pores with the morphology described in the previous section are not found in real world. Common porous materials are composed of non-identical pores. Semi-phenomenological models involve several physical parameters of porous materials that can be measured and used to accurately predict sound propagation within porous materials. These physical parameters are based on the macroscopic characteristics of porous materials that were already introduced in section 4.1.1.

The **Johnson-Champoux-Allard (JCA)** is one of the most popular semi-phenomenological models. The method is based on the works of Johnson [21] and Champoux and Allard [37]. First, Johnson et al. derived an expression for the dynamic density of the equivalent fluid for rigid frame porous media with random pore geometry. They introduced the viscous characteristic length parameter $\wedge$ which has already been presented in section 4.1.1. $\wedge$ replaces the hydraulic radius that was used to predict the dynamic density and bulk modulus of porous materials with simple cross-sectional pore geometry given by Eq. (120) and (121). The dynamic density of the JCA model is calculated as:

$$\rho_d(w) = \frac{\alpha_\infty\rho_0}{\phi}\left[1 + \frac{\sigma\phi}{jw\rho_0\alpha_\infty}\sqrt{1 + \frac{j4\alpha_\infty^2\eta\rho_0 w}{\sigma^2\wedge^2\phi^2}}\right] \tag{125}$$

Where η is the dynamic viscosity of air, σ is flow resistivity, ϕ is porosity, w is the angular frequency, and α_∞ is a parameter equivalent to tortuosity (different authors denoted tortuosity using different symbols).

It has been proved [38] that expression (125) matches the asymptotic behaviour of the dynamic density. The imaginary low-frequency limit tends to σ/w, whereas the real high-frequency limit tends to $\rho_0\alpha_\infty/\phi$. The real low frequency limit remained inexact. Later, Pride et al. [40] made some modifications to the dynamic density expression of Johnson et al. to adjust the real low-frequency limit. Pride introduced a new parameter that was related to cross-sectional variations and constrictions in the pores, thus accounting more precisely for the inertia of the fluid.

The JCA model was completed with the expression for the bulk modulus for rigid frame porous materials developed by Champoux and Allard [20]. Their expression was also developed to match the asymptotic behaviour of the dynamic bulk modulus, going from an isothermal process at low frequencies to an adiabatic process at high frequencies. However, their formulation remained inexact at low frequencies.

$$\kappa_d(w) = \frac{\frac{\gamma P_0}{\phi}}{\gamma - (\gamma-1)\left[1 - \frac{j8\eta}{N_{pr}\rho_0 w \wedge'^2}\sqrt{1 + \frac{jN_{pr}\rho_0 w \wedge'^2}{16\eta}}\right]^{-1}} \tag{126}$$

Where γ is the adiabatic index, P_0 the static pressure, ϕ is the porosity, η is the dynamic viscosity, N_{Pr} is the Prandtl number (0.7 for air), $\wedge$' is the thermal characteristic length which has been defined previously (see Eq. (108)), ρ_0 is the static density, and w is the angular frequency.

In a effort to improve the performance of the model at low frequencies, Lafarge introduced a new parameter known as the *static thermal permeability*. Later, in order to achieve more accurate behaviour at low frequencies, the model of Lafarge was improved and one more geometrical parameter was introduced to derive an expression for the dynamic bulk modulus [39].

Champoux and Allard presented a model to predict the acoustic characteristics of fibrous porous materials that used expresions (125) and (126) to calculate the acoustic characteristics [20]. In their work, fibres were modelled as circular-cylindrical rods of diameter d_f and length l_f that were lying in layers perpendicular to the direction of the sound. Expressions for the viscous and thermal characteristic lengths were provided:

$$\wedge = \frac{1}{\pi d_f l_f} \tag{127}$$

$$\wedge' = \frac{2}{\pi d_f l_f} \tag{128}$$

Champoux and Allard provides the following expressions for the calculation of the dynamic density and bulk modulus of fibrous materials:

$$\rho(w) = 1.2 + \left[-0.0364\left(\frac{\rho_0 f}{\sigma}\right)^{-2} - j0.1144\left(\frac{\rho_0 f}{\sigma}\right)^{-1}\right]^{\frac{1}{2}} \quad [kg/m^3] \tag{129}$$

$$\kappa(w) = 101320 \frac{j29.64 + \left[2.82\left(\frac{\rho_0 f}{\sigma}\right)^{-2} + 24.9\left(\frac{\rho_0 f}{\sigma}\right)^{-1}\right]^{\frac{1}{2}}}{j21.17 + \left[2.82\left(\frac{\rho_0 f}{\sigma}\right)^{-2} + 24.9\left(\frac{\rho_0 f}{\sigma}\right)^{-1}\right]^{\frac{1}{2}}} \quad [N/m^2] \tag{130}$$

While the JCA model was developed to approximate the asymptotic behaviour of dynamic density and bulk modulus to the exact theoretical limits, at least at high frequencies, other models, such as the model provided by Wilson [36], were elaborated to match the middle frequency range. For a more in-detail review of the Wilson model the reader is directed to [39].

5.3 Empirical models

Empirical models provide expressions to directly calculate the acoustic characteristics without previous calculations of dynamic density and bulk modulus. The expressions are obtained by applying regression models to several acoustical measurements of porous materials with predetermined properties.

Among the empirical models reported in the literature, the model of **Delany and Bazley**, $D\&B$, is the most popular [41]. Delany and Bazley derived expressions for the acoustic characteristics of porous media by fitting a large number of measurements of glass and rock wools with specific flow resistivity ranging from 2000 to 80000 $[Pa\,s\,m^{-2}]$. The model requires a single parameter, flow resistivity, to predict the acoustic characteristics of porous materials. Delany and Bazley defined a dimensionless variable E that was found to be the parameter that collapsed all the measured data used in the development of their model [18].

$$E = \rho_0 f/\sigma \tag{131}$$

However, the model of Delany and Bazley has widely been criticised due to its poor performance at low frequencies. The reason is that the frequency range of validity of the model is limited by the flow resistivity of the material under study:

$$0.01 \leq \frac{f}{\sigma} \leq 1 \tag{132}$$

This constriction at low frequencies leads to incapabilities and inaccuracies of the model. For example, the lowest frequency valid for a porous material of flow resistivity equal to 300 000 $mks\,rayls\,m^{-1}$ is 2500 Hz, which may not be sufficient to completely describe porous materials. Additionally, the poor performance at low frequencies may cause non-physical behaviour in the real part of the surface impedance and/or absorption coefficient of a sample of porous material.

Many authors have proposed modifications to the $D\&B$ model to improve its performance at low frequencies. **Miki** [42] and **Komatsu** [43] introduced adjustments to avoid the non-physical behaviour of surface impedance and absorption coefficient, respectively. Miki reported that the poor performance at low frequencies was due to the real component of the surface impedance becoming negative at low frequencies.

This phenomenon is undesirable, and Miki made new regression models to provide new empirical equations that corrected the adverse behaviour for the surface impedance given by the $D\&B$ formulae, thus providing larger frequency range of validity at low frequencies. Komatsu focused his work on correcting the non-physical behaviour of the sound absorption coefficient. He provided new empirical expressions that avoided negative values of the sound absorption coefficient.

Despite the corrections and more accurate results given by the models of Miki and Komatsu, some authors have criticised the models. Kirby [44] stated that the models of Miki and Komatsu have no physical basis, and that they just adjusted the expressions of the $D\&B$ model to improve the non-physical behaviour of the surface impedance and absorption coefficient, without analysing the most fundamental properties of porous materials, dynamic density and bulk modulus.

Kirby based his criticism on the fact that any modifications on the $D\&B$ must first avoid anomalies of the fundamental properties of the material. He showed that the real component of the dynamic density computed by the models of Miki and Komatsu presented clear irregularities. The real component of the dynamic density computed by Miki's model became negative at low frequencies. Using the model of Komatsu the real part of the dynamic density increased to very large values at low frequencies. These results were more incorrect than the results computed by the model of $D\&B$. Kirby suggested the model of Mechel as a superior alternative empirical model that avoids the non-physical behaviour presented by the models of $D\&B$, Miki, and Komatsu.

Hongisto and Oliva [45] showed that the model developed by **Mechel** offers one of the most accurate predictions of the acoustic characteristics when compared to other empirical and semi-phenomenological models. Mechel's model overcomes the model of $D\&B$ by giving more accurate results at low frequencies. Mechel studied the acoustic characteristics of wool fibres by analysing two types of fibres separately (glass and rock wool). Furthermore, he divided the normalized dimensional parameter E defined by Delany and Bazley (see Eq. (131)) into two ranges, thus providing different empirical equations for each range. The coefficients used by Mechel's formulae can be found in table 3.

Hongisto and Oliva compared the accuracy of one semi-phenomenological and six empirical models with real measurements performed using the transfer function method of impedance tube. The characteristic impedance and propagation constant were calculated for all the models using the following notation:

$$Z_a = Z_{a0}(1 + C_1\hat{X}^{C_2} - jC_3\hat{X}^{C_4}) \tag{133}$$

$$\Gamma_a = \frac{w}{c_0}(C_5\hat{X}^{C_6} - j(1 + C_7\hat{X}^{C_8})) \tag{134}$$

Where $\hat{X}$ is a dimensionless parameter that is equal to the dimensionless parameter E defined by Delany and Bazley for the models of $D\&B$, Miki, Mechel, and Allard-Champoux ($\hat{X} = \frac{\rho_0 f}{\sigma}$), and it becomes Eq. (135) for the model of Komatsu.

$$\hat{X} = 2 - \log \frac{f}{\sigma} \tag{135}$$

Additionally, Hongisto and Oliva provided regression coefficients for the semi - phenomenological model of Allard and Champoux. The coefficients were obtained by applying regression models to the results obtained using the original equations developed by Allard and Champoux in [20]. Table 3 shows the empirical coefficients $c1 - c8$ for the more relevant models found in the work of Hongisto and Oliva ($D\&B$, Miki, Komatsu, Mechel, Qunli, and Allard and Champoux models).

The work on Hongisto and Oliva concluded that the semi-phenomenological model proposed by Allard and Champoux is the most accurate. The model of Mechel was proved to be slightly more accurate than the model of Miki, whereas Komatsu's model excessively overestimates the values of the sound absorption coefficients at frequencies below 1000 Hz. They also tested the model of Qunli which was developed to predict sound absorption of plastic foams. Their results showed that this model is not suitable for predicting sound absorption of fibrous materials.

It was reported by Garai and Pompoli [33] that the models available in the literature to predict the sound absorption coefficients of fibrous materials do not work accurately for materials made of polyester fibres. They attributed the incorrect predictions to variation in the physical characteristics of the fibres, such as length and fibre diameter. Garai and Pompoli provided new empirical expressions for polyester fibre materials by applying regression methods to acoustical measurements obtained from 38 polyester fibre materials (see model $G\&P$ in Table 3).

More recently, Berardi and Iannace [46] provided empirical coefficients for the prediction of the acoustic characteristics of natural fibre materials. Analogously to Garai and Pompoli, they reported that previous models have a poor performance in the prediction of the sound absorption properties of natural fibre-based materials. The main reason is attributed to the more irregular shape and greater diameter of natural fibres. Moreover, the structures formed by natural fibres when they aggregate is notably different to the structures formed by the combination of wool fibres.

The empirical coefficients given by Berardi and Iannace were computed based on a single sample of specific density and thickness. Consequently, their empirical coefficients can only predict the sound absorption of materials with the same density and thickness than they used for their calculations. Table 3 shows the empirical coefficients calculated for the following samples: wood fibres of density $100\,kg/m^3$ and thickness 60 mm; kenaf fibres of density $50\,kg/m^3$ and thickness 60 mm; kenaf fibres of density $100\,kg/m^3$ and thickness 40 mm; and kenaf fibres of density $100\,kg/m^3$ and thickness 40 mm.

Arenal et al. [28] also developed a model that could predict the sound absorption properties of porous materials made of unbleached cellulose fibre crumbs. Their computed empirical coefficients can be also found from Table 3.

Other empirical models have been developed to predict sound propagation in fibrous media without the needs of defining complex parameters. Voronina [47] presented an empirical model that predicts the acoustic characteristics of fibrous porous material based on the following physical characteristics of the fibres: diameter,

	Raw material	Model		c1	c2	c3	c4	c5	c6	c7	c8
Synthetic Fibres	Mineral wool	D&B		0.05710	-0.75400	0.08700	-0.73200	0.18900	-0.59500	0.09780	-0.70000
		Miki		0.07000	-0.63200	0.10700	-0.63200	0.16000	-0.61800	0.10900	-0.61800
		Komatsu		0.00027	6.20000	0.00470	4.10000	0.00690	4.10000	0.00040	6.20000
		Mechel (Glass Wool)	$\hat{X} \leq 0.025$	0.06880	-0.70700	0.19600	-0.54900	0.39600	-0.45800	0.13500	-0.64600
			$\hat{X} \geq 0.025$	0.02350	-0.88700	0.08750	-0.77000	0.17900	-0.67400	0.10200	-0.70500
		Mechel (Rock wool)	$\hat{X} \leq 0.025$	0.08100	-0.69900	0.19100	-0.55600	0.32200	-0.55600	0.13600	-0.64100
			$\hat{X} \geq 0.025$	0.05630	-0.72500	0.12700	-0.65500	0.17900	-0.66300	0.10300	-0.71600
	Polyester	G&P		0.07800	-0.62300	0.07400	-0.66000	0.15900	-0.57100	0.12100	-0.53000
Natural Fibres	Wood (40 Kg/m^3, 60 mm)	B&I		0.0770	-2.4825	0.8795	0.6510	0.4505	-1.3031	-0.0965	0.8289
	Kenaf (50 Kg/m^3, 60 mm)	B&I		0.0238	-1.0683	0.1115	-0.6167	0.1858	-0.5462	0.1568	-0.4173
	Kenaf (100 Kg/m^3, 40 mm)	B&I		1.2405	0.0370	-0.4082	-0.3840	0.8666	0.6454	3.6462	20.7484
	Kenaf (100 Kg/m^3, 40 mm)	B&I		0.0406	-1.5843	0.0345	-1.7689	0.2014	-1.0106	0.2966	0.9598
	Unbleached loose-fill cellulose	Arenas		0.6224	-0.0892	-0.481	0.614	0.3952	0.127	0.5823	0.087
Foams	Plastic	Qunli		0.20900	-0.54800	0.10500	-0.60700	0.16300	-0.59200	0.18800	-0.55400

Table 3: Empirical coefficients for the models of Delany & Bazley, Miki, Komatsu, Mechel, Garai and Pompoli, Berardi and Iannace, Arenal et al., and Qunli.

specific density of the material, and bulk density of the sample. In his model, porosity is defined as:

$$\phi = 1 - \frac{\rho_s}{\rho_m} \tag{136}$$

Where ρ_s is the bulk density of the sample, and ρ_m is the specific material density (density of one single fibre). This model defines a parameter known as *structural characteristic*, denoted as Q:

$$Q = \frac{(1-\phi)\,(q_0)}{\phi\, d_f}\sqrt{\frac{8\eta}{k_0\rho_0 c_0}} \tag{137}$$

Where η is the dynamic viscosity, ρ_0 and c_0 the static density of air and speed of sound in air, k_0 is the wave number in air, d_f is the fibre diameter, and q_0 is given by the following empirical expression:

$$q_0 = 1 + 0.25 \cdot 10^{-4}\,(1-\phi)^{-2} \tag{138}$$

The acoustic characteristics of fibrous porous materials can be calculated as follows:

$$Z_a(w) = 1 + Q - jQ \tag{139}$$

$$\Gamma_a(w) = k_0 \frac{Q\,(2+Q)}{1+Q} + jk\,(1+Q) \tag{140}$$

The frequency range of validity of this model is defined by the diameter of the fibres:

$$k_0 \cdot d_f \cdot 10^4 > 0.5 \tag{141}$$

The limitation imposed by the diameter of the fibre implies incorrect predictions of the acoustic characteristics for materials made of very thin fibres. For example, for

fibres of diameter 10 μm, the minimum frequency that can be accurately predicted is 273 Hz. This constriction can be explained by the fact that the model of Voronina does not consider the motion of very thin fibres. In a later work [48], Voronina improved his model to account for the motion of *superthin* fibres, and therefore, the model became suitable for materials made of fibres with very small diameter ($d_f < 1\mu m$). However, the improved model is not discussed here because the previous model is suitable for the diameters of fibres used in this work.

While the theoretical models presented above are more suitable for fibrous and reticulated cellular porous materials, other models have been specifically developed for granular media. Voronina and Horoshenkov [49] presented an empirical model that can be used to calculate the acoustic characteristics of loose granular media. Their model computes the characteristic impedance and propagation constant based on the following four measurable parameters, porosity, tortuosity, characteristic particle dimension and specific density, thus not requiring knowledge of complex parameters related to pore geometries.

In their model, Voronina and Horoshenkov neglected energy losses due to thermal effects as, for granular media, losses due to thermal effects are much smaller than losses due to viscous forces. Viscous effects are accounted for by the parameter ξ. This parameter was also used to make a new classification for grain size:

$$\xi = \frac{D\rho_0 c_0}{\eta} 10^{-4} \tag{142}$$

Where ρ_0 is the static air density, η is the dynamic viscosity, c_0 is the speed of sound in air, and D is the characteristic particle dimension of a grain and it is calculated as:

$$D = \sqrt[3]{\frac{V_g}{0.5233}} \tag{143}$$

Where V_g refers to the equivalent volume of one grain. V_g can be calculated by doing the ratio between the number of particles needed to fill an unit volume. According to the characteristic particle dimension, D, grains are classified as follows:

$$\begin{cases} \xi \leq 1 & \rightarrow Small\ grains \\ 1 \leq \xi \leq 2 & \rightarrow Medium\ grains \\ \xi \geq 2 & \rightarrow Large\ grains \end{cases}$$

Additionally, this model introduces a parameter, denoted as M, that relates the specific density, ρ_m, to the static density of air ρ_0:

$$M = \frac{\rho_m}{\rho_0 10^3} \tag{144}$$

It is believed that decreasing the specific density, ρ_m, results in greater sound absorption. This may be related to two main factors. In first place, the extra high-frequency absorption occurring within the micro-pores located in individual particles due to thermal losses; and secondly, higher friction between elements of lower specific density may increase absorption at low frequencies.

The model calculates the acoustic characteristics, $Z_a = Z'_a + jZ''_a$ and $\Gamma_a = \Gamma'_a + j\Gamma''_a$, based on the structural characteristic parameter, Q, and three more empirical expressions. The real part of the characteristic impedance can be divided into two frequency ranges. Above the transition frequency, f_{cr}, Z'_a is relatively independent of frequency and it tends to its higher-frequency limit. Below f_{cr}, Z'_a depends on the structural characteristic Q:

$$\begin{cases} Z'_a = s/\phi & \rightarrow f \leq f_{cr} \\ Z'_a = 1 + Q & \rightarrow f \geq f_{cr} \end{cases} \tag{145}$$

Where s is the tortuosity. The transition frequency (f_{cr}) and tortuosity are defined as:

$$s = \sqrt{1 + \frac{1-\phi}{2\phi}} \tag{146}$$

$$f_{cr} = \frac{200\eta \left(1-\phi\right)^2 \left(1+\phi\right)^4}{\pi \rho_0 D^2 \left(s-\phi\right)^2} \tag{147}$$

The imaginary part of the characteristic impedance and real and imaginary parts of the propagation constant are calculated as follows:

$$Z''_a = \frac{Q\phi}{1+\hat{C}} \tag{148}$$

$$\Gamma'_a = \frac{kQ\phi}{1+\hat{A}} \tag{149}$$

$$\Gamma''_a = k\left[1 + Q\phi\left(1+\hat{B}\right)\right] \tag{150}$$

Expression for the empirical coefficients $\hat{A}$, $\hat{B}$, $\hat{C}$ and for the structure factor Q are given below:

$$Q = \frac{0.2\left(1-\phi\right)\left(1+\phi\right)^2}{\phi\sqrt{kD\xi}} \tag{151}$$

$$\hat{A} = \frac{\left(1-\phi\right)M}{1+Q} \tag{152}$$

$$\hat{B} = \frac{1}{\sqrt{Q}\left(1+\phi\right)\left(1+Q^2 M\right)} \tag{153}$$

$$\hat{C} = \frac{1-H}{\sqrt{Q}} \tag{154}$$

Voronina and Horoshenkov showed that the predictions provided by their model are in good agreement with acoustical measurements. Furthermore, their work suggested that unconsolidated granulate porous materials made of smaller size grains, $\xi \leq 2$, provide more efficient sound absorbing surfaces.

6 Sound absorption of cellulosic materials

Cellulose is the main component of vegetable fibres. It is a renewable and biodegradable polymer that is considered a potential green alternative to fossil-fuel based polymers. Cellulose is used in many fields, but it finds its main application in the paper industry. In the building sector, the natural and sustainable properties of cellulose fibres make them an excellent material for the production of thermal and acoustical insulation materials as well as for the developing of sound absorbing surfaces for room acoustic designs.

There is a wide variety of cellulose sources, including plants, animals and bacterias. Plant fibres can be classified according to the part of the plant the fibres have been obtained from [32]

- stalk or wood fibre (straw of wheat, softwood, hardwood,...)
- bast fibre or skin fibre (flax, jute, kenaf, hemp,...)
- leaf fibre (sisal, palm, ...)
- seed fibre (cotton)
- fruit fibre (coconut)

The morphology of fibres is one of the main attributes determining their properties [51]. The morphology is determined by the type of fibre and plant source. Fibre diameter, length and shape are some of the physical characteristics of fibres that defined their performance in different applications.

The structure of plant fibres resemble tubes. They have a hollow central space which is called lumen. The lumen is surrounded by cell walls. Cell walls of plants are composed of three main organic substances: cellulose, lignin and hemicellulose. From these three compounds cellulose is the dominant, typically accounting for 40-50% in wood fibres, and 60-70% in most plant fibres. This amount is larger for some plants such as cotton, with almost 100% of its components being cellulose [52].

The arrangement of cellulose units in the cell walls of plants is shown in Fig. 20. Cellulose is a linear polymer of D-glucose units that are connected by β-1,4-glycosidic bonds. The linked glucose units form cellulose chains. These chains are connected by hydrogen bonds, and they are arranged in parallel to form cellulose microfibrils. The cell walls are formed by the association of microfibrils embedded in a hemicellulose-lignin matrix. The association between the glucose units of the cellulose chains determines crystalline and amorphous regions in microfibrils. Glucose units arranged in a highly order defined crystalline regions, whereas arrangements in low order determine amorphous regions. Crystalline regions are one of the factors responsible for the higher mechanical properties of cellulosic materials [51]. The grade of crystanillinity as well as many other properties of cellulose depends on the source .

Lignocellulosic materials can be broken down physically or chemically to generate discrete liberated fibres than can be dispersed in water and reformed into a mass

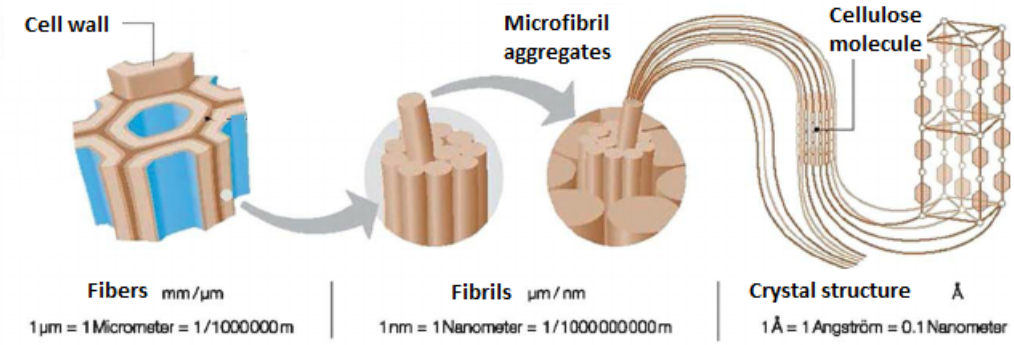

Figure 20: Ilustration of the arrangement of cellulose units in the plant cell wall. Adapted from [51].

known as pulp. The various methods for the production of pulp can be classified as chemical or mechanical processes. Mechanical methods separate fibres based on physical actions and avoiding chemicals. Chemical pulping methods rely on the effects of chemicals to separate fibres. Chemical methods provide pulp that has lower content of lignin as the chemicals tend to remove it [53].

The most popular pulping method is known as the Kraft method. The Kraft process efficiently removes lignin and produces cellulosic fibres with high strength properties [52]. The original Kraft process could not be considered as environmental-friendly. However, the method has been developed into a more ecological process that reuses wastes and employs less damaging chemicals.

In this work sound absorbing porous materials composed of natural wood cellulose fibres as well as microcrystalline cellulose spherical particles were measured. The chapter started with a brief introduction to cellulose. For a more in-depth definition of cellulosic materials the reader is referred to [51],[53]. The chapter continues with an introduction to wood cellulose and nanocellulose. Then the preparation of the samples made of wood cellulose fibres and microcristalline cellulose spheres is described. Finally, the section finishes with an analysis of the results and a discussion of the sound absorption properties of granular and fibrous porous materials. It is demonstrated that the models developed to predict the sound absorption properties of fibrous materials are not valid for cellulose fibres.

6.1 Wood cellulose

The main source of cellulose is wood obtained from forest trees, accounting for over 90% of the world's cellulosic fibres. Trees are classified into two categories known as *hardwood* and *softwood*. Wood fibres obtained from softwood and hardwood differs in many physical aspects, such as length and diameter. These physical differences make some fibres more suitable for specific purposes. For example, according to previous research on fibrous porous materials [25], narrower and shorter fibres generally produce more efficient sound-absorbing materials. This is due to an increase in the number of fibres needed to fill the same volume, which results in a higher number of

pores and geometries, thus leading to an increase in friction and consequently sound absorption.

Softwood species are characterized by their needle-like leaves. Example of softwood trees are pine, spruce, and cypress. Softwood fibre length ranges between 2 and 6 mm and its diameter within 25-60 μm. On the other hand, hardwood trees have broad leaves that are generally lost in winter. Hardwoods include birch, aspen and oak. Hardwood fibres are shorter and narrower, ranging from 0.9 to 1.5 mm, and they are characterized by the presence of pores in their surface [53].

Cellulose fibres are obtained from wood fibres by removing lignin and hemicellulose. This process results in a reduction in the diameter of the fibres. Another significant physical characteristic of cellulose fibres is that they are hollow, like drinking straws. The air contained in the lumen is communicated with air outside through pores located in the walls of the fibre [54]. Furthermore, the wall of a single cellulose fibre is composed of a large number of nanofibres. Sound waves propagating within cellulose materials set these nanofibres into motion, thus causing dissipation of sound absorption [55]. It is shown later that these characteristics endow cellulose fibres with comparable sound absorption to that of typical sound absorbing materials used in the building sector.

6.2 Previous work on the sound absorption properties of cellulose

Arenas et al. [28] investigated the sound absorption properties of unbleached loose cellulose crumbs obtained from pine trees through the Kraft pulping process. Cellulose crumbs can be regarded as fibrous-granular materials. The bleaching process whitens the pulp by removing lignin, which is the compound that provides the brown color to the unbleached pulp. Due to the presence of lignin in the fibres, unbleached cellulose fibres have larger diameter than bleached fibres. In their work, Arenas et al. demonstrated that unbleached cellulose crumbs can attain similar sound absorption than mineral-fibre-based products. They measured the sound absorption of four samples with the following physical properties: bulk density equal to 96.4 kg/m^3, flow resistivity 3471 $\pm$ 158 Ns/m^4, porosity 0.98, and tortuosity 1.01. The thickness of each sample was 25, 50, 75 and 100 mm.

	Thickness [mm]	Bulk density [kg/m^3]	Porosity	Flow resistivity [Pa s m^{-2}]	α (500 Hz)	α (2000 Hz)
1	25	96.4	0.98 $\pm$ 0.01	3471 $\pm$ 158	0.2	0.5
2	50	96.4	0.98 $\pm$ 0.01	3471 $\pm$ 158	0.5	0.9
3	75	96.4	0.98 $\pm$ 0.01	3471 $\pm$ 158	0.7	0.8
3	100	96.4	0.98 $\pm$ 0.01	3471 $\pm$ 158	0.75	0.9

Table 4: Physical properties and sound absorption measured for the unbleached loose cellulose crumbs porous materials studied in [28]. Measurements were performed using an impedance tube.

Table 4 shows the measured sound absorption coefficients at 500 and 1000 Hz for four samples with thickness as the only varying parameter. The same samples were also measured having 69 % relative humidity. The results showed no significant variations in the sound absorption curves with respect to the results obtained for the dry samples. Obviously, these results would not be the case for a material explicitly exposed to water. In such situation the wet material would cause the growth of fungal which would ruin the acoustic properties of the material.

In [50], the authors in an effort to support the use of environmentally-friendly products studied the sound absorption properties of materials made of cigarette filters. Cigarette filters are mainly made of cellulose acetate, which is a non-biodegradable material that consists of cellulose treated with acetic acid. Production of sound absorbing materials made of waste cigarette filters involves the use of natural fibres and recycled materials. This combination results in a sustainable alternative for acoustic purposes. Samples made of used and non-used cigarette filters were produced and measured. The results showed that samples made of used-filters were characterized by lower porosity and higher flow resistivity, which led to higher sound absorption coefficients. These results can be explained by the increase in mass that the fibres experienced when they are smoked. However, the sound absorption properties of the two types of samples were very similar. For samples of lower bulk density this difference was slightly more noticeable.

Comparisons between the sound absorption provided by samples made of cigarette filters and commercial sound porous absorbers showed that cigarette filters could be used to produce sound absorbing materials that can be used in the building industry. Table 5 showed the sound absorption coefficients at 500 Hz for some of the samples studied in [50].

	Thickness [mm]	Bulk density [kg/m^3]	Porosity	Flow resistivity [Pa s m^{-2}]	α (500 Hz)	α (2000 Hz)
CFu1	14	104	0.953	23,447	0.12	0.72
CFu2	26.5	89.75	0.96	20,113	0.29	0.98
CFu3	52	92	0.959	21,314	0.75	0.9

Table 5: Physical properties and measured sound absorption coefficients of CFu (Cigarette Filters Used) based samples studied in [50].

6.3 Equipment and Measurement method

Acoustical measurements were performed using the two-microphones transfer-function method described in the standard EN ISO 10534-2:2001 and in section 3.1.2 of this work. The impedance tube used was the *Brüel&Kjaer* type *4206A* with the large tube set up (100 mm diameter). The space between microphones was 5 cm. This configuration allowed us to obtain reliable measurements within the frequency range

[300 - 2000] Hz, according to Eq. (94) and (95). Increasing the distance between microphones to 10 *mm* would vary the valid frequency range to [170 - 1640] Hz.

The excitation signal used in the measurements was a sweep that covered wider frequency range than the allowed by the impedance tube set-up limitations. The use of a sweep required calculations of the impulse responses by convolving the measured pressures at each microphone with the inverse sweep, as explained by Farina in [10]. As a result, all the transfer functions H_{12} computed in this work are based on impulse responses instead of pressures.
The excitation signal was amplified using a power amplifier of the type *Yamaha MX-70*. Two 1/4"-microphones of the type *Brüel&Kjaer* 2670 were used to measured the pressures at each microphone location. The measured signals were amplified using a pre-amplifier of the type *Brüel&Kjaer Nexus*. The audio interface used was the *UltraLite-mk3 Hybrid*. All the signal processing was performed in Matlab. The layout of the measurement equipment is shown in Fig. 21.

The method chosen to eliminate the phase mismatch between microphones was the computation of a predetermined calibration factor. The specimen in the calibration process was a 70 mm thick foam.

Figure 21: Ilustration of the setup used to measure the sound absorption coefficient of porous materials using the transfer-function method with an impedance tube.

6.4 Materials and sample preparation

This section describes the materials and processes followed to make the cellulosic porous samples that were measured using an impedance tube. Fibrous samples have been made of dry loose hardwood and softwood cellulose fibres. Fibrous materials were obtained from pulp mill located in eastern Finland. Softwood fibres were obtained from pine and spruce, and hardwood fibres from birch. Hardwood fibres are shorter than softwoods. Generally, hardwood fibres are thinner. However, fibre diameter varies with species and even among trees of the same specie.

SEM images were taken of the cellulose fibres used to make the samples. This images were visually inspected to estimate the diameter of the fibres. The estimated diameters were 15 - 30 μm for hardwood and and 25 - 50 μm for softwood fibres.

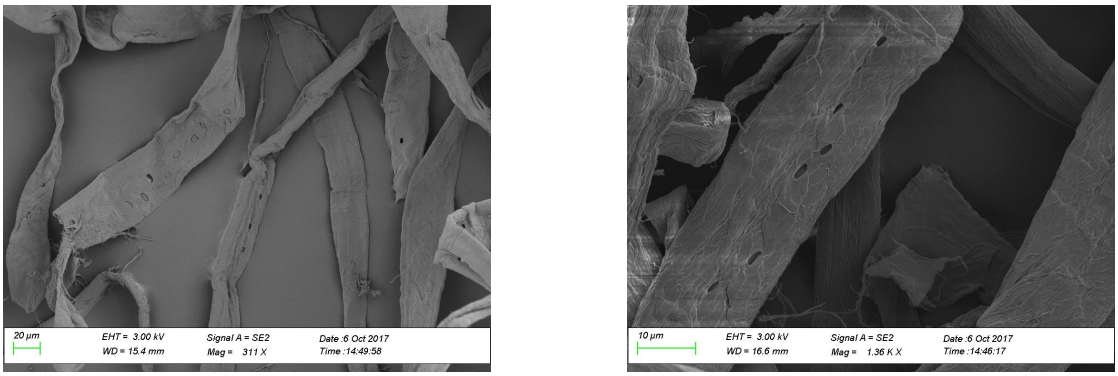

(a) Softwood cellulose fibres (b) Hardwood cellulose fibres

Figure 22: Scanning electro microscopy (SEM) images of softwood and hardwood cellulose fibres.

Unconsolidated granular samples were made of microcrystalline cellulose spheres (MCC) provided by the company JRS Pharma. There were three different diameter of grains: 100, 350 and 700 μm.

Figure 23: Raw materials used to make the granular and fibrous cellulosic samples. On the left, MCC spheres of diameter 100, 350 and 700 μm. On the right, hardwood and softwood cellulose fibres.

Preparation of fibrous samples

Fibrous samples were made of dry loose cellulose fibres. Creating the samples in such a way is appropriate because the artefacts caused by the drying process of the wet mixtures can be avoided. Furthermore, the use of dry particles allows the production of more homogeneous samples.

The dry loose cellulose fibres were obtained from softwood and hardwood pulp sheets. The process followed to obtained loose fibres from the dried pulp sheets is described below:

1. Bleached softwood/hardwood dry pulp, 30 g, was soaked in deionized water, 2 litres, for 1 day at room temperature. The use of deionized water is a common practice when doing chemistry experiments. Deionized water is water that has been treated to remove all its mineral ions, thus preventing samples under study from being contaminated.

2. After one day the solution was disintegrated using a pulp disintegrator (manufactured by Mavis Engineering, Ltd., London, England) set to a rotational frequency of 1200 rpm. This process aims to separate the interlaced fibres without modifying their structural properties.

3. The suspension was then filtered using filter-paper of particle retention 12-15 μm.

4. Fibres washed with water tend to aggregate, thus forming cumulus. In order to avoid this tendency and obtain more dispersed fibres, fibres were washed using solvents of decreasing polarity. First, one washing with excess ethanol, and then two washings with excess acetone.

   The process of drying pulp from polar solvents, for example water, causes formation of hydrogen bonds between fibres. This does not occur with non-polar solvents. By washing the fibres with solvents of decreasing polarity the polar solvent can be removed, thus avoiding formation of hydrogen bonds which can be seen as aggregation.

5. Finally, the wet fibres were dried over 72 hours and then stored in sealed plastic bags.

Once the dispersed wood cellulose fibres were obtained they were used for the preparation of the fibrous samples 6. Fibres were compacted in a cylindrical mould (100 mm external diameter and 95 mm internal diameter) to achieve the desired bulk density and thickness. During the production of the fibrous samples, steam was applied to the fibres in order for the fibres to aggregate and form a more compacted and homogeneous surface. As fibres were added into the mould, mechanical pressure was applied to the fibres to achieve the desired density. Finally, the samples were dried at room temperature for 72 hours. It should be noted that due to the low "technology manufacturing techniques" the samples could not be produced to be very homogeneous, and this may have influenced some of the results.

Images of the process and equipment used to separate cellulose fibres from the pulp sheets are shown in *Appendix A*.

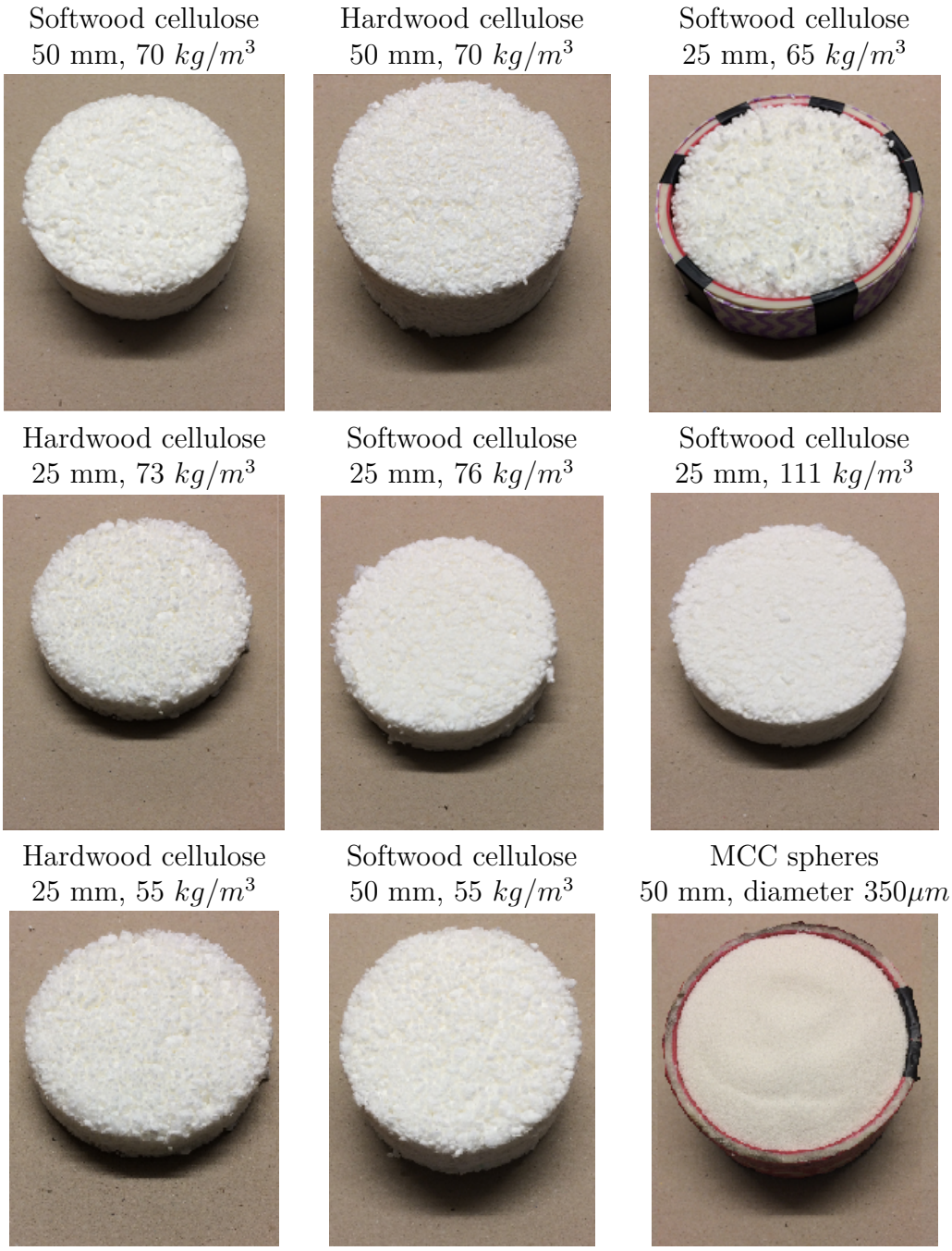

Table 6: Pictures of the samples measured in this work.

Preparation of granular samples

Unconsolidated granular samples were made of microcrystalline cellulose spheres. The samples were prepared by adding microcrystalline cellulose spherical particles of desired diameter into a cylindrical mould of desired thickness, and 95 mm and 100 mm of internal and external diameter. No compaction nor shaking was applied to the samples in order to prevent larger grains from going to the bottom, and in this

way achieve a more homogeneous sample. Measurements of the granular media with a layer of air gap behind were made by placing the particles on top of an acoustically transparent felt that was attached to a honeycomb structure to prevent the felt from behaving as a spring-mass system. Sound absorption measurements of the honeycomb structure and felt were made to verify that they do not influence the sound absorption coefficient of the materials.

6.5 Results and discussions

6.5.1 Results of unconsolidated granular samples

Granular samples have been measured according to thickness, air gap between sample and the rigid back, and particle diameter. Fig. 24 shows the absorption coefficient measured for unconsolidated granular media for different diameter of particles (0.1, 0.35 and 0.7 mm), and sample thickness of 50 and 25 mm. The results have been compared to the sound absorption predictions computed using the model of Voronina [49].

Absorption of granular media has already been described in section 4.3. Porous granular media absorbs sound through two mechanisms. The first mechanism causes absorption due to visco-thermal losses, and the second mechanism is related to the destructive interference at the surface of the sample between the direct and the sound reflected from the rigid surface behind the sample. The former becomes prominent when the attenuation happening inside the material is high, so that reflected waves from the rigid back reach the front of the sample very attenuated and therefore there is no significant interference with the direct sound. This effect can be seen from Fig. 24.

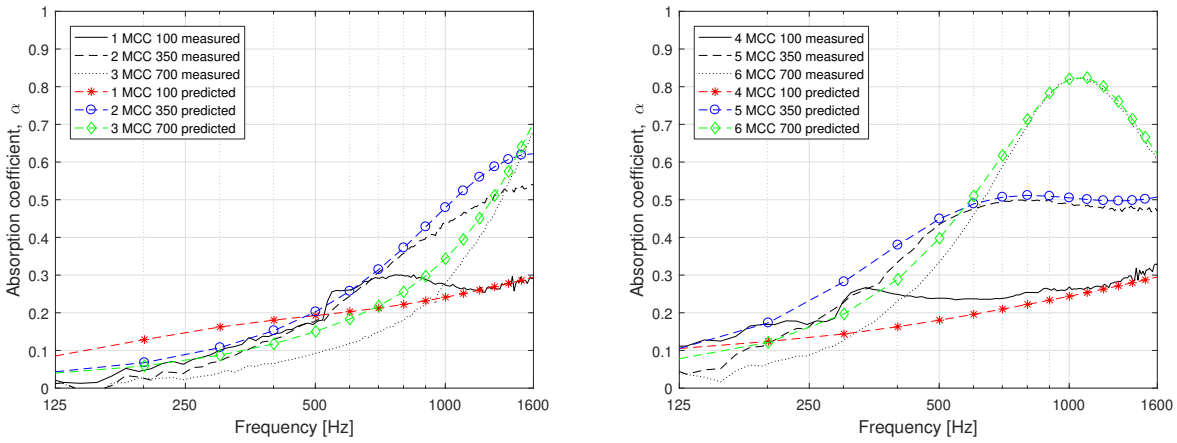

(a) (b)

Figure 24: Granular samples made of microcrystalline cellulose spheres of different grain size. MCC 100, MCC 350 and MCC 700 correspond to sphere diameter of 100 μm, 350 μm and 700 μm, respectively. The thickness of the samples in Fig. *a* and *b* were 25 and 50 mm, respectively.

For particles of size 700 μm there is a clear first resonance at 1 kHz. This first resonance is flattened and moved towards low frequencies for samples of particle size 350 μm. This effect is due to visco-thermal losses within the material becoming the dominant sound absorption mechanism for such particle size. When the particle size is reduced to 100 μm the sound absorption properties of the granular samples are considerably diminished. This degradation may be attributed to an excessive reduction in the size of the pores, which causes higher reflections rates at all frequencies. The measured results agree with the predictions computed using the model of Voronina with the following input parameters:

	Particle diameter $[\mu m]$	Sample thickness $[mm]$	Bulk density $[kg/m^3]$	Porosity
1	100	25	800	0.32
2	350	25	800	0.26
3	700	25	800	0.48
4	100	45	800	0.32
5	350	45	800	0.32
6	700	45	800	0.48

Table 7: Physical properties of the six granular samples measured. The four parameters are required by the model of Voronina [49] to predict the sound absorption coefficients of granular media.

The porosity of the granular samples could not be measured due to the no availability of the necessary equipment to perform the measurements. However, it has been shown that the porosity of a packing of idealized spheres of uniform size must fall between 0.26 and 0.48 [56]. Based on this theory, the porosity values for the model were adjusted to match the measurements. The only restriction was to respect the maximum and minimum possible value of porosity expected for a packing of uniform spheres, 0.48 and 0.26, respectively.

The effect of increasing the thickness of unconsolidated granular media has also been studied. It can be seen from Fig. 24 that increasing the thickness of the samples results in a shift of the sound absorption curve towards low frequencies. The combination of the two absorption mechanisms results in the appearance of peaks and dips in the absorption curve (only for larger particle sizes). These peaks and dips also move towards low frequencies when the sample thickness is increased. Therefore, as stated in [29], increasing the thickness of the material does not result in an overall enhancement in absorption at all frequencies. However, this effect may be less prominent when measurements are done in diffuse field.

It is noted here that in order to match the predictions with the measured results for the sample of thickness 50 mm, the input thickness parameter introduced in the model had to be reduced to 45 mm. This inconsistency may be attributed to the presence of leakages during the measurements, or simply to the no accuracy of the model due to the no perfect uniformity in the diameter of the grains. This problem was not encountered for the samples of thickness 25 mm.

From a practical point of view, the samples made of MCC spheres of diameter 350 μm provide the most suitable particle size for manufacturing optimal absorbers. The reason is that in a diffuse field, sound absorption caused by destructive interferences between direct and reflected sound may not be as efficient as that happening in the impedance tube, where only incident sound waves propagating perpendicularly to the sample are considered.

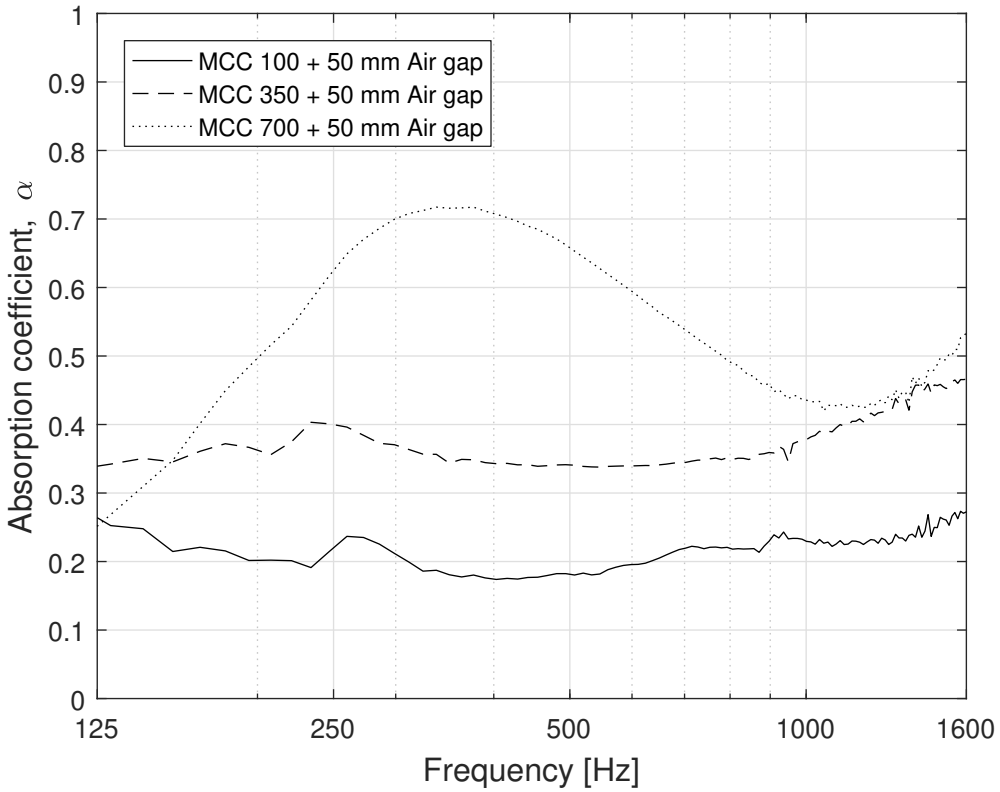

Figure 25: Sound absorption coefficient measured for the 25 mm thick granular samples of diameter 100, 350 and 700 μm with an air layer of 25 mm behind them.

Fig. 25 shows the absorption coefficient for the samples 4, 5 and 6 from Table 7 with an extra air layer of 50 mm thickness. As expected, the resonance found for the sample 4 is shifted towards low frequencies due to the increase of the total thickness of the system. The added air layer behind the samples 5 and 6 has the effect of increasing sound absorption at lower frequencies.

6.5.2 Results of cellulosic fibrous samples

The sound absorption coefficient of cellulosic fibrous samples have been measured according to thickness, bulk density, air space behind the porous samples, and fibre diameter and length.

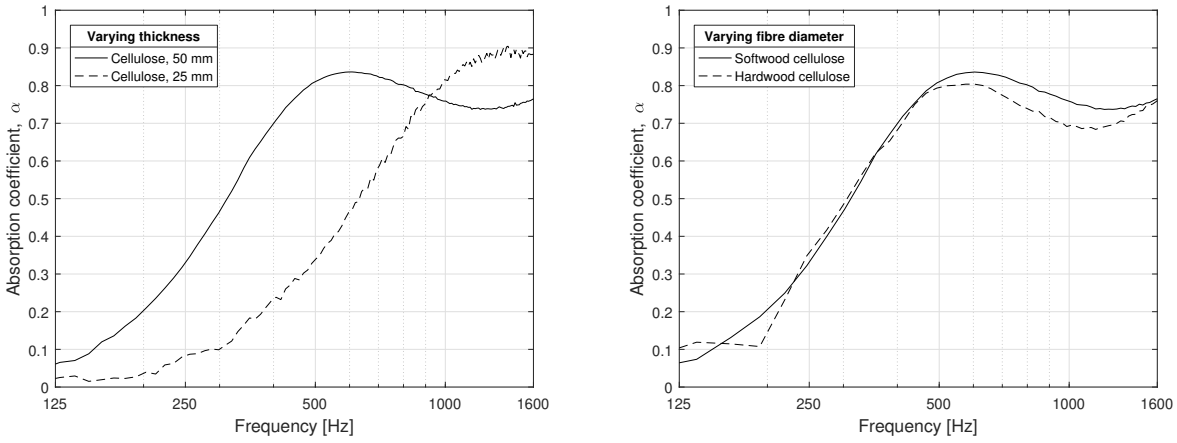

(a) (b)

Figure 26: Fig. a) shows the sound absorption coefficient of cellulosic fibrous materials of varying thickness. Fig. b) shows the sound absorption coefficient for cellulose fibres of varying diameter.

Thickness Fig. 26a shows the sound absorption coefficient for softwood samples of thickness 25 and 50 mm, and comparable densities of 76 and 70 kg/m^3, respectively. It can be seen that the sound absorption coefficient increases at all frequencies with thicker samples. It is specially interesting to note that for cellulose samples, sound absorption does not follow the theory that states that maximum sound absorption occurs at the point where particle velocity is maximum (1/4 wavelength from the rigid back surface). According to this principle, for samples of thickness 25 and 50 mm, the peak of maximum absorption should appear at around 3400 and 1700 Hz, respectively. However, as can be observed from Fig. 26a, these values considerably differ from the absorption peaks measured for these cellulose samples, which are found at 1400 and 600 Hz.

Fibre diameter Koizumi [25] proved that fibre diameter is a relevant factor determining the efficiency of fibrous materials in absorbing sound. When thinner fibres are used, a greater number of fibres is needed to fill a volume. This results in more fibres creating paths within the porous materials, and therefore giving rise to more tortuous paths. Additionally, thinner fibres are lighter and hence, they are more easily to set in motion.

Because hardwood fibres are narrower and shorter than softwood fibres, samples made of hardwood cellulose fibres should be more efficient in absorbing sound. The influence of the fibre diameter on sound absorption is shown in Fig. 26b. The results do not agree with the theory as softwood cellulose fibres provided slightly greater sound absorption.

However, it should be noted here that the difference shown in Fig. 26b could have been caused by other properties of the samples, such as their non-homogeneity. The technology used in the preparation of the samples was not accurate enough to ensure that the fibre diameter was the only divergence between the samples.

Bulk density Sound absorption coefficients for the cellulosic samples with densities 55, 65, 76, and 111 kg/m^3, and thickness of 25 mm are shown in Fig. 27a. The densest sample absorbs more sound up to 720 Hz. Above this frequency, less dense cellulose samples absorb more sound. This can be explained by a slight reduction in porosity and an increase in flow resistivity for denser samples. By increasing flow resistivity sound absorption enhances at all frequencies, however, when flow resistivity exceeds a particular value sound absorption enhancement only happens at lower frequencies, whereas at higher frequencies sound absorption deteriorates because these frequencies are reflected from the surface of the material.

Fig. 27b shows the sound absorption coefficients for samples of thickness 50 mm and densities 55 amd 70 kg/m^3. The effect is the same than in the previous case.

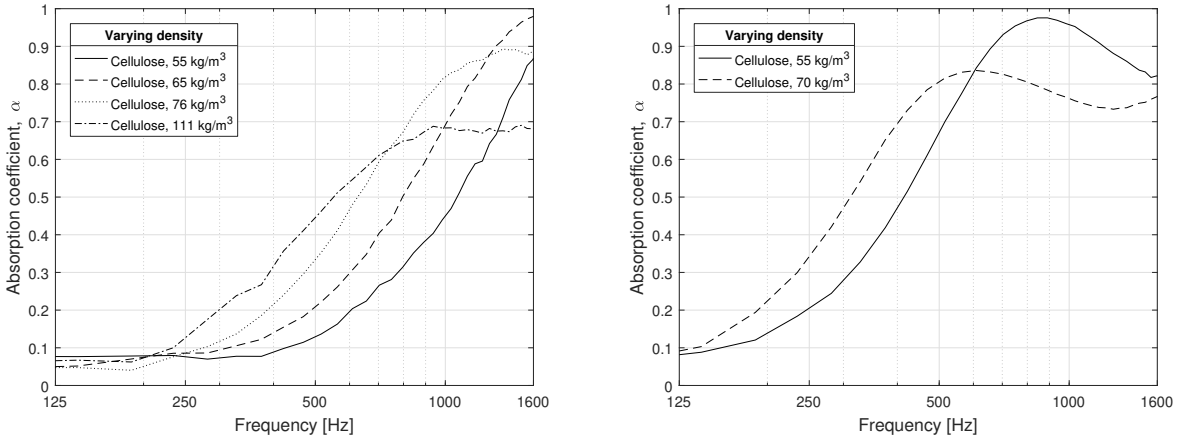

(a) (b)

Figure 27: Sound absorption coefficients for softwood cellulose samples of varying density. Fig. a) Fixed thickness of 25 mm. Fig. b) Fixed thickness of 50 mm.

Air space behind the porous layer It has already been explained in section 4.1.2, that adding a layer of air gap behind the porous materials increases sound absorption at lower frequencies. Figs. 28a and 28b depict this phenomenon for fibrous cellulose samples of thickness 50 mm and densities 55 and 70 kg/m^3, respectively.

The sample of density 55 kg/m^3 shows maximum peaks of very high absorption at frequencies 870, 545 and 405 Hz, for the three different sample configurations. According to the theory of *maximum absorption at one-quarter wavelength*, the decrease from 870 to 545 Hz of the first maximum peak should correspond to an increase of the total thickness of the sample equal to 59 mm (calculations are shown in Eq. (155)). However, the thickness of the layer of air added to the porous sample was only 25 mm. Analogously, the decrease of the maximum peak from 545 to 403 Hz would correspond, according to the same theory, to an increase of the total thickness of the sample equal to 55 mm. Again, this does not correlate with the thickness of the air layer added, which was again 25 mm. A similar analysis with analogous results can be conducted for the measurements shown in Fig. 28b.

$$\frac{\left(\frac{c_0}{870} - \frac{c_0}{545}\right)}{4} = 59\,mm \tag{155}$$

Where c_0 is the speed of sound in air, and 403 and 545 are the frequencies in Hz of the first maximum peak measured for the samples having a layer of air of 50 and 25 mm, respectively.

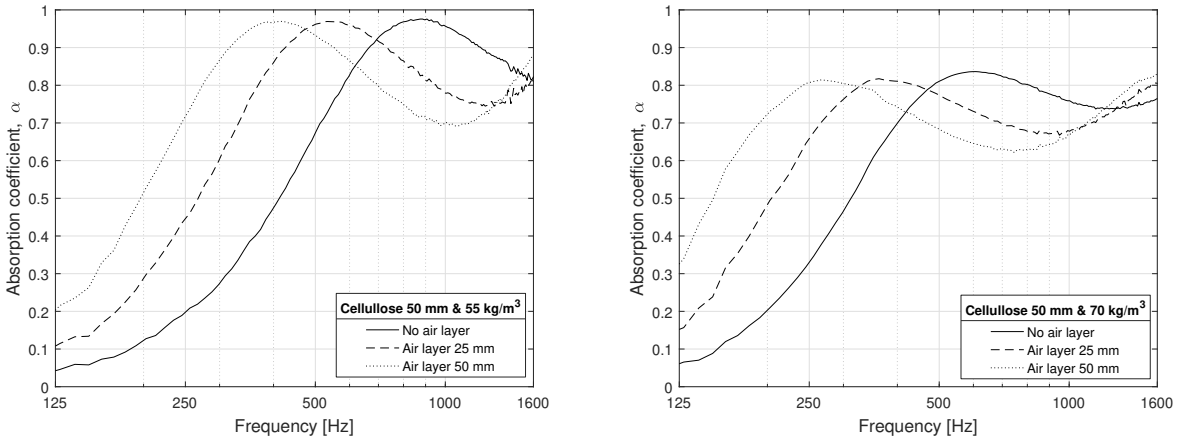

(a) (b)

Figure 28: Effect of a layer of air behind the cellulosic fibrous samples.

Comparison of cellulose fibres with rock and glass wool The physical characteristics of cellulose fibres were explained previously in this chapter. Cellulose fibres are hollow and porous, and they are made of microfibrils. These are convenient attributes that enhance the mechanisms of sound absorption of other typical fibrous porous materials, such as glass and mineral wools. While cellulose fibres are hollow, fibres glass and mineral wools are solid, cylindrical and non-porous. Their average diameter is about 6-13 μm for fibre glass, and 3-10 μm for glass and mineral wool [15], which is much smaller than the diameter found for cellulose fibres in this work (ranging from 15 to 30 μm for hardwood and from 25 to 50 μm for softwood cellulose fibres).

Cellulosic fibrous samples have two levels of porosity, which improves viscous and thermal losses within the material. The first level of porosity is given by the presence of pores in single fibres (microporosity), while the second porosity level (macroporosity) is given by the combination and interconnection between the fibres. Additionally, sound waves propagating within porous materials cause fibres and microfibrils to vibrate, which is one more mechanism for sound energy dissipation.

Fig. 29 shows measurements of the sound absorption coefficients obtained for two cellulose samples of thickness 50 mm and density 70 and 55 kg/m^3, a sample of high density glass wool and 50 mm thick, and a sample of low density rock wool of thickness 40 mm. The dip present in the sound absorption curve of the sample of rock wool must be attributed to some physical irregularities in the lateral surface of

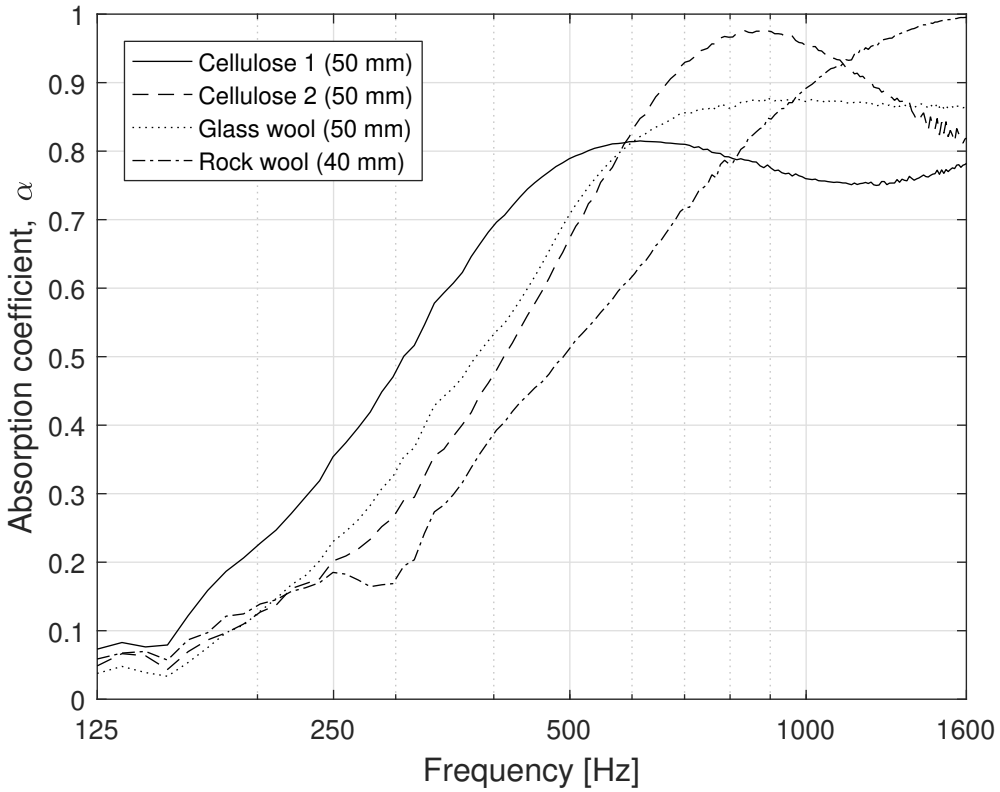

Figure 29: Comparison between the sound absorption coefficients of cellulose-fibre-based materials with glass and rock wool. The thickness and bulk density of the materials are: Cellulose 1, 50 mm and 70 kg/m^3; Cellulose 2, 50 mm and 55 kg/m^3; Glass wool, 50 mm and high density; Rock wool, 40 mm and low density.

the sample. The specimens of rock and glass wool were obtained from a larger layer of material by cutting them using a regular kitchen knife.

It can be observed that cellulose fibres can provide comparable sound absorption to glass and rock wool. Cellulose fibres can even improve the performance of these materials at lower frequencies. However, at higher frequencies, wool seem to be more efficient. Nevertheless, the samples of glass and rock wool used are products that have been optimized to achieve high sound absorption. On the other hand, the samples of cellulose fibres were made by using very simple tools without optimization process. Therefore, it is believed that the samples of cellulose fibres can be optimized to attain higher sound absorption.

6.5.3 Comparison of cellulose fibrous samples with modelling predictions

The sound absorption coefficients measured for the different cellulosic fibrous samples were compared to predictions computed by some of the models to predict the sound absorption of porous materials described in section 5.3. The models employed to make the predictions are the semi-phenomenological model of Allard and Champoux

[20] for fibrous porous materials, and the model given by Arenas et al. for unbleached cellulose crumbs [28] (the coefficients of the models can be found from Table 3). The model of Allard and Champoux ($A\&C$) was chosen because it was shown by Hongisto and Oliva [45] that it is one of the most accurate models. The model developed by Arenas et al. was chosen because the raw material used to make the samples is very similar to the raw material used in this work (cellulose fibres used in this work are bleached, which results in fibres of smaller diameter).

Fig. 30 shows the experimental and predicted results obtained using the model of Arenas et al.. Before examining the results, it should be noted that this model provides acceptable results for $0.04 \leq \rho_0 f/\sigma \leq 1$. This constriction limits the valid frequency range at low frequencies for higher values of flow resistivity ($\sigma = 12000\,Ns/m^4 \longrightarrow f_l = 400Hz$), and at high frequencies for lower values of flow resistivity ($\sigma = 500\,Ns/m^4 \longrightarrow f_u = 416Hz$).

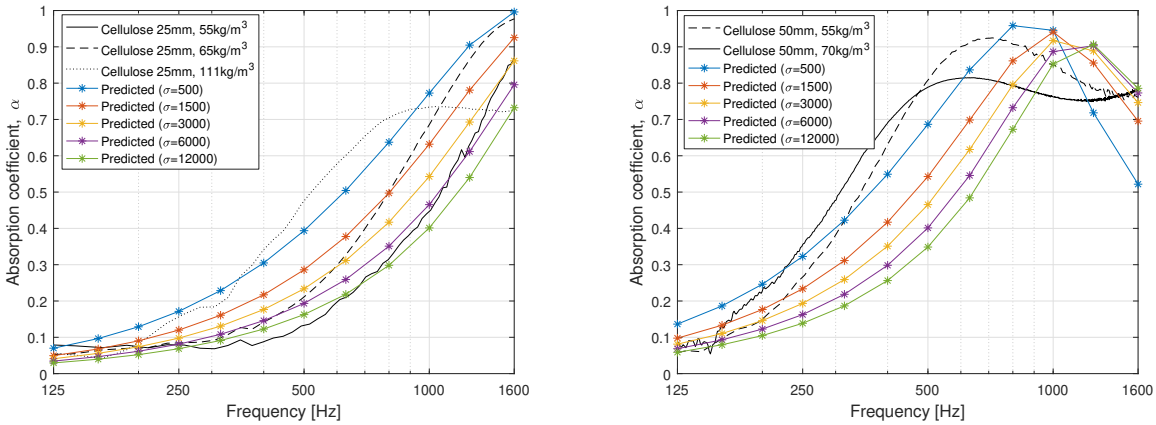

(a) (b)

Figure 30: Comparison between experimental and predicted results obtained by using the model of Arenas et al. [28]. Fig. a) Measured cellulosic fibrous samples of thickness 25 mm and densities 55, 70 and 111 kg/m^3. Fig. b) Measured cellulosic fibrous samples of thickness 50 mm and densities 55 and 70 kg/m^3. The flow resistivity values used as input parameter for the model were 500, 1500, 3000, 6000 and 12000 Ns/m^4.

According to the results obtained by using the model of Arenas et al., the sound absorption coefficients measured for the denser samples correspond to predictions obtained for lower values of flow resistivity. The flow resistivity values of the cellulosic samples could not be measured in this work due to the no availability of the equipment required to perform the measurements. However, no measurements are needed to infer that this finding is in disagreement with the logic. Obviously, denser samples should correspond to higher values of flow resistivity, at least for the bulk density values used in these measurements. Therefore, it can be concluded that the model developed by Arenas et al. is not suitable to predict the sound absorption of bleached cellulose fibres.

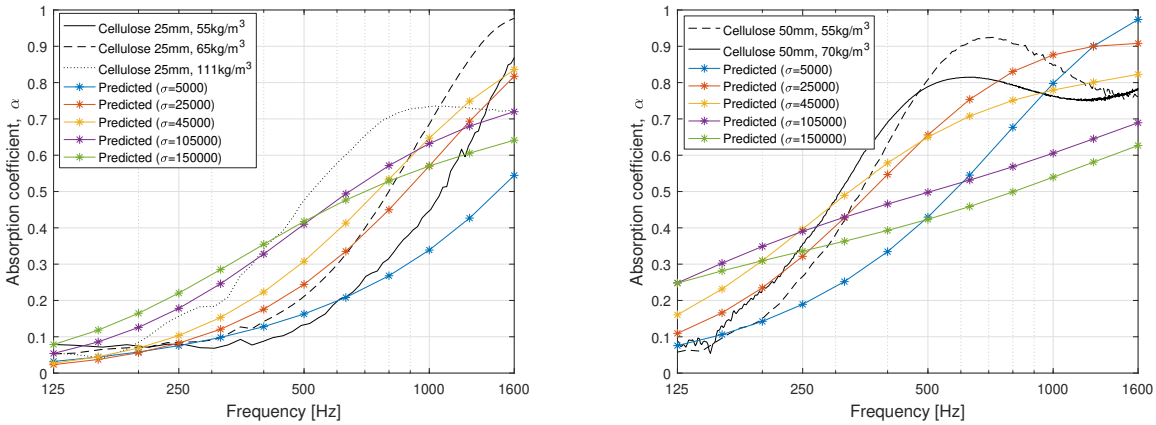

(a) (b)

Figure 31: Comparison between experimental and predicted results obtained by using the model of Allard and Champoux. [20]. Fig. a) Measured cellulosic fibrous samples of thickness 25 mm and densities 55, 70 and 111 kg/m^3. Fig. b) Measured cellulosic fibrous samples of thickness 50 mm and densities 55 and 70 kg/m^3. The flow resistivity values used as input parameter for the model were 5000, 25000, 45000, 105000 and 150000 Ns/m^4.

Fig. 31 shows comparisons between the same cellulose fibrous samples and predictions computed by the model of Allard and Champoux for varying value of flow resistivity. The predictions correlate well with the measurements in the sense that higher values of flow resistivity result in greater sound absorption at lower frequencies and lower sound absorption at higher frequencies. However, it can be seen that no prediction matches the first peak of the measured results. This can be explained by the fact that the model is not able to predict the first interference maximum that appears in the measurements obtained for samples of low bulk density. However, the measured sound absorption coefficients for the sample of thickness 25 mm and bulk density 111 kg/m^3 has no interference peak, and still no prediction can reach its sound absorption within the frequency range $[450 - 1000]$ Hz.

The failure of the models in their attempt to predict the sound absorption of bleached cellulosic fibres must be attributed to the physical differences between the raw materials. The semi-phenomenological model of Allard and Champoux was optimized to account for fibrous porous materials where fibres where modelled as identical solid circular-cylindrical rods of constant radius. This modelling does not correspond to natural cellulose fibres, which are hollow, may be porous, their radius varies along the fibre, and in general, they are different from each other. Arenas et al. described the raw material used to make their samples as particles that are a combination of grains and fibres. This description could be correctly used to describe the raw material used to make the fibrous samples in this work. However, there must be relevant differences in the raw materials because the predictions were totally in disagreement with the measurements done in this study.

Fig. 32 shows the normalized real and imaginary components of the surface impedance for cellulosic fibrous samples of different thickness and density. The surface impedance of porous materials can be measured using an impedance tube. It is computed from the reflection factor R, and the characteristic impedance of air, Z_0, as follows:

$$Zs = Z_0\left(\frac{1+\mid R \mid}{1-\mid R \mid}\right) \tag{156}$$

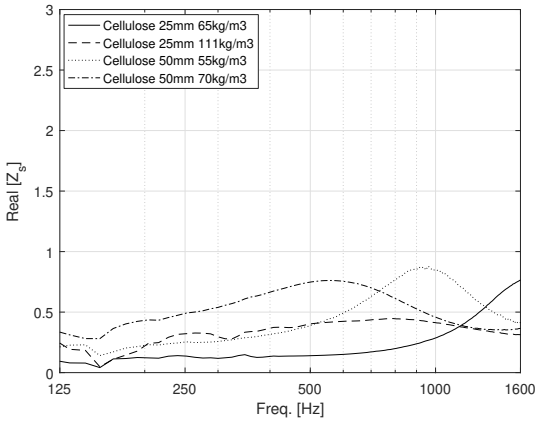

(a) Real component of Z_S

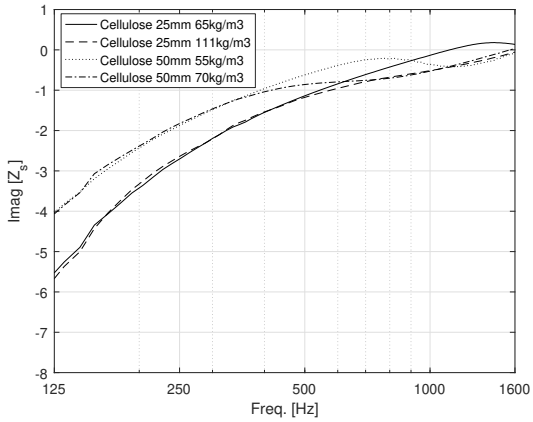

(b) Imaginary component of Z_S

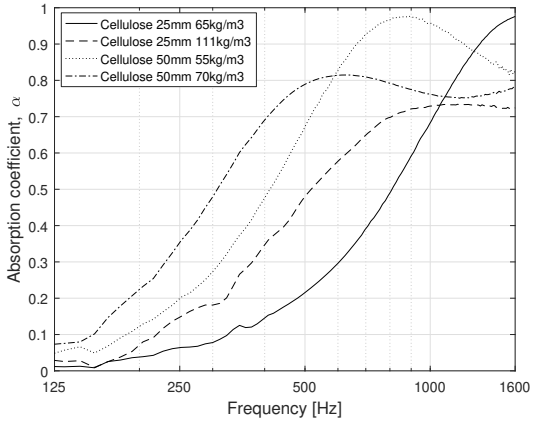

(c) Sound absorption coefficient.

Figure 32: Fig. a) and b) show the real and imaginary components of the surface impedance. Fig. c) shows the corresponding sound absorption coefficients.

The real and imaginary components of the surface impedance are associated with energy losses and phase changes, respectively [2]. When the real component approaches the characteristic impedance of air, most of the sound energy penetrates the porous media, thus causing higher dissipation of sound energy. On the other hand, the imaginary part of the surface impedance approaching zero is interpreted as a reduction in the sound energy reflected from the surface of the porous material.

It can be seen that the real part of the surface impedance shows a well defined bump for all the samples except for the densest one. The bumps are caused by the interference between the incident and reflected sound waves from the rigid surface

behind the porous sample. When the samples are dense enough the interference phenomenon at the surface of the samples does not occur.

The imaginary part of the surface impedance shows that thicker samples reflect less sound energy at lower frequencies. At higher frequencies the effect of the thickness is not as relevant, and the parameter that determines the sound absorption of the material is the bulk density (less dense samples correspond to lower values of flow resistivity).

It can be observed in Fig. 32 that the frequency range of highest sound absorption correspond to the frequency range where the normalized real and imaginary parts of the surface impedance approach the characteristic impedance of air and zero, respectively.

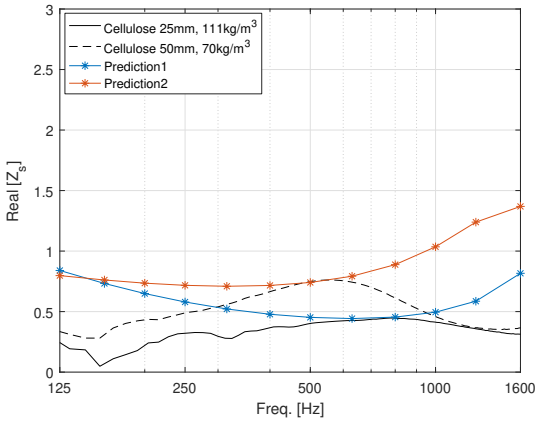

(a) Predicted and measured real component of Z_S

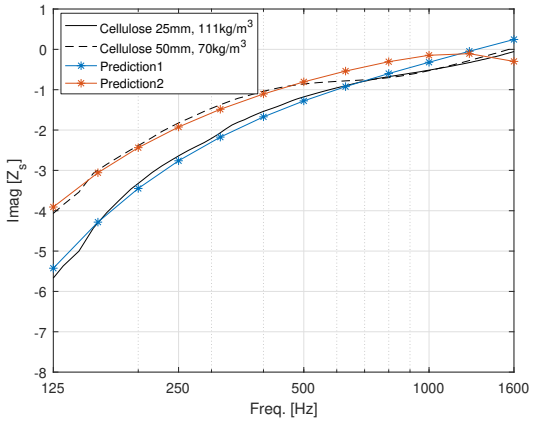

(b) Predicted and measured imaginary component of Z_S

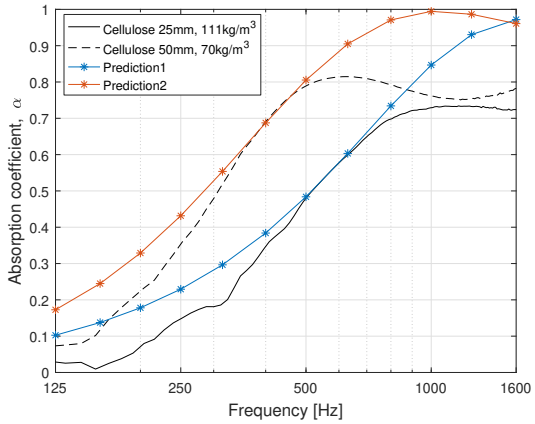

(c) Predicted and measured sound absorption

Figure 33: Measured and predicted results using the model of Allard and Champoux. The parameters of the model where set to match the real and imaginary parts of the surface impedance.

Note that the imaginary part of the surface impedance at low frequencies only depends

on the thickness of the samples. Based on this fact, a model for predicting the acoustic properties of mineral wools can be used to determine the thickness required for a sample of mineral wool to achieve the sound absorption at low frequencies provided by cellulosic fibrous materials of specific thickness. The required flow resistivity can be derived by varying the value of flow resistivity in the model to match the real part of the surface impedance and the high frequency range of the imaginary part. This has been implemented using the model of Allard and Champoux, and the results are shown in Figs. 33. Predictions only have been obtained for the samples of higher bulk density, where the interference effect is lower, and consequently, the model may provide better matching with the measurements.

For the cellulosic fibrous sample of thickness 25 mm and density $111kg/m^3$, the thickness and flow resistivity that best match the measured values of real and imaginary surface impedance are 63 mm and 2700 Ns/m^4. For the sample of thickness 50 mm and density $70kg/m^3$, the best matching is given for a layer of mineral wool of thickness 83 mm and flow resistivity 5500 Ns/m^4. The predicted thickness of the layer of mineral wool depends on not only the thickness of the cellulosic samples but the bulk density.

7 Conclusions

In this work an investigation has been conducted on the ability of sound absorbing porous materials to dissipate sound energy. A modified wave equation that depends on the properties of the porous material (flow resistivity, porosity and tortuosity) was derived to describe the propagation of plane sound waves in porous materials. The transfer matrix method was also explained as an accurate tool to predict the sound absorption properties of multilayer porous materials.

The impedance tube and the reverberation room methods were studied as the two most commonly used laboratory methods to measure sound absorption coefficients. The use of the impedance tube method, in particular the transfer function technique, is more convenient for the development of sound absorbing materials as it can be used to obtain, in addition to the absorption coefficient, the surface impedance and the acoustic characteristics of the absorbers. Furthermore, the impedance tube method requires much smaller samples, which allows much faster preparation of samples and consequently, faster optimization of the products. However, the impedance tube method only measures normal incident sound absorption, which is far away from real situations, where sound arrives surfaces from all directions. In this context, the reverberation room method is much more realistic as it can be used to determine the random incident sound absorption coefficient.

It was shown that the main macroscopic parameters determining the ability of porous materials to attenuate sound waves and change the speed of sound are flow resistivity, porosity, tortuosity, as well as the viscous and thermal characteristic lengths. These parameters are used as input parameters in the different models developed to predict the sound absorption of porous materials. Moreover, the physical properties of the sound absorbing system, including thickness, bulk density, fibre/particle diameter, and the addition of an air cavity behind the porous material, determine the final sound absorption properties of the absorber.

The main mechanisms responsible for the sound absorption of porous materials are related to viscous, thermal and inertial effects. Viscous effects are significant at low frequencies, where the size of the viscous boundary layer is comparable to the size of the pores. At high frequencies, interaction between the fluid and the solid frame causes changes in the motion of the air particles, which results in loss of momentum in the direction of wave propagation. Viscous and inertial losses cause an increase in the effective density of the fluid within the porous materials. Furthermore, thermal losses are substantial at low frequencies, where sound propagation is considered an isothermal process, which involves thermal exchange between the fluid and the solid frame at the compressions and rarefractions of the sound waves. At high frequencies sound absorption is considered an adiabatic process, compressions and rarefractions happen so fast that there is no time for the heat to flow.

Reducing the speed of sound within porous materials implies more efficient sound absorption at low frequencies. This can be achieved in two ways, by increasing effective density of the fluid at low frequencies, or by decreasing the effective bulk modulus. The latter is limited to the isothermal value (P_0), whereas the effective density can be increased by decreasing the size of the pores, thus increasing viscous

losses. However, decreasing excessively the size of the pores may cause a rise in the reflected sound energy from the surface due to a deterioration of the matching between the impedances of air and the porous material. Therefore, a process of optimization has to be done to reduce the size of the pores while keeping a good impedance matching.

Granular porous materials backed by a rigid surface exhibits one more mechanism of sound absorption. This mechanism involves a destructive interference occurring at the surface of the granular layer between the direct and the reflected sound waves coming from the rigid wall. At high frequencies, viscous-thermal effects dominate, whereas at low frequencies the destructive interference is the main mechanism of sound absorption. However, the destructive interference mechanism losses significance as the size of the grains is reduced.

A review of the models developed to predict the sound absorption properties of porous materials was presented. These models were divided into three categories, fully theoretical, semi-phenomenological, and empirical models. Theoretical models can be used to predict the sound absorption of porous materials characterized by simple pore geometries. It has been shown by many authors that the semi-phenomenological model developed by Allard and Champoux to predict the sound absorption properties of fibrous materials, provide accurate results at wide range of frequencies. However, the method requires measurements of the macroscopic parameters of the porous material, which generally involve complicated measuring techniques. Empirical models were also shown to provide accurate predictions when the model is applied to materials for which they were developed. Otherwise, the accuracy of empirical models is rather low.

The sound absorption coefficient of natural cellulose fibrous porous materials were measured using the transfer function impedance tube method. It has been shown that cellulose fibrous materials possesses acoustic properties comparable to those of sound absorbing materials typically used in the building industry. Materials made of cellulose fibres have two levels of porosity, which increases viscous and thermal losses within the material. Furthermore, the microfibres that form the cell walls of cellulose fibres are set in motion as sound waves propagate within the materials, which is one more mechanism of sound energy dissipation. Additionally, the cellulose samples of lower bulk density showed an additional peak in the sound absorption curve that was related to a destructive interference taking place at the surface of the porous layer. This phenomenon is caused by the interference between the direct and the reflected sound from the rigid surface.

According to the measurements obtained in this study, the author strongly believes that by optimizing the design of cellulosic fibrous materials to optimal values of flow resistivity, cellulose fibre materials may overcome the sound absorption performance of synthetic fibre materials. Furthermore, natural fibres are sustainable and biodegradable materials. These properties not only favour the environment, but provide a great point for the marketing of the products. Additionally, obtaining cellulose fibres may be very economical, as many industries have tons and tons of plant waste that could be used to obtain these fibres.

It has also been shown that there is no model which could accurately predict

the sound properties of cellulosic fibrous materials (at least to the knowledge of the author). In order to obtain more accurate predictions for cellulose fibres materials using semi-phenomenological models, new parameters should be added that consider the physical structure of natural cellulose fibres. An empirical model could also be developed by measuring cellulose samples of different physical properties. A regression method is then applied on the set of measurements to obtain empirical formulae. This is left for future work.

References

[1] Fahy, Frank J., *Foundations of Engineering Acoustics.* Academic Press, London, UK, (2000).

[2] Cox, Trevor J. and D'Antonio, Peter., *Acoustic Absorbers and Diffusers: Theory, Design and Applications.* Taylors and Francis, New York, USA, (2009).

[3] Dunn, F., et al., *Handbook of Acoustics.* Springer, (2015).

[4] Yamaguchi, Michiyuki, Nakagawa, Hiroshi, and Mizuno, Takuya, *Sound absorption mechanism of porous asphalt pavement.* The Journal of the Acoustical Society of Japan (E) 20, 1 (1999).

[5] Utsumo, H., Tanaka, T., and Fujikawa, T., *Transfer function method for measuring characteristic impedance and propagation constant of porous materials.* The Journal of the Acoustical Society of America 86, 637-643 (1989).

[6] Hongisto, V., *Meluntorjunta.* Book of the course S89.3471 - Noise Control (in Finnish), Aalto University, Acoustics and Audio Technology Department, (2015).

[7] EN ISO 354:2003, *Acoustics - Measurement of sound absorption in a reverberation room.*

[8] EN ISO 10534-1:1996, *Acoustics - Determination of sound absorption coefficient and impedance in impedance tubes. Part 1: Method using standing wave ratio.*

[9] EN ISO 10534-2:1998, *Acoustics - Determination of sound absorption coefficient and impedance in impedance tubes. Part 2: Transfer function method.*

[10] Farina, A., *Simultaneous measurement of impulse response and distortion with a swept-sine technique.* Proceedings 108th Convention Audio Engineering Society, Paris 18-22, (2000).

[11] Naoki, Kino, Takaayasu, Ueno, *Investigation of sample size effects in impedance tube measurements.* Applied Acoustics. 68(11), 1485-1493, (2007).

[12] Cops, A., Vanhaecht, J., & Leppens, K., *Sound absorption in a reverberation room: Causes of discrepancies on measurement results.* Applied Acoustics 46(3), 215-232, (1995).

[13] Rouquerol, et al., *Recommendations for the Characterization of Porous Solids.* Pure & Applied Chemistry, 66(8), 1739-1758, (1994).

[14] D'Alessandro, F., Pispola, G.„ *Sound absorption properties of sustainable fibrous materials in an enhanced reverberation room.* INTER-NOISE and NOISE-CON Congress and Conference Proceedings. Vol. 2005. No. 6. Institute of Noise Control Engineering, (2005).

[15] Arenas, Jorge P., Crocker, Malcolm J., *Recent Trends in Porous Sound-Absorbing Materials.* Sound & Vibration, 44(7), 12-18, (2010).

[16] *Supplier of microcrystalline cellulose spheres:* http://www.jrspharma.com/pharma_en/products-services/excipients/carriers/vivapur-mcc-spheres.php Accessed: 25.10.2017.

[17] Dunne, R., Desai, D., Sadiku, R., *A Review of the Factors that Influence Sound Absorption and the Available Empirical Models for Fibrous Materials.* Australian Acoustical Society, 45(2), 453-469, (2017).

[18] Vér, István L. and Beranek, Leo L., *Noise And Vibration Control Engineering.* John Wiley & Sons, Inc., Hoboken, New Yersey, USA, (2006).

[19] Attenborough, Keith, Umnova, O., *Cell model calculations of dynamic drag parameters in packings of spheres.* The Journal of the Acoustical Society of America 107(6), 3113-3119 (2000).

[20] Allard, Jean-F., Champoux, Yvan, *New empirical equations for sound propagation in rigid frame fibrous materials.* The Journal of the Acoustical Society of America 91, 3346 (1992).

[21] Johnson, D.L., Koplik, J. and Dashen, R., *Theory of dynamic permeability and tortuosity in fluid saturated porous media.* J. Fluid Mech. 176, 379-402 (1987).

[22] Zwikker, C. and Kosten, C.W., *Sound absorbing materials.* Elsevier, Amsterdam, (1949).

[23] Groby, J-P., Huang, W., Lardeau, A., Aurégan, Y. *The use of slow waves to design simple sound absorbing materials.* Journal of Applied Physics 117(12) (2015).

[24] Hongisto, V. , Oliva, D., Häggblom, H., *Sound absorption of multi-layer structures - Experimental study* Indoor Environmental laboratory, Turku, Finnish Institute of Occupational Health, Helsinki, Finland, (2010).

[25] Koizumi, T., Tsujiuchi, N., Adachi, A., *The development of sound absorbing materials using natural bamboo fibers and their acoustic properties.* INTER-NOISE and NOISE-CON Congress and Conference Proceedings. Institute of Noise Control Engineering, 5, 713-718, (2002).

[26] Asdrubali, F., *Survey on the acoustical properties of new sustainable materials for noise control.* Proceedings of Euronoise. Vol. 30. (2006).

[27] IARC, *IARC Monographs on the Evaluation of Carcinogenic Risks to Humans.* Vol. 81, Man-made Vitreous Fibres, Lyon, IARCPress, (2002).

[28] Arenas, J. P., Rebolledo, J., del Rey, R., & Alba, J., *Sound absorption properties of unbleached cellulose loose-fill insulation material.* BioResources 9(4), 6227-6240, (2014).

[29] Swift, M.J., Bris, P., and Horoshenkov, K.V., *Acoustic absorption in re-cycled rubber granulate.* Applied Acoustics 57, 213-212, (1999).

[30] Venegas, R., Umnova, O., *Acoustical properties of double porosity granular materials.* The Journal of the Acoustical Society of America 130(5), 2765-2776, (2011).

[31] Bechwati, F., Avis, M. R., Bull, D. J., Cox, T. J., Hargreaves, J. A., Moser, D., & Venegas, R., *Low frequency sound propagation in activated carbon.* Acoustical Society of America, 239-248, (2012).

[32] Berardi, U, Iannace, G, *Acoustic characterization of natural fibers for sound absorption applications.* Building and Environment 94, 840-852, (2015).

[33] Garai, Massimo, Pompoli, Francesco. *A simple empirical model of polyester fibre materials for acoustical applications.* Applied Acoustics 66(12), 1383-1398, (2005).

[34] Biot, M.A., *Theory of propagation of elastic waves in a fluid-saturated porous solid. I Low frequency range.* The Journal of the Acoustical Society of America 28(2), 168-78, (1956).

[35] Biot, M.A., *Theory of propagation of elastic waves in a fluid-saturated porous solid. II Higher frequency range.* The Journal of the Acoustical Society of America 28(2), 179-91, (1956).

[36] Allard, Jean-F., Atalla, N., *Propagation of Sound in Porous Media: Modelling Sound Absorbing Materials.* 2 Edition. John Wiley & Sons, (2009).

[37] Allard, Jean-F., Champoux, Yvan, *Dynamic tortuosity and bulk modulus in air-saturated porous media.* The Journal of the Appl. Phys. 70, 1975-1979, (1991).

[38] Panneton, Raymond, Olny, Xavier, *Acoustical determination of the parameters governing viscous dissipation in porous media.* The Journal of the Acoustical Society of America 119(4), 2027-2040, (2006). Academic Press, London, UK, (2000).

[39] Panneton, Raymond, Olny, Xavier, *Acoustical determination of the parameters governing thermal dissipation in porous media.* The Journal of the Acoustical Society of America 123, 814, (2008).

[40] Pride, Steven R., Morgan, Frank Dale, Gangi, Anthony F., *Drag forces of porous-medium acoustics.* Physical review B 47(9), 4964, (1993).

[41] Delany, M. E., Bazley, E. N. *Acoustical properties of fibrous absorbent materials.* Applied Acoustics 3(2), 105-116, (1970).

[42] Miki, Yasushi, *Acoustical properties of porous materials-Modifications of Delany-Bazley models.* Journal of the Acoustical Society of Japan (E) 11(1), 19-24, (1990).

[43] Komatsu, Takeshi, *Improvement of the Delany-Bazley and Miki models for fibrous sound-absorbing materials.* Acoustical Science and Technology 29(2), 121-129, (2008).

[44] Kirby, Ray, *On the modification of Delany and Bazley fomulae.* Applied Acoustics 86, 47-49, (2014).

[45] Oliva, David, Hongisto, Valtteri, *Sound absorption of porous materials–Accuracy of prediction methods.* Applied Acoustics 74(12), 1473-1479, (2013).

[46] Berardi, Umberto, Iannace, Gino. *Predicting the sound absorption of natural materials: Best-fit inverse laws for the acoustic impedance and the propagation constant.* Applied Acoustics 115, 131-138, (2017).

[47] Voronina, N. *Acoustic properties of fibrous materials.* Applied Acoustics 42(2), 165-174, (1994).

[48] Voronina, N. *Improved empirical model of sound propagation through a fibrous material.* Applied Acoustics 48(2), 121-132, (1996).

[49] Voronina, N.N., Horoshenkov, K.V., *A new empirical model for the acoustic properties of loose granular media.* Applied Acoustics 64(4), 415-432 (2002).

[50] Maderuelo-Sanz, Rubén, Gómez Escobar, Valentín, & Meneses-Rodríguez, Juan Miguel, *Potential use of cigarette filters as sound porous absorber.* Applied Acoustics 129, 86-91, (2018).

[51] Kalia, Susheel, B. S. Kaith, & Inderjeet Kaur, (Eds.), *Cellulose fibers: bio-and nano-polymer composites: green chemistry and technology.* Springer Science & Business Media, (2011).

[52] Gullichsen, Johan, Paulapuro, Hannu, *Forest Products chemistry.* Fapet Oy, Helsinki, Finland, (2000).

[53] Biermann, Christopher J., *Handbook of pulping and papermaking.* Elsevier, 1996.

[54] Wassilieff, Con, *Sound Absorption of Wood-Based Materials.* Applied Acoustics, 48(4), 339-356, (1996).

[55] Yang, W. & Li, Y., *Sound Absorption Performance of Natural Fibers and Their Composites.* Science China Technological Science, 55(8), 2278-2283, (2012).

[56] Nimmo, J. R., *Porosity and pore size distribution.* Encyclopedia of Soils in the Environment 3, 295-303, (2004).

A Appendix: Equipment used in the process of obtaining cellulose fibres from pulp sheets.

All the process was carried out in the facilities of the School of Chemical Technology, Aalto University.

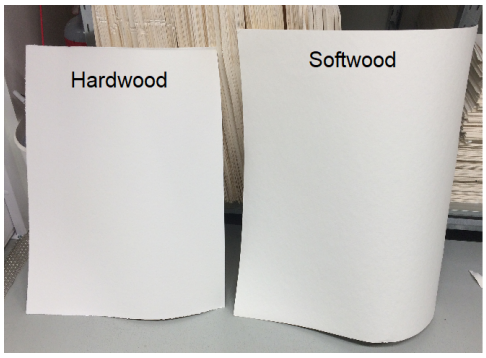

(a) Hardwood and Softwood pulp sheets.

(b) Pulp disintegrator, manufactured by Mavis Engineering, Ltd., London, England.

(c) Filter-paper of particle retention 12-15 μm.

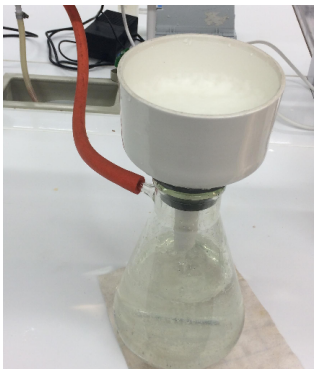

(d) Set-up used to filter the pulp suspension.

(e) Washing cellulose fibres with solvent of decreasing polarity to remove water.

(f) Separated hardwood and softwood cellulose fibres obtained at the end of the process.